DIRECT RADIATIVE FORCING BY AEROSOLS OVER SOUTHERN AFRICA

Antonio Joaquim Queface

Student Number 0000709Y

A thesis submitted to the Faculty of Sciences,
University of the Witwatersrand, Johannesburg,
in fulfilment of the requirements for the degree of Doctor of Philosophy

February 2013

Declaration

I declare that this thesis is my own unaided work in fulfilment of the degree of Doctor of Philosophy in the School of Geography, Archaeology and Environmental Studies in the University of Witwatersrand, Johannesburg. This thesis has not been submitted previously for any degree or examination at any other university.

I further declare that the work presented in the thesis:

DIRECT RADIATIVE FORCING BY AEROSOLS OVER SOUTHERN AFRICA

is authentic and original unless clearly indicated otherwise and in such instances full reference to the source is acknowledged and I do not pretend to receive any credit for such acknowledged quotations, and that there is no copyright infringement in my work. I declare that no unethical research practices have been used and no material gained through dishonesty. I understand that plagiarism constitutes a serious offence and, should I contravene the Plagiarism Policy (notwithstanding signing this affidavit), I may be found guilty of a serious criminal offence (perjury) that would compel the University to inform all other tertiary institutions of the offence. The University would also be able to issue a corresponding certificate of reprehensible academic conduct to whoever may request such a certificate from the institution.

_____

Antonio Joaquim Queface

26th day of February 2013

Abstract

A thorough understanding of the optical properties of aerosols, their spatial and temporal distribution and their radiative effects in the atmosphere, is needed for the better assessment of the impacts of aerosols on regional climate systems. Monitoring of aerosol parameters and solar radiation fluxes has been conducted in southern Africa by the AERONET programme since the middle of the last decade. These valuable data, combined with model estimates products, plus the intensive field experiments such as SAFARI 2000, provided key information, contributing towards a better overall understanding of the main characteristics of tropospheric aerosols over southern Africa and how these aerosols impact the direct aerosol forcing in the region. Two long-term AERONET sites, at Mongu in Zambia and Skukuza in South Africa, formed the core sources of data in this study. Secondary sites in Saudi Arabia (Solar Village) and United Arad Emirates (Hamin and Dhadnah) were used for comparison purposes.

Aerosol optical properties and the direct aerosol radiative forcing over southern Africa both change significantly from one season to another, following the strong seasonal cycle of aerosol optical thickness (AOT). Consequently, the evaluation of aerosol forcing using static values throughout the year is not suitable for describing the aerosol climate effects in this region.

Results show that the seasonal variations of aerosol optical thicknesses at 500 nm over southern Africa can be defined into three periods:

- December to May with relatively clean atmospheric conditions, with monthly averages AOT values at 500 nm between 0.1 to 0.2, mainly associated with air masses from which aerosols have been washed during the wet season, and minimal regional biomass burning;
- followed by a transition period towards high AOT values, from June to August, with a moderately turbid atmosphere (0.2 – 0.3);
- September to November, with high levels of AOT (0.3 – 0.5) –mainly associated with biomass burning.

Within this region a reversal gradient of AOT can be observed along the annual timeline; the north has higher magnitudes than the south, i.e. a north–south gradient, during the

biomass-burning season and the opposite applies in the non-biomass burning season, i.e. a south–north gradient. From the currently available aerosol data, no long-term discernible trends are observable in aerosol loadings over this region. Direct aerosol radiative forcing evaluations, in southern Africa, need to take into account the differences between both the non-biomass burning and the biomass burning seasons. Direct aerosol forcing magnitudes during the biomass burning period are almost double those of the non-biomass burning at BOA and TOA. The impact of biomass burning on the direct aerosol forcing is not limited to the bottom of atmosphere (BOA), but also influences the forcing at top of atmosphere (TOA). Direct aerosol radiative forcing values for all of southern Africa are estimated at -33 $W\,m^{-2}$ for BOA and -6 $W\,m^{-2}$ for TOA. However, seasonal values may differ considerably from these levels.

Monthly averages of direct aerosol radiative forcing at BOA are frequently less than -30 $W\,m^{-2}$ from December to May (non-biomass burning period) with a slightly south-north gradient. From July to October, a strong north-south gradient of direct aerosol radiative forcing is observed and forcing magnitudes are frequently recorded at -50 $W\,m^{-2}$ (and, on occasion well above that level) during September, i.e. at the peak of biomass burning. June and November are regarded as transitional months when levels move towards the higher or and lower values of forcing respectively. At TOA monthly averages of direct aerosol radiative forcing from December to May are frequently less than -9 $W\,m^{-2}$ and, during biomass burning, direct aerosol radiative forcing values almost double. From the seasonal perspective, it is also possible to depict the reversal gradient behaviour at TOA.

This study has contributed to improving the understanding and knowledge about of the direct aerosol radiative effects in this region - necessary step towards addressing the indirect and semi-direct aerosol effects. This study also emphasises the need for obtaining further data for defining the aerosol optical characterisations by regions or sub regions as demonstrated by the identifiable overall differences in the aerosol optical properties between the southern Africa and Middle Eastern regions. This process will require improving the quantity and quality of aerosol measurements at regional scales.

Dedication

In memory of my Grandfather

Queface Chicatsa Savanguane

1912-1979

Preface

Particles injected into the atmosphere, i.e. aerosols such as dust, salt from sea spray; small smoke particles from combustion of vegetation or power plants, interact with incoming solar radiation. These particles have the ability to change the radiative balance of the Earth's climate system. Aerosols modify the Earth-atmosphere energy budget through diverse atmospheric processes. The direct aerosol effect acts by scattering and absorption of solar and Earth radiation; the indirect effect acts by changing particle sizes and lifetimes of cloud droplets that act as cloud condensation nuclei, leading to changes of cloud microphysics.

A process that alters the energy balance of the climate system is known as 'radiative forcing'. The radiative effects of aerosols on the Earth's system form a major component of global and regional climatic patterns, influencing processes in the troposphere, the hydrological cycle and surface temperatures over the entire globe. The addition of anthropogenic aerosols to the atmosphere may change the radiative fluxes at the top of atmosphere (TOA), at bottom of atmosphere (BOA) and throughout the atmospheric column thereby perturbing the whole climate system.

The focus of this research is direct aerosol radiative forcing, defined as the change in the net downward minus upward radiative flux at a particular level in the atmosphere, at TOA or BOA. A positive direct aerosol forcing at the TOA indicates additional energy reaching the Earth-atmosphere system, i.e. a warming effect; a negative forcing indicates a net loss of energy, i.e. a cooling effect. The magnitude of cooling by anthropogenic aerosols may be comparable to greenhouse gas warming when examined on a global scale, but can be much larger on a regional scale.

Large uncertainties exist in the current estimates of direct aerosol forcing because of incomplete knowledge concerning both the distribution of aerosols, and their physical and chemical properties and aerosol-cloud interactions. The uncertainty in determining the level of the aerosol direct forcing is a factor of approximately 2 to 3; the uncertainty for the indirect forcing is much larger and more difficult to quantify. Reduction in these uncertainties requires a coordinated research strategy aimed at successfully integrating data from multiple platforms, e.g. ground-based networks, satellite, ship, aircraft, and multiple

techniques, e.g. in-situ measurement, remote sensing, numerical modelling and data assimilation.

During the late 1990s, a great deal of effort was invested in improving aerosol measurements and data sets by:

- including their integration into the sophisticated surface-radiation networks such as AERONET (Aerosol Robotic Network);
- the validation and implementation of new and enhanced satellite sensors (MODIS in TERRA or AQUA satellites);
- the execution of intensive aerosol radiation field experiments in various aerosol regimes around the globe (including in southern Africa).

The aim of this research is to study the direct radiative forcing of aerosols and the aerosol optical properties of southern Africa. Of particular interest is the estimation of the variations of aerosol direct forcing directly attributable to changes in aerosol loadings over the atmospheric column of this region. For this study the following questions were posed:

1. What are the aerosol optical properties (AOP) over southern Africa?
2. How do these AOP change within different seasons (including identifying any likely long-term trends)?
3. What are the main characteristics of AOP in southern Africa that differ from those in other environments?
4. What are the magnitudes of daily and seasonal direct aerosol radiative forcing (ARF) at bottom of atmosphere and top of atmosphere over southern Africa?
5. How does the change of aerosol amounts in the tropospheric column influence the change of direct ARF at bottom of atmosphere and at top of atmosphere?
6. What is the likely regional magnitude of direct radiative forcing of aerosols for southern Africa?

A synergy of ground-based remote sensing measurements and model radiation estimates were utilised to deduce the direct radiative forcing at BOA and at TOA. The levels of aerosol optical properties, derived from long-term measurement sites at Mongu in Zambia and Skukuza in South Africa, were used as basic data to improve the understanding of direct radiative forcing by aerosols in this region. For comparison purposes, data from a secondary region in Middle East were also analysed.

This thesis is divided into six chapters.

Chapter 1 provides the necessary background information related to the radiative effects of aerosols in the Earth system, solar radiation measurements instruments, a summary of aerosol research in southern Africa and the research questions of this study.

Chapter 2 describes the data sets, analytical tools and methodologies.

Chapter 3 describes the climatology of aerosol optical properties over southern Africa, a comparison of aerosol optical properties between southern Africa and the Middle East is discussed, analyses in separate size modes (coarse and fine) is also presented.

Chapter 4 presents the surface solar fluxes measurements in Skukuza during SAFARI 2000, identifies the clear sky days and the associated atmospheric aerosol parameters and solar radiation fields. Backward trajectories are analysed for the selected clear sky days.

Chapter 5 includes the analysis of direct aerosol forcing estimates over southern Africa (Mongu and Skukuza) for top of atmosphere and bottom of atmosphere, describes the seasonal changes, and discusses the inter-linkages between the estimated direct radiative forcing values, the surface radiation measurements during clear sky periods and the aerosol optical properties for final evaluation of direct aerosol forcing at regional scale. In addition direct aerosol radiative forcing magnitudes between southern Africa and Middle East regions are compared.

Finally, in **Chapter 6,** key results from each posed research questions are summarised and conclusions presented. Furthermore a brief significance of this study is presented

Material from Chapter 3: 'Climatology of aerosol optical properties in southern Africa' has been published in the *Journal of Atmospheric Environment* (Queface *et al.*, 2011). Parts of this research have also been presented at the International Geosciences & Remote Sensing Symposium (IGARSS 2009) held in Cape Town, South Africa (13 – 17 July 2009); the South African Society of Atmospheric Science (SASAS), SASAS 2006 Conference (Bloemfontein, Free State, 4-6 October 2006).

Acknowledgments

During the course of this research, permissions and assistance in accessing data were obtained through various laboratory and field experiments undertaken at NASA's Goddard Space Flight Center (GSFC). These activities were conducted at the Radiation and Climate Branch (under the AERONET and SMART research groups) and during the United Arab Emirates Unified Aerosol Experiment in 2004.

The investigations into aerosol optical properties and solar fluxes estimates were made possible through the AERONET project, NASA Goddard Space Flight Center. Mention must be made of the support and assistance gratefully received from the Climatology Research Group of The University of Witwatersrand, Johannesburg and the Physics Department of Eduardo Mondlane University during this work.

I am grateful to the SMART team, for their invaluable support in providing guidance on data analysis and MatLab programming, in particular the principal investigator Si-Chee Tsay and Jack Ji. I would also like to thank the AERONET site managers at Mongu and Skukuza for their continuous maintenance of the sun photometer instruments. The work reported in this study also formed part of the SAFARI 2000 Regional Science Initiative.

This research has been conducted under the guidance of Prof. Stuart John Piketh (Director of the Climatology Research Group at The University of the Witwatersrand) and Dr Si-Chee Tsay (SMART Group at NASA GSFC), who are here thanked for their supervision and continuous encouragement. They are also thanked for providing funding for several trips – both to United States for short-term training at NASA GSFC and to the field experiment in United Arab Emirates (UAE) during the Unified Aerosol Experiment. I thank Prof. Harold Annegarn from the University of Johannesburg in South Africa for his long support and encouragement of Mozambican students and Ms. Lisanne Frewin for proofreading this thesis.

I thank the Sida-SAREC of Sweden, for supporting the long-standing research cooperation with the Faculty of Sciences at Eduardo Mondlane University, through the financial support of the research programme "Energy, Environment and Climate" and currently "Environment and Climate". Also I thank Prof. Harold Annegarn for financial contribution to accommodation in Johanneburg.

Finally, yet importantly, I thank Eduardo Mondlane University for extensive leave for research in Southern Africa, study breaks at Wits and in the USA. Thanks to colleagues who carried extra teaching loads during my absence.

Contents

List of Figures

List of Plates

List of Tables

Chapter 1.

The necessary background information related to the radiative effects of aerosols in the Earth system, key definitions, the principles of solar radiation measurement, and the summary of aerosol research in southern Africa are given in this chapter. The research goals and research questions are also outlined.

1 Introduction and Literature Review

1.1 Introduction

The main processes that determine the overall state of the climate system are twofold: heating by the incoming solar radiation and cooling by outgoing long-wave (infrared) terrestrial radiation (Coakley *et al*., 1983; Ramanathan *et al*., 1989). Any process that can disturb the overall energy balance can cause climate perturbation (Kaufman & Fraser, 1997). A process that alters the radiative balance of the climate system is known as 'radiative forcing' (Coakley *et al*., 1983; Coakley & Cess, 1985). Changes in the composition of the atmosphere constitute a major forcing mechanism; the best examples are greenhouse gases and aerosols particles (Crutzen & Andreae, 1990; Charlson *et al*., 1992). Changes in the greenhouse gas or aerosol content of the atmosphere affects the radiative balance of the climate system.

The addition of anthropogenic aerosols to the atmosphere may change the radiative fluxes at the top-of-atmosphere (TOA), at the surface, and within the atmospheric column. Aerosols have two main effects on the Earth's radiation budget. The first is a direct effect when aerosol particles scatter and absorb the solar and thermal radiation (Charlson *et al.*, 1992). The other is an indirect effect when aerosols change the particle size and lifetime of cloud droplets by acting as cloud condensation nuclei, leading to a cloud albedo change (Twomey, 1977).

The focus of this research is 'direct aerosol radiative forcing' (DRF), which is defined as the change in the net downward minus upward radiative flux at a particular level in the atmosphere (IPCC, 1995), e.g. at top of atmosphere (TOA) or bottom of atmosphere (BOA). A positive DRF at the TOA indicates an addition of energy to the Earth-

atmosphere system, i.e. a warming effect. A negative effect indicates a net loss of energy, i.e. a cooling effect.

Aerosol forcing assessments have been based largely on model calculations although, to some degree, these models have been initialised and evaluated against satellite and surface measurements. Large uncertainties exist in the current estimates of aerosol forcing because of an incomplete knowledge of aerosols, i.e. their distribution, their physical and chemical properties, and aerosol-cloud interactions. The uncertainty for the aerosol direct forcing is about a factor of two to three and for the indirect forcing is much larger and more difficult to quantify (IPCC, 2001; Haywood & Boucher, 2000).

Reduction in these uncertainties requires a coordinated research strategy to successfully integrate data from multiple platforms, e.g. ground-based networks, satellites, ships and aircraft, and multiple techniques, e.g. in-situ measurements, remote sensing, numerical modelling and data assimilation (Penner *et al*., 1994; Kaufman *et al*., 2002; Diner *et al*., 2004; Anderson *et al*., 2005).

In late 1990s, a great deal of effort was put into improving aerosol measurements and data sets, including integration into sophisticated surface-radiation networks such as AERONET (Aerosol Robotic Network) (Holben *et al*., 1998). The validation and implementation of new and enhanced satellite sensors, such as MODIS aboard the TERRA or AQUA satellites, and the execution of intensive aerosol radiation field experiments in various aerosol regimes, also contributed to improved measurement and data results from around the globe (Yu *et al.*, 2006).

Because of these efforts, it has now become increasingly feasible to shift the focus of the estimates of aerosol direct forcing away from largely model-based calculations towards measurement-based datasets. In this new approach, remote sense measurements provide a baseline for regional to global-scale assessments. Chemical transport models are used to interpolate and supplement data in regions/conditions where observational data are not available. Measurements from ground-based networks and intensive field experiments are required for evaluating the accuracy of the satellite retrievals and model simulations. Model simulation is an indispensable tool for estimating past aerosol forcing and projecting future climate conditions related to changes in atmospheric aerosols. Observations can be used to improve and constrain model simulations of aerosol impacts through synthesis and integration (Collins *et al*., 2001; Yu *et al*., 2004).

Errors in estimating aerosol optical properties can have a tremendous influence on estimates of impacts of the aerosol direct radiative effect. In recent years, the characterisation of aerosols in southern Africa has been significantly improved through intensive field experiments — ground-based network measurements, and satellite remote sensing and its integration with model simulations. However, studies of aerosols are few in Southern Africa compared with other regions, e.g. in the Northern hemisphere, despite the climatic vulnerability of this region.

The main objective of this research is to study the direct radiative forcing of aerosols and the aerosol optical properties of southern Africa. Of particular interest is the estimation of the variation in aerosol direct forcing to be attributed to changes in atmospheric aerosol loadings over this region. A synergy of ground-based remote sensing measurements and model radiation estimates were utilised to deduce the direct radiative forcing at the bottom-of-atmosphere (BOA) and at top-of-atmosphere (TOA). The aerosol optical properties, derived from two long-term measurement sites at Mongu in Zambia and Skukuza in South Africa, were used as basic data to improve the understanding of direct radiative forcing by aerosols. For comparison purposes, data from a secondary region in Middle East were also analysed.

1.2 Literature review

1.2.1 Definition of radiation and aerosol optical parameters

Radiation fluxes: The total amount of radiation that the Earth and its atmosphere absorb or emit, expressed in watts per square meter [W m^{-2}].

Irradiance: The amount of incident radiation on a given surface, expressed as energy per unit time and unit area or watts per square meter [W m^{-2}].

Aerosol optical thickness — AOT: The quantitative measurement of the extinction of solar radiation (by aerosol scattering and absorption between the point of observation and the top of the atmosphere). The higher the AOT value, the more aerosols there are within a column. AOT is also the most important parameter for evaluating direct radiative forcing. The AOT value can be determined from the ground or from space through measurements of the spectral transmission of solar radiation through the atmosphere using sun photometers or filter radiometers.

Ångström exponent — α or AE: An indirect measure of the aerosol size distribution. Generally when α is close to zero, coarse particles dominate; for α close to 2, fine particles are the most prevalent. In practical applications, the AOT are measured at two or more wavelengths in the ultraviolet, visible, or near infrared spectral regions and the Ångström exponent can be calculated from a pair of the spectral values of AOT, by using the Ångström turbidity formula.

Single scattering albedo — ω or SSA: The single scattering albedo is the probability that, given an interaction between the photon and particle, the particle will be scattered rather than absorbed. The single scattering albedo is equal to zero ($\omega = 0$) for a perfectly absorbing aerosol and equal to one ($\omega = 1$) for pure scatter.

Size parameter— x: The ratio of particle circumference to the wavelength of incoming radiation ($x = 2\pi r/\lambda$). This parameter will define the type of theory to be applied in scattering problems. When $x << 1$, i.e. when particles are very small compared to the wavelength of incident radiation, the Rayleigh theory is used. In the case of very large particles, $x \rightarrow \infty$, geometrical optics may be used to estimate the scattering field, i.e. rays of light can be traced by the classical laws of refraction and reflection. When the size of particles is comparable with the wavelength of the incident beam, the Mie theory is applied.

Scattering angle — θ: Represents the angle between the forward direction of the incident beam and the scattered radiation.

Phase function — P(θ): Represents the angular distribution of the scattered energy (angular dependence of scattering), which has units of [Sr^{-1}] and describes the probability of a photon scattering into a unit solid angle oriented at an angle θ relative to the photons original trajectory. An *isotropic* phase function, i.e. $P(\theta) = 1/4\pi$, would scatter light with equal efficiency in all possible directions.

Asymmetry factor — g: The asymmetry factor (dimensionless) is a measure of the amount of forward direction retained after a single scattering event. If a photon is scattered by a particle so that its trajectory is deflected by a deflection angle θ, then the component of the new trajectory, which is aligned in the forward direction, is shown as cos(θ). There is commonly an average deflection angle and the mean value of cos(θ) is defined as g. Theoretically, the asymmetry factor can vary

between -1 and 1 ($-1 \leq g \leq 1$). The more the particles scatter in the forward direction, the higher the asymmetry factor. Particles with *isotropic* scattering properties have an asymmetry factor equal to zero ($g = 0$).

Radiative forcing — RF: The perturbation to the energy balance of the Earth-atmosphere system following, for example, a change in the concentration of greenhouse gases; changes in aerosols or a change in the output of the sun. The magnitude of the RF can be obtained by calculating the difference between the net — downward minus upward — radiative flux at a particular level in the atmosphere and is measured in [W m^{-2}], i.e. heat per area of the Earth's surface. A positive RF implies a warming of the surface; a negative RF implies a cooling of the surface.

Radiative Forcing efficiency — RFE: The aerosol radiative forcing efficiency is defined as the rate at which the irradiance at a certain wavelength range is "forced" (changing) per unit of aerosol optical thickness.

1.2.2 Aerosols in the atmosphere

Physical and chemical properties

An aerosol is a distribution of solid or liquid particles of varying physical size and chemical composition suspended in the air. Aerosol particles can originate from a variety of sources, e.g. biomass burning, pollution from power plants, sea salt from oceans, dust that has been lifted into the atmosphere (Magi, 2006). Most aerosol particles occur in the lowest 5 km of the atmosphere, with lifetime ranging from a few days to weeks — short compared with the decades long lifetimes of greenhouse gases such as carbon dioxide.

The aerosol chemical composition is dependent on the particle source and there are significant variations from one region to another. Common chemical compositions of aerosols are ionic species like sulphate (SO_4^{2-}) and various carbonaceous mixtures, often broadly classified as organic carbon (OC) and black carbon (BC). Biomass burning emissions, a major source of aerosols in southern Africa, are dominated by a range of carbonaceous particles, including organic carbon (OC) and black carbon (BC) particles. Smaller contributions comprise inorganic particles like sulphates (Magi, 2006). Aerosol chemical composition also changes over time as the aerosols originating from the various sources interact. The changes are also dependent on their mixing state, i.e. externally or internally mixed.

Aerosols are important to the Earth system because they play a fundamental role in the cloud formation process and interact with the climate system in two important ways. First, they scatter and absorb radiation in the atmosphere; second, they change the microphysical structure (and possibly the lifetime and extent of clouds) within the atmosphere. Aerosol scattering and absorption depend strongly on particle size and therefore will change relative to the aerosol size distribution (Van de Hulst, 1981).

Size distribution

Aerosols cover a wide range in size, from ~1 nm (0.001 μm) to 1 mm (1000 μm) diameter, but frequently are grouped in different size modes that are linked to the particle age and source (Raes *et al*., 1995). Three size modes are commonly defined: the nucleation mode (with particle diameter (D_p) less than 0.1 μm); the accumulation mode (with D_p between 0.1 to 1 μm) and the coarse mode (with D_p greater than 1 μm). Nucleation mode particles are generally produced by the chemical conversion of gaseous precursors into liquid or solid products (gas-to-particle conversion). Accumulation mode particles are formed mainly by combustion processes, including biofuel or biomass burning, and these particles have much greater impact on visible radiation. Coarse particles are derived from the break-up and suspension of bulk material by wind or mechanical forces, producing soil dust and sea salt aerosols.

Particle size is the most important parameter for characterising the physical properties of aerosols. The amount of light scattered from a particle is an extremely sensitive indicator of particle size and forms the basis for several types of aerosol measuring instruments (Hinds, 1982). The accumulation mode (fine fraction) aerosols are the most important in terms of radiative forcing. Because of their size, they have low impaction efficiencies, and low sedimentation velocities (unlike coarse particles). They can, therefore, be transported long distances and also be taken up to altitudes where the particles are able to interact with clouds (Raes *et al*., 1995).

An aerosol size distribution gives the relative concentrations (probability distribution) of aerosol particles present in the atmosphere, sorted according to size. This is often described mathematically using a lognormal distribution function, because it was observed experimentally that most aerosol size distributions exhibit a skewed distribution function (long tail at large sizes) that do not fit a normal distribution pattern (Reist, 1993; Hinds,

1982). Figure 1.1 shows typical shapes of the normal distribution function (left panel) and of the lognormal distribution function (right panel).

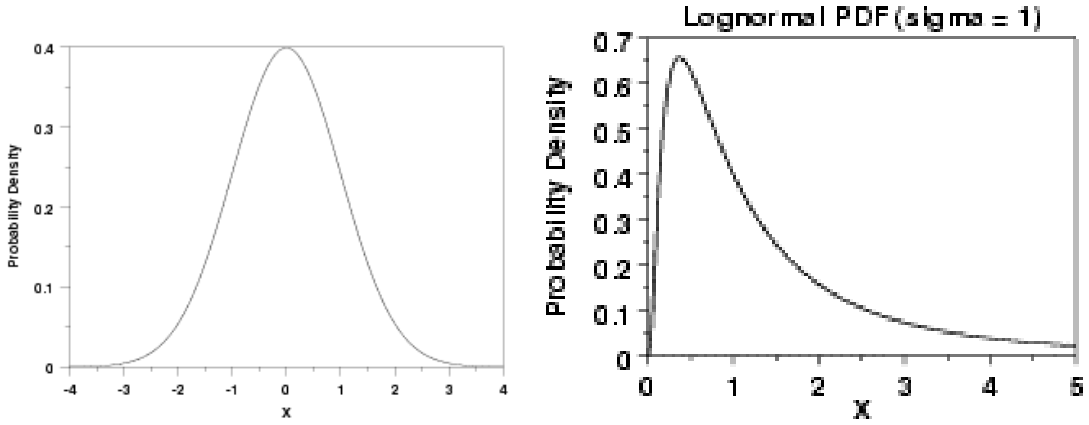

Figure 1-1 Typical shapes of normal distribution function, also known as a Gaussian distribution or bell curve (left panel) and lognormal distribution function, characterised by long tail at large variables (right panel).

Since Junge (1955) proposed the existence of a continuous atmospheric aerosol size distribution, more sophisticated models have been developed that describe the aerosol size distribution by a lognormal distribution (Harrison & Van Grieken, 1998):

$$\frac{dN}{d\ln r} = \frac{N_0}{\sqrt{2\pi}\ln\sigma_g}\exp\left[-\frac{1}{2}\frac{\ln\left(\frac{r}{r_m}\right)}{\ln\sigma_g}\right]^2 \qquad (1.1)$$

where *dN/dlnr* is the number size distribution (number of particles per volume and logarithmic diameter interval *dlnr*) in m^{-3}; N_0 is the total aerosol number concentration; $\ln\sigma_g$ is the geometric standard deviation of *lnr*; *r* the radius of the particle and r_m the median number radius. For spherical particles with density ρ the volume size and mass distributions can be obtained by:

$$\frac{dV}{d\ln r} = \frac{4\pi}{3}r^3\left(\frac{dN}{d\ln r}\right) \qquad (1.2)$$

and

$$\frac{dM}{d\ln r} = \frac{4\pi}{3}r^3\rho\left(\frac{dN}{d\ln r}\right) \qquad (1.3)$$

where *dV/dlnr* is the volume size distribution (volume of particles in unit area and logarithmic diameter interval *dlnr*) in [$\mu m^3\ \mu m^{-}2$] and *dM/dlnr* is the mass size distribution (mass of particles per volume) in [$g\ m^{-3}$].

For determining the columnar aerosol size distribution from extinction measurements, an inversion algorithm is required (King *et al*., 1978; Dubovik & King, 2000). It should be emphasised that the aerosol properties are themselves important since they have a significant impact on climate variations through their potential to scatter and absorb incoming solar radiation. The role of aerosols in climate forcing will be discussed in the next section.

1.2.3 Aerosols and climate

After a period of focusing almost exclusively on greenhouse gas enhancement (as the principal cause of climate change), it has become clear (on the basis of numerical climate modelling) that atmospheric aerosols contribute substantially to global annual air surface temperature variability, with an important role being played by aerosols of both natural and anthropogenic origin (Kondratyev, 1999).

Aerosols modify the Earth-atmosphere energy budget through various atmospheric processes, including the direct effect — the scattering and absorption of solar and Earth radiation (Charlson *et al*., 1992); the semi-direct effect — changing atmospheric thermodynamics and cloud formation (Koren *et al*., 2004); and the indirect effect — changing cloud microphysics (Rosenfeld & Lensky, 1998). The addition of anthropogenic aerosols to the atmosphere may change the radiative fluxes at the top-of-atmosphere (TOA), at the bottom-of-atmosphere (BOA) and within the atmospheric column and thereby perturb a whole regional climate system.

The impact of aerosols to the Earth's radiation budget is a major component of global and regional climatic patterns, influencing processes in the troposphere (Yu *et al*., 2002); the hydrological cycle (Ramanathan *et al*., 2001) and surface temperatures all over the globe. Uncertainties remain substantial for the direct and for the indirect effect (IPCC, 2007). However it is important to recognise that, since the Second Assessment Report of the Intergovernmental Panel on Climate Change (IPCC, 1995), significant progress has been made in improved characterisation of the radiative roles of different types of aerosols in different environments and regions.

Several intensive field experiments have been conducted in recent years in a variety of aerosol regimes around the globe (Table 1.1). During each of these comprehensive missions, aerosols were studied in great detail, using combinations of in-situ and remote sensing observations from various platforms, including aircraft, ships, satellites and ground-networks (Seinfeld *et al*., 2004). In spite of their relatively short duration, these missions acquired comprehensive data sets of regional aerosol properties, leading to the better understanding of the complex interactions of aerosols within the Earth-atmosphere system (Yu *et al*., 2006) (Table 1.1).

Aerosol radiative forcing

Current interest in atmospheric aerosols derives in part from the assessment conducted by the Intergovernmental Panel on Climate Change (IPCC) of the potential importance of radiative forcing of climate by tropospheric aerosols (IPCC, 1995).

The impact of aerosols on the Earth´s energy budget can be quantified in terms of aerosol radiative forcing (ARF). ARF is defined as the difference between atmospheric radiative fluxes when aerosols are present and when they are absent (Vogelmann *et al*., 2003). The total ARF can be broken down into the direct effect (actual interactions of the aerosols with radiation) and the indirect effect (aerosol induced changes in the radiative properties of clouds). For the purpose of this study, the direct effect will be the core focus for analysis.

Table 1-1 List of major intensive field experiments that are relevant to aerosol research in a variety of aerosol regimes around the globe conducted in the past decade.

Aerosols Regimes	Intensive Field Experiments		
	Name	**Location**	Time
Industrial Pollution from North America and West Europe	TARFOX	North Atlantic	July, 1996
	NEAQS	North Atlantic	July–August, 2002
	SCAR-A	North America	1993
	CLAMS	East Coast of U.S.	July–August, 2001
	INTEX-NA, ICARTT	North America	Summer 2004
	ACE-2	North Atlantic	June–July, 1997
	MINOS	Mediterranean region	July–August, 2001
	LACE98	Lindberg, Germany	July–August, 1998
	Aerosols99	Atlantic	Jan–Feb, 1999

Aerosols Regimes	Intensive Field Experiments		
	Name	**Location**	Time
Brown Haze in South Asia	INDOEX	Indian subcontinent and Indian Ocean	January–April, 1998 and 1999
	ABC	South and East Asia	March-April, 2005
Pollution and dust mixture in East Asia	ACE-Asia	East Asia and Northwest Pacific	April, 2001
	TRACE-P	East Asia and Northwest Pacific	March–April, 2001
	PEM-West A & B	Western Pacific off East Asia	Sep–Oct, 1991 Feb–Mar, 1994
Biomass burning smoke in the tropics	BASE-A	Brazil	1989
	SCAR-B	Brazil	Aug–Sep, 1995
	LBA-SMOCC	Amazon basin	Sep–Nov 2002
	SAFARI2000	Southern Africa Region	Aug–Sep, 2000
	SAFARI92	South Atlantic and South Africa	Sep–Oct, 1992
	TRACE-A	South Atlantic	Sep-Oct, 1992
Mineral dusts from North Africa and Arabian Peninsula	SHADE	West coast of North Africa	September, 2000
	PRIDE	Puerto Rico	June–July, 2000
	UAE[2]	Arabian Peninsula	Aug-Sep, 2004
Remote Oceanic Aerosol	ACE-1	Southern Oceans	December, 1995

(Adapted from Yu *et al.*, 2006)

From a modelling perspective, direct radiative forcing (DRF) by aerosols can be calculated, at least in principle, once the optical constants, size distribution and atmospheric concentration of the aerosol are known (Lacis & Mishchenko, 1994).

An expression for global average aerosol direct forcing, that takes into account both scattering and absorption, is:

$$\Delta F = -\tfrac{1}{2} F_0 T^2 (1 - A_c) \tau \bar{\beta} \omega \left\{ (1-R)^2 - 2R(1-\omega)/\bar{\beta}\omega \right\} \quad (1.4)$$

where ΔF is the change in outgoing shortwave flux at the TOA; F_0 is the incoming solar flux at the TOA; T is the transmittance of the atmosphere above the aerosol layer; Ac is the fractional cloudiness, τ is mean aerosol optical depth; $\bar{\beta}$ is the mean up-scatter fraction

(fraction of radiation scattered into the upward hemisphere); ω is the single scattering albedo, and R is the surface reflectance. (Charlson *et al.*, 1992; Haywood & Shine, 1995)

The IPCC 1995 assigns a low confidence to the estimate of direct aerosol forcing and a very low confidence to the estimate of the indirect effect. The low confidence in the estimates of DRF is caused by the highly non-uniform compositional, spatial and temporal distribution of tropospheric aerosols, on the global scale, because of their heterogeneous sources and short lifetime. Therefore, it is crucial to establish a sound observational basis for estimating the magnitude of the aerosol optical parameters that are the key parameters for the DRF calculations.

The magnitude of DRF also can be obtained by a combination of observations and models. This is achieved by subtracting the energy budget in clean conditions (no aerosols) and loaded conditions (with the presence of aerosols).

$$\Delta F = F_{clearsky} - F_{loaded} \qquad (1.5)$$

where $F_{clearsky}$ denotes the radiation flux obtained under clear sky conditions and F_{loaded} is the radiation flux for a given aerosol state in the atmosphere. The equation (1.5) can be applied at the TOA or BOA.

The interpretation of the direct aerosol forcing cannot be explained by measurements alone because the instrumentation being used has limitations in that one measurement will only be able to represent one condition (either clean or loaded atmosphere). The results of both a clean and a loaded atmosphere cannot be combined in one measurement. Furthermore, the 'clean' atmosphere is hypothetical; therefore to simulate the clean atmosphere, a model is used and the assumption is made that no aerosols are present. Large uncertainties exist in the current estimates of aerosol forcing because of the incomplete knowledge of both the distribution and physical and chemical properties of aerosols. This study will also contribute to improved understanding of the aerosol optical properties within southern Africa.

Aerosol optical properties

The complex interaction of aerosols with radiation is usually defined using three main optical parameters: aerosol optical thickness (AOT, τ); the single-scattering albedo (SSA, ω_0) and the phase function P(θ). AOT measures the magnitude of solar radiation extinction by aerosols, integrated in the vertical column (through either scattering or absorption).

AOT levels vary with the wavelength of radiation; the wavelength-dependence of the aerosol optical thickness is usually represented by the Ångström exponent parameter (Ångström, 1929, 1930), which is an indirect measure of aerosol particle size. High values of Ångström exponent (α) are indicative of small particles and low values are representative of large particles.

Single-scattering albedo (SSA or ω_0) is the ratio of the scattering coefficient to the extinction coefficient, measuring the relative importance of scattering and absorption (Yu *et al*., 2006). The chemical composition of aerosols will determine the ability of particles to scatter or absorb solar radiation and this can be seen in the SSA spectral trend. At visible wavelengths, the SSA decreases with wavelength for non-dust aerosols and increases for dust aerosols (Dubovik *et al*., 2002).

The angular distribution of scattering radiation is described by the phase function, i.e. a ratio of the scattered intensity (at a specific direction) to the integral of the scattered intensity (in all directions). In principle, given the size distribution of an assumed spherical aerosol, the phase function can be calculated from the Mie theory (van de Hulst, 1981; Bohren & Huffman, 1983). In practice, approximations, such as the Henyey-Greenstein (HG) phase function (Henyey & Greenstein, 1941) have been used in most radiative transfer models (Fu & Liou, 1993). The HG phase function is defined in terms of a single parameter - the asymmetry factor (g); with g=1 for completely forward scattering and g=0 for symmetric scattering. Typical values of g range from 0.5 to 0.8. The asymmetry factor *g* decreases with wavelength because of the decrease in the scattering-effective particle size (Hansen & Travis, 1974).

Aerosol optical properties also depend strongly on the *size distribution* (relative concentrations of aerosol particles sorted according to size). Therefore, any factors affecting the size distribution will affect the aerosol optical properties. One critical factor is the relative humidity (RH). Some aerosol types are hygroscopic, meaning that they grow as they take up water vapour. As a result, as their size increases, their refractive indices change, in turn leading to changes in their optical properties. The aerosol optical properties also depend on aerosol composition as that impacts refractive index, especially when absorbing material is present. In contrast to greenhouse gases, aerosol loading and optical properties exhibit large spatial and temporal variability. Because of the variability in sources and sinks, different aerosol components are associated with different geographical

areas, and the residence time in the troposphere is relatively short (about 1 week). The vertical distribution of aerosols varies substantially; this variable distribution is determined by the injection height and a variety of atmospheric processes. Such variations complicate the calculations of estimated aerosol direct effect in cloudy skies and in the thermal infrared region.

1.2.4 Solar radiation measurement

Atmospheric circulation is driven by radiation and energy fluxes. Determining the solar radiation and its interaction with the atmosphere and the Earth's surface is important since solar radiation accounts for almost all the energy available to the Earth. There are two ways solar radiation reaches the Earth's surface. The first is direct solar radiation - i.e. where the solar radiation is directly transmitted through the atmosphere. The second is via diffuse solar radiation where the incoming solar radiation is scattered or reflected to the Earth's surface. There are several instruments (generally called radiometers) for measuring solar radiation.

Radiometers

Radiometers are used for quantifying solar and terrestrial radiation. For this research, the most commonly used were *pyranometers*, *pyrheliometers* and *pyrgeometers*. In addition to these, a more sophisticated sun/sky spectral radiometers was used, namely the CIMEL™ Sun Photometers.

Pyranometers or Precision Spectral Pyranometers (PSPs) are radiometers designed to measure the broad band solar radiation, on a plane surface, resulting from radiant fluxes in the wavelength range from 0.3 to 3 μm. Pyranometers measure the total radiation or sum of the direct and diffuse solar radiation arriving from the whole hemisphere (usually across a complete arc of the sky) (Plate 1.1). The instrument sensor converts the radiant energy to heat energy, which, in turn, is measured by a thermopile as voltage.

The Pyrheliometer or Normal Incidence Pyrheliometer (NIP) is used for measurement of the broadband direct solar radiation from 0.2 to 4.0 μm, i.e. solar radiation that passes directly though the atmosphere from the sun without being scattered or absorbed by the atmosphere. Typically, it is measured on a surface that is kept normal to the direction of the centre of the sun's disk. That surface is held normal to the sun's position by a solar tracker.

The Pyrgeometer or Precision Infrared Pyranometer (PIR) is used for the measurement of the broadband infrared radiation. The PIR is sensitive to radiation between 4 and 50 μm. It constitutes a thermopile sensor (covered by a silicon dome) internally coated with an interference filter with a transmission range of approximately 3.5 to 50 μm (Plate 1.2).

Plate 1-1 Precision Spectral Pyranometer (PSP) showing the dome (external glass) and the case (internal glass) covering the sensor.

Plate 1-2 Precision Infrared Pyranometer (PIR), manufactured by Eppley Laboratories.

Calibration of short wave radiometers

The calibration of shortwave radiometers should be done in compliance with the World Radiation Reference (WRR). In the field two procedures should be followed to check for constancy of instrument sensitivity. One method is by comparing an accurately calibrated pyranometer alongside the field instruments (at least once a year and ideally under cloudless conditions). A linear regression can be used to determine the calibration coefficients. Another method is to repeat the basic radiometric calibrations by using a pyrheliometer or a thermopile-type derived standard (Iqbal, 1983). The calibration factor is the ratio of the measurement from the test pyranometer to the measurement from the reference pyranometer. Good calibration of the precision spectral pyranometers will usually reproduce the WRR to within ± 1%.

Sun sky spectral radiometers

Sun sky spectral radiometers measure the spectral sky radiances at selected wavelengths. Widely used instruments for aerosol studies are the CIMEL™ Sun Photometers, manufactured in France. This automatic scan radiometer takes only two basic measurements, direct Sun radiation and sky radiation, each measured within several programmed sequences. The direct solar radiation measurements are taken in eight spectral bands (in the standard wavelengths 340, 380, 440, 500, 670, 870, 940 and 1020 nm). Sky measurements are performed at 440 nm, 670 nm, 870 nm, and 1020 nm. These measurements are used to compute aerosol optical thickness $\tau_a(\lambda)$ at each wavelength, with the exception of the 940 nm channel, which is used to calculate precipitable water (PW) in cm.

The CIMEL™ Sun Photometers are the instruments widely used by AERONET network (Holben *et al*., 1998). The calibration of CIMEL™ direct sun measurements is performed by a transfer of calibration from reference CIMEL™ instrument; for sun sky measurements, calibration is performed by comparison with a reference integrating sphere at the NASA Goddard Calibration Facility. Typically, the total uncertainty in spectral aerosol optical depth for CIMEL™ field instruments ranges from 0.01 to 0.02 under cloud-free conditions for air mass equal one (Eck *et al*., 1999). For the sky radiance measurements, the accuracy is of ±5% or better (Holben *et al*., 1998).

Data Acquisition System

The process of measuring the solar radiation requires a data acquisition system, to record the parameters gathered by a sensor that converts the information into electrical signals. The signals from the sensors are transferred (by wire, optical fibre or wireless links) to an instrument which conditions, amplifies, measures, scales, processes, displays and stores the sensor signals - the data acquisition instrument.

Data acquisition can be divided into two broad classifications – real time data acquisition and data logging. Real time data acquisition is when data acquired from sensors is used either immediately or within a short period, such as in process control. Data logging is where data acquired from sensors are stored for later use. In this study, data logging was used.

Data Loggers

A data logger is an electronic instrument that records measurements, such as temperature, relative humidity, light intensity, over time. Typically, data loggers are small, battery-powered devices that are equipped with a microprocessor, data storage and sensor. Most data loggers utilise turnkey software on a personal computer to initiate the logger and for reviewing the collected data.

Selection of an appropriate data logger depends mainly on the type, number, precision, and speed of measurements. During SAFARI 2000 field experiment, the solar measurements, a CR7 data logger from Campbell Scientific was used *(http://www.campbellsci.com)*. The CR7 is suitable for applications that require high resolution or a large number of input channels (Plate 1.3).

Plate 1-3 The CR7 data logger used during solar radiation measurements at Skukuza site during SAFARI 2000 field experiment (September 2000).

Total Sky Imager

The Total Sky Imager (TSI) is a full-colour digital imaging and software system designed to automatically monitor cloud conditions at any site. The TSI uses an advanced charge-coupled device (CCD) to take pictures of the sky at user-defined intervals during day time conditions. The TSI Manager software, a JAVA application running on a host computer, captures and analyses the images, providing fractional cloud cover data in nearly real time. Unlike remote-sensing satellite photos, with coarse spatial resolution (~1 km), TSI images are in 24-bit colour with much higher spatial resolution.

The TSI Model 440 (Plate 1.4) basic components include an imager, an automatically rotating hemispherical mirror (with strip of protective tape on the mirror to prevent reflected sunlight from damaging the imager optics). The TSI imager looks downward onto the hemispherical mirror. The 'shadowband' on the mirror is positioned by an ephemeris calculation that tracks the sun for any time and location on the Earth, and prevents direct sunlight from saturating the imager and damaging the CCD. The TSI Model 440 is manufactured by Yankee Environmental Systems from USA *(http://www.yesinc.com)*.

An Ethernet port on the TSI connects to a local PC or network computer running the TSI image capture and processing software. The capture tool samples the TSI output images at user-defined intervals and stores them in industry-standard JPEG image format, 288 X 352 pixel resolution, 24-bit colour on the host computer. The image processing tool then

applies a sophisticated filtering algorithm to the raw images to distinguish clouds from clear sky. Processed images are stored in Portable Network Graphic (PNG) format. Cloud cover results are stored in ASCII reports, organised by date. The sampling rate interval is variable, with maximum of one image every 10 seconds.

Plate 1-4 Total Sky Imager (in the mounted position) at Goddard site (January 2004).

1.2.5 Aerosol research in Southern Africa

Two major field campaigns were conducted over southern Africa region in the period 1999 - 2001. SAFARI 2000 was conducted in three different periods: August – September 1999, February – March 2000 and August – September 2000. This experiment was a joint initiative between southern African countries and the National Aeronautic and Space Administration (NASA). As result of this experiment, a huge data set is available; including ground-based remote sensing measurements, in-situ measurements and satellite observations (Swap *et al*. 2003).

The second field campaign was the Aerosol Recirculation and Rainfall Experiment (ARREX), which was conducted in January 1999 (mid-wet season) and March/April 2001 (late wet season). ARREX was designated to investigate the long-range transport of aerosols and trace gases over southern Africa and the effects of industrially derived aerosols on rainfall-producing systems (Piketh *et al*., 1999).

Taken during these experiments, and of particular interest to this study, are the ground based sun photometer measurements that form part of the aerosol robotic network

(AERONET), alongside data on solar radiation fluxes measured using a set of ground based radiometers.

SAFARI 2000 has contributed significantly to the regional scale aerosol mapping and current studies on aerosol radiative effects. Detailed scientific results arising from SAFARI 2000 were published in a special issue of the Journal of Geophysical Research (Swap *et al*., 2003). The most important results under review in this study are the aerosol characterisations, including the physical and chemical aerosol parameters in southern Africa or, more precisely, in selected sites representing the region.

Aerosol types and their vertical distribution

The aerosol types in southern Africa predominately include smoke, dust, industrial pollution and sea salt particles. During the dry season period, from August to October, the predominant aerosol type over the region is smoke, generated from biomass burning on land and transported over the adjacent southern Atlantic and Indian Oceans (Ichoku *et al*., 2003; Eck *et al*., 2003; Haywood *et al*., 2003). It also became clear, from the SAFARI 2000 results, that the eastern seaboard (consisting of southern Mozambique and Kwazulu-Natal, South Africa) is the main atmospheric exit corridor for continental air masses (Stein *et al*., 2003).

Prior to SAFARI 2000 it was also noted that subsidence from anti-cyclonic circulation is a dominant feature during much of year, with four stable vertical layers identified in the troposphere (Garstang *et al*., 1996; Cosijn & Tyson, 1996). The two layers most important in controlling aerosol vertical and horizontal transport occurred at 1.5 km and the (very persistent layer) at 3.5 km above the surface. Additional to these earlier findings is a previously unreported phenomenon in the vertical structure. Hobbs (2003) documented thin regions of very clean air (clean slots), separating polluted air above and below, all within the depth of the planetary boundary layer.

The abovementioned information is of paramount importance in studying the direct aerosol radiative effects, because the radiative forcing of aerosols depends not only on the type of aerosols but also on how they are distributed vertically in the atmosphere.

Aerosol optical thicknesses in southern Africa

Emerging from SAFARI 2000, the aerosol optical parameters in the region (aerosol optical thickness, size distribution, single scattering albedo and the phase function), were retrieved

from ground based and in-situ measurements. The definitions of all these parameters are given early in the section on the literature review.

In general, for southern Africa, the average aerosol optical thickness (AOT) at 500 nm is approximately 0.24. This value is an indication of the average amount of aerosols in the region. Values higher than 0.24 can be observed north of Zambia, while values less than 0.24, are often registered at Bethlehem, in the southern region of South Africa. The magnitude of AOT decreases from north to south, following the north-south gradient in the regional precipitation (Eck *et al.*, 2003; Queface *et al.*, 2003; Barenbrug, 2003; Eck *et al.*, 2001). However, this study demonstrates that this north-south gradient is only valid for a specific period of the year and the variability of the gradient will be discussed in Chapter 3.

One of the atmospheric features that drew particular attention during SAFARI 2000 was the widespread haze exiting off shore towards the Indian Ocean. This phenomenon was named the River of Smoke (Annegarn *et al*., 2002). A massive thick plume of smoke was advected from central Zambia, southeast over southern Africa, exiting the subcontinent over Inhaca Island, Mozambique (Eck *et al*., 2003; Schmid *et al*., 2003).

The abovementioned features of aerosol optical thickness, and their seasonal variability in southern Africa, may significantly affect the radiation budget of this region and hence the regional climate.

Ångström exponent and size distribution

The attenuation of solar radiation by aerosols particles is strongly dependent on particle size. The size of particles suspended in the atmosphere may cover a broad range of sizes; in practice there are two ways of estimating the particle sizes from sun photometer measurements. The first (easy but less precise) is to compute the so-called Ångström exponent from the aerosol optical thickness spectral dependence; this parameter gives an overall idea of the size of particles dominating over certain locations, i.e. whether fine or coarse. In this method it is important to consider the wavelength pair used to calculate the Angstrom exponent when making qualitative assessments about the corresponding aerosol size distributions. Angstrom exponents calculated from longer wavelength pairs (λ = 670, 870 μm) are sensitive to the fine mode fraction of aerosols; conversely, shorter wavelength pairs (λ = 380, 440 μm) are sensitive to the coarse mode fraction (Eck *et al*. 1999). The second way is more complicated but, with more information related to the number of particles within certain size interval, the estimate is obtained by using an algorithm for size

distribution retrieval (as reported in Dubovik & King, 2000). In practical applications, the Ångström exponent can be calculated from the spectral values of the AOT according to the following equation.

$$\alpha = -\frac{d \ln \tau_a}{d \ln \lambda} = -\frac{\ln\left(\frac{\tau_{a_2}}{\tau_{a_1}}\right)}{\ln\left(\frac{\lambda_2}{\lambda_1}\right)} \qquad (1.6)$$

where λ is the wavelength in microns of the corresponding aerosol optical thickness (τ_a

The Ångström exponent ($\alpha_{440-870}$), as observed at various sites during SAFARI 2000 (the experiment was widespread across southern Africa; from Zambia to the southern part of South Africa; from Mozambique in the East to Namibia in the West), exhibited significant regional variability. This showed that the tropospheric aerosol loading had a diverse number of contributing sources. High values of Ångström exponent (~2) are frequently observed in northern Zambia throughout the year; an indication of the strong influence of fine particles from biomass burning (Holben *et al*., 2001). Relatively low values are observed at Skukuza, South Africa and Inhaca Island, Mozambique, possibly because of the influences of aeolian dust and sea salt aerosols (Eck *et al*., 2003). The southernmost Safari 2000 site (Bethlehem in South Africa) displayed values well above those observed at Inhaca, Mozambique, but less than those recorded at Mongu, Zambia. Bethlehem is more likely to be influenced by mixed dust/industrial aerosols because of its locality and the higher concentration of human activity.

The retrieved aerosol size distribution, from ground-based and in-situ measurements from selected sites in southern Africa, clearly shows the presence of both fine and coarse mode aerosols. In many cases, especially during the biomass-burning season, the submicron fraction dominates all over the region (Haywood *et al*., 2003). Under the submicron fraction (where the particles are more optically active) it has been noted that biomass burning aerosols tend to have a larger median diameter (up to 0.19 μm compared to 0.11 μm of the industrial aerosols) (Ross *et al*., 2003).

The overall assessment of aerosol particle size in the southern African subcontinent shows a wide range of particles sizes. However, it is important to note the particles in the fine mode fraction have a peak radius at approximately 0.1 μm; in the coarser fraction the peak

radius is around 5 µm (Eck *et al*., 2003). During the non-biomass burning season the ratio of fine to coarse mode is well balanced, with fine particles representing approximately 50% of the total volume size distribution. This proportional representation is noticeably unbalanced during the biomass burning season when the fine fraction may represent double the volume size distribution of the coarse fraction.

Single scattering albedo (SSA)

The type of direct forcing that aerosols can cause in the atmosphere, whether it is positive (warming) or negative (cooling), is strongly related to their chemical composition. The chemical composition of aerosols will determine the ability of particles to scatter or absorb solar radiation. Under the radiative transfer calculations this ability is given by the single scattering albedo (SSA) parameter. The computation of the SSA is very sensitive to the complex refractive indices of the particles (difficult to determine in a mixture of particles) therefore the SSA computations will include a relatively high degree of uncertainty. The error estimates of SSA from AERONET retrievals range between 0.01 – 0.03 (Dubovik *et al*., 2000).

The main feature of SSA in southern Africa is the decreasing of single scattering albedo with wavelength, characteristic of the absorption by small black carbon particles (Bergstrom *et al.,* 2003). Black carbon is a result of the combustion processes that take place from diverse activities in the region, including burning of fossil fuels for power generation, wild fires and burning of coal/wood for domestic purposes. These activities appear to be the main sources of fine particles in the region.

Dubovik *et al*. (2002) in their analysis of the single scattering albedo from biomass burning aerosol over African savanna determined a mean value of the SSA as 0.90 ± 0.03. Recent studies, based on long term measurements observations with AERONET sun photometers, suggest that lower SSA values of 0.88 and 0.84 at 440 nm and 670 nm wavelengths respectively would be more applicable to southern Africa (Eck *et al.*, 2003; Ichoku *et al.*, 2003; Magi *et al.*, 2003).

It was noted that small variations of SSA can occur within the region because of aerosol aging during transport and from the contributions made by other aerosol sources, i.e. Aeolian dust, fossil fuel combustion aerosols, etc. The observed regional differences in aerosol SSA need to be considered when assessing regional aerosol radiative forcing

(Haywood *et al*., 2003). Therefore, in this study, a more detailed analysis by sub-regions will be given in Chapter 3.

Direct aerosol forcing during SAFARI 2000

From a regional climate perspective, the overall analysis of direct aerosol radiative forcing and the aerosol optical properties is the aim of this thesis, and individual aerosol events analysis are intermediate objectives. Direct aerosol radiative forcing calculations in southern Africa are rare (only a few case studies) and limited in spatial coverage. The effect of aerosols on solar radiation can be separated into two stages: the aerosol direct forcing at the top of atmosphere (TOA) and at bottom of atmosphere (BOA). Satellites are deemed suitable for deriving aerosol forcing at the TOA; ground-based solar measurements are better applied for discerning the BOA aerosol forcing.

Estimates of the direct aerosol forcing during SAFARI 2000 revealed that, during the high levels of aerosol optical thickness, both a strong BOA and TOA aerosol forcing were created. For instance, Bergstrom *et al*. (2003) computed the direct radiative effects of aerosols on two different and contrasting days: 24 August (low AOT day) and 6 September (high AOT day). The TOA direct aerosol forcing were -13 W m^{-2} and -17 W m^{-2}, respectively and the surface (BOA) direct aerosol forcing was -57 W m^{-2} and -200 W m^{-2}, respectively (Bergstrom *et al*., 2003; Keil & Haywood, 2003). Ichoku *et al*. (2003), used aerosol information from the MODIS instrument as input to calculate direct aerosol radiative forcing over the southern Atlantic Ocean for September 2000; the results showed a forcing of -10 W m^{-2} at the TOA and -26 W m^{-2} at the BOA.

1.2.6 AERONET radiative transfer module description

A new radiative transfer module has been integrated into operational AERONET inversion code. This module uses the detailed size distribution, complex refractive index and fraction of spherical particles retrieved by AERONET (Dubovik & King, 2000, Dubovik *et al*. 2006) and provides the fluxes and aerosol radiative forcing values as part of AERONET operational product (Garcia *et al*., 2008).

The AERONET computations of solar fluxes account for the absorption and multiple scattering effects using the Discrete Ordinates DISORT approach (Stamnes *et al*., 1988). The solar broadband fluxes are calculated by spectral integration from 0.2 to 4.0 μm, using more than 200 size sub-intervals. In each of these sub-intervals the extinction, single

scattering albedo and phase function are calculated using the retrieved size distribution in the exact same manner as in the AERONET retrieval scheme (Dubovik *et al*. 2006, Garcia *et al*., 2008).

The integration of atmospheric aerosol scattering and absorption, gaseous absorption, molecular scattering and underlying surface reflection effects are conducted using developments employed in the GAME (Global Atmospheric ModEl) code. In the GAME code, gaseous absorption (mainly H_2O, CO_2 and O_3), is calculated from the correlated k-distribution (Garcia *et al*., 2008). The correlated k-distribution allows for the interactions between gaseous absorption and multiple scattering to be accounted for with manageable computational time. Coefficients of the correlated k-distribution were estimated from reference calculations using a line-by line code (Dubuisson *et al*., 2004). Regarding the gaseous content in the atmospheric column, the GAME model accounts for spectral gaseous absorption: ozone in the ultraviolet-visible spectral range (0.2-0.35 μm and 0.5-0.7 μm) and water vapour in the shortwave infrared spectrum (0.8-3 μm). The instantaneous water vapour content retrieved by AERONET (Smirnov *et al*. 2000) is employed, while the total ozone content is taken from monthly climatology values (1978-2004) based on the NASA Total Ozone Mapping Spectrometer (TOMS) measurements (http://ozoneaq.gsfc.nasa.gov/). The atmospheric gaseous profile, US standard 1976 atmosphere model, was scaled to match with the gaseous concentrations in column. The GAME code has a fixed spectral resolution of 100 cm^{-1} from 2500 to 17700 cm^{-1} (4 to 0.6 μm) and 400 cm^{-1} from 17700 cm^{-1} to 50000 cm^{-1} (0.6 to 0.2 μm).

The AERONET module results (specifically the broadband flux estimates), which allow the computation of direct aerosol forcing, have been validated in recent works by using ground-based solar measurements from global networks and during intensive field campaigns. As a result, AERONET solar fluxes estimates agree with solar fluxes observations within 10% or better (García *et al*., 2008). In global terms, a small overestimation of +9±12 W m^{-2} is found on the observed solar radiation at surface, which means a relative error of +2.1±3.0% (García *et al*., 2008).

Moving on, from simply investigating case studies, to the regional integration of the aerosol optical properties and the regional direct aerosol forcing represents the main challenge of this research.

1.3 Research aim and objectives

The main aim of this research is to study the direct radiative forcing of aerosols and the aerosol optical properties of southern Africa. Of particular interest is to estimate the variations of aerosol direct forcing attributed to changes in aerosol loadings over the atmosphere of this region.

During this study the following questions are posed:

1. What are the aerosol optical properties (AOP) over southern Africa?
2. How do these AOP change within different seasons (including identifying the likelihood of long-term trends)?
3. What are the main characteristics of AOP in southern Africa that differ from other environments?
4. What are the magnitudes of daily and seasonal direct aerosol radiative forcing (ARF) at bottom of atmosphere and top of atmosphere over southern Africa?
5. How does the change of aerosol amounts in tropospheric column influence the change of direct ARF at bottom of atmosphere and at top of atmosphere?
6. What is the likely regional magnitude of direct radiative forcing of aerosols for southern Africa?

****

Key definitions of aerosol optical parameters, the physical and chemical properties of aerosols, have been outlined. The role of aerosols in the Earth´s climate system and their impacts were discussed in this chapter. The aerosol and solar measurements instruments and retrieval process were described. The progress on aerosol studies worldwide and within the southern Africa region was also outlined. Data and methodology used are discussed in Chapter 2.

Chapter 2.

Chapter 2 outlines the study area, measurement sites, data used, their sources and methods used for analysis. The chapter explains the data sets and methodologies used to compile the climatology of aerosol optical properties in southern Africa; the identification of clear sky conditions; air mass transport analysis and the direct aerosol radiative forcing analysis from the AERONET radiative transfer model outputs.

2 Data and Methodology

2.1 Study area and selected sites

The study area being considered is the southern African region bounded by latitudes 6° - 30°S and longitudes 5° - 45°E. For this research, the area was subdivided into two sub-regions - the tropical (6° - 18°S) and subtropical (18° - 30°S). Each sub-region is represented by one measurement site - Mongu in Zambia (15º 15' S; 23º 09' E; elev. 1107 m) and Skukuza in South Africa (24º 59' S; 31º 35' E; elev. 150 m) (Figure 2.1). The selection of these sites was based on their geographical location and the availability of long time series i.e. at least five years of continuous measurements, of aerosol optical parameters in southern Africa, coupled with other measurements, e.g. radiation solar fluxes. Mongu represents the area of major biomass burning activities in southern Africa and is located far from industrial sources; Skukuza represents a region of relatively low biomass burning, but with some influence from industrial and maritime aerosol sources. These differences provided the basis for comparing and contrasting the aerosol optical properties and their influence on direct forcing between the two sub-regions.

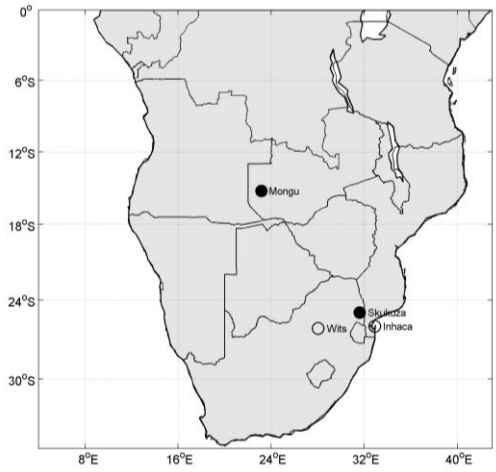

Figure 2-1 Map of southern African region showing the study area and the position of Mongu in Zambia and Skukuza in South Africa (black dots).

With a view to better understanding the regional differences of aerosol optical properties, a secondary region of study in Middle East was selected. The interest in this region was engendered by the fact that Middle East is located at similar geographical latitudes to those of southern Africa, but in the northern hemisphere. The Middle East also represents an environment quite different from southern Africa. Additionally, the Climatology Research Group (CRG) at Wits University (under which this study has been conducted) have been actively part of the aerosol research teams in Middle East during the decade starting in 2004 — the United Arab Emirates Unified Aerosol Experiment UAE2.

The Middle East region selected as a secondary study area is bounded by latitudes 6^o to 36^o N and longitudes 32^o to 72^o E (Figure 2.2). The predominant local sources of aerosols include desert dust, maritime and petrochemical combustion (Reid *et al*., 2004). The primary area of study for this research, the southern African region, is correspondingly bounded by latitudes 6^o to 30^o S and longitudes 5^o to 45^o E. For this secondary region of study, three sites were selected, Solar Village in Saudi Arabia, and Dhadnah and Hamin in the UAE.

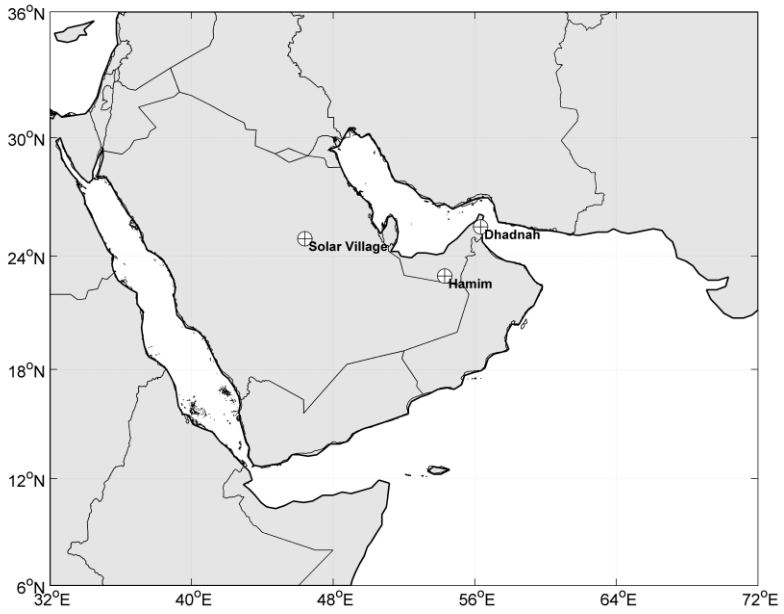

Figure 2-2 Middle East region showing the geographic positions of Solar Village in Saudi Arabia, Dhadnah and Hamin in United Arab Emirates. The three locations are AERONET sites in this region.

2.2 Data sets and tools

Aerosol forcing estimates requires quantification of aerosol optical properties, for a particular time and location; each of these depends on the wavelength of the incident radiation, the zenith angle and relative humidity. This section will describe the processes used to acquire and analyse the data used in this study.

2.2.1 Aerosol Robotic Network (AERONET)

AERONET is one of the most useful global networks for monitoring atmospheric aerosols and data archive conducted by NASA Goddard Space Flight Center (Holben *et al.*, 1998). The AERONET program has provided high quality aerosol products for the past decades from approximately 180 stations globally (http://aeronet.gsfc.nasa.gov/).

The AERONET primarily uses the CIMEL Sun photometer instrument (Holben *et al.*, 1998) to measure aerosol optical thickness (τ_λ) at seven wavelengths (λ = 340, 380, 440, 500, 670, 870 and 1020 nm), but also retrieves aerosol volume size distribution and single scattering albedo (ω); an asymmetry factor (g) and a complex refractive index (m = n + *i*k) (at four wavelengths (λ = 440, 670, 870 and 1020 nm) using information from sky radiances scans) (Dubovik & King, 2000).

For this study, the long-term measurements and derived aerosol optical properties for Mongu, Zambia (1995 – 2009) and Skukuza, South Africa (1998 - 2009) were the key

input datasets to study the aerosol optical properties in southern Africa. Additional sites from Middle East, namely Solar Village (1999 – 2008) in Saudi Arabia, and Hamin and Dhadnah (2004 – 2007) in UAE, were also used.

The calibration of the instruments was performed regularly at the Goddard Space Flight Center (GSFC) by a transfer of calibration from reference instruments, calibrated by the Langley method at Mauna Loa Observatory. The combined effects of uncertainties in calibration, atmospheric pressure, and ozone amount (climatology is used) resulted in a total uncertainty in derived aerosol optical thickness of ~0.01 - 0.02, (the largest errors falling in the UV range (Eck *et al*., 1999). Data were quality checked and cloud-screened following the methodology of Smirnov *et al. (*2000). Two major criteria were employed in the cloud-screening procedure. First, retained stable triplets (three AOD measurements) were made, within a 1 minute interval, to eliminate high-frequency changes. It was assumed that the aerosol optical depth (in the total atmospheric column) should show a variation of less than 0.02 across all wavelengths within one triplet for the atmosphere to be considered stable and cloud free.

A flexible inversion algorithm for the retrieval of optical properties, developed by Dubovik and King (2000), was used for retrieving aerosol volume size distributions, single scattering albedo, refractive index and phase function. In addition, a spectral de-convolution algorithm, developed by O'Neil *et al*. (2006), was used to extract the elemental optical parameters of each mode (fine and coarse). All data sets utilised in this study were Level 2, i.e. final calibrations and quality assurance had been applied.

2.2.2 Surface radiation fluxes

Radiometers were used to quantify broadband solar and terrestrial radiation fluxes and for this research, the three types of solar radiometers used were Precision Spectral Pyranometers (PSP), Normal Incidence Pyrheliometer (NIP) and Precision Infrared Pyranometer (PIR). All these instruments are described in detail under Chapter 1 (literature review section).

PSP was used to measure global (unshaded) and diffuse (shaded) solar irradiances within the broadband intervals of 0.3 to 3 μm at the Earth surface. NIP was used for measurement of the broadband direct solar radiation from 0.2 to 4.0 μm. This is the solar radiation band that passes directly from the sun through the atmosphere without being scattered or

absorbed by the atmosphere. The PIR was used for the measurement of the broadband infrared radiation between 4 and 50 μm.

In the process of measuring the solar radiation, the sensor instruments convert the radiant energy to heat energy, which, in turn, is converted by a thermopile into electrical signals in Volts (V). The measured voltage output is then processed, using the manufacturer and laboratory calibration constants, as solar radiation fluxes (usually expressed in W $m^{-2)}$.

Solar fluxes data used in this study were collected during the dry season campaign of SAFARI 2000 (Swap *et al.*, 2003). A mobile Laboratory for Ground-based Remote Sensing of Atmospheric Radiation, from the SMART group at NASA's Goddard Space Flight Center; (SMART, http://smartlabs.gsfc.nasa.gov) was operated at Skukuza in the Kruger National Park, South Africa. Alongside other sensors, three Eppley PSPs (SN: 32759, 32107 and 32188); one NIP (mounted in a solar tracker); one Eppley PIR (SN: 32194); one Total Sky Imager (TSI) and a Micro Pulse Lidar (MPL) were used.

Solar fluxes were measured and recorded at one-minute intervals from 17 August to 18 September in 2000. In addition, cloud cover fraction and aerosol layer heights were also measured by TSI and MPL instruments respectively. The data acquired in this dry season field campaign were used in this study to identify accurately the cloud free conditions (for better assessment of the direct aerosol radiative forcing in southern Africa). Details of this analysis are given in Chapter 4.

Plate 2-1 The SMART mobile laboratory in operating position.

2.2.3 Direct solar effects of aerosols under cloud free conditions

Radiative transfer theory quantifies the interaction of atmospheric aerosols with radiation. In principle, if the physical and chemical properties of aerosols are known, the direct solar effects of aerosols can be estimated.

Recent advances in AERONET measurements and retrievals provided an extended set of physical and optical aerosol parameters - key information for estimating the aerosol radiative effects. In addition, spectral and broadband fluxes at the bottom and top of atmosphere have been included. This information, combined with the radiative transfer model, provided long-term direct aerosol radiative forcing and aerosol radiative forcing efficiency estimates for cloud free days at bottom of atmosphere and top of atmosphere at both Mongu and Skukuza.

Daily direct aerosol forcing estimates covering the period of 1995-2007 (for Mongu) and 1997-2007 (for Skukuza) were combined with other data sets and analysis (as previously discussed) to assess and validate the magnitude and variability of direct forcing of aerosols in southern Africa.

2.2.4 Backward trajectory model

The NOAA Air Resource Laboratory in Silver Spring, Maryland provided online models for computing trajectories (http://ready.arl.noaa.gov/HYSPLIT.php). The HYSPLIT_4 (HYbrid Single-Particle Lagrangian Integrated Trajectory) model is a complete system for computing data, ranging from simple trajectories to complex dispersion and deposition simulations (Draxler & Hess, 1998).

Gridded meteorological data, on a latitude-longitude grid or along one of three conformal map projections (Polar, Lambert, Mercator), are required at regular time intervals. The input data are interpolated to an internal sub-grid centred to reduce memory requirements and increase computational speed. Calculations can then be performed, either sequentially or concurrently, on multiple meteorological grids, usually specified from fine to coarse resolution (Draxler *et al*., 2009).

The routine meteorological data fields required for the calculations were obtained from existing archives or from forecast model outputs already formatted for input to HYSPLIT. In addition, several different pre-processor programs are available to convert NOAA, NCAR (National Center for Atmospheric Research) re-analysis, or ECMWF (European

Centre for Medium-range Weather Forecasts) model output fields to a format compatible for direct input to the model.

The modelling system included a Graphical User Interface (GUI) to set up a trajectory. The post-processing part of the model package incorporates graphical programs for generating multi-colour or black and white publication-quality Postscript printer graphics. This system can be accessed and used online at http://ready.arl.noaa.gov/HYSPLIT.php.

In this study, this model was used to assess the air mass origins (backward trajectories) for specific days at Skukuza during the SAFARI 2000.

2.2.5 The MATLAB mathematical computing software

MATLAB (Matrix Laboratory) is a programming environment for algorithm development, data analysis and visualization (developed by the MathWorks Corporation, who specialise in mathematical computing software). MATLAB allows matrix manipulations, plotting of functions and data, implementation of algorithms, creation of user interfaces, and interfacing with programs written in other languages, including C, C++, Java, and Fortran.

In this study MATLAB was used as the mathematical and statistical tool for data handling, processing, analysis and plotting. For this purpose many MATLAB computer scripts were developed.

2.3 Data analysis

2.3.1 Climatology of aerosol optical properties

The long-term AERONET measurements and retrievals of atmospheric aerosols at Mongu and Skukuza provided a good opportunity for understanding the spatial and temporal distribution of aerosol optical properties in southern Africa. The aerosol optical thickness, Ångström exponent and retrieved single scattering albedo and size distribution, were analysed and compiled into a southern Africa climatology of aerosol optical properties. These aerosol properties directly determine how atmospheric aerosols interact with the solar radiation and their relative importance in the scattering and absorption processes (Garcia *et al*., 2008). The data used for this analysis are taken from the highest available AERONET quality version (Version 2.0 at level 2.0, Dubovik *et al*., 2006).

Analysis covered the seasonal variation, day to day and inter-annual variability, to evaluate the possible trend of aerosol loading in this region. The analysis was also performed for

two different size modes - coarse and fine fractions. Assumptions on aerosol load classification were proposed and defined for late applications. Specific attention was given to two periods: the peak biomass burning period (August, September and October) and the non-biomass burning period, outside rainy season (April, May and June). Similar analyses were extended to regions other than southern Africa: specifically the Middle East region (Saudi Arabia and United Arab Emirates).

Frequency distribution analyses of the aerosol optical thickness (AOT) and Ångström exponent (AE) were performed. The results allowed for seasonal and interannual variations interpretation of AOT and AE values for each site.

All data handling and analysis were supported by the MATLAB computational suite the statistical tools within MS Excel™. The detailed results on the climatology of aerosol optical properties are presented in Chapter 3.

2.4 Identification of clear sky conditions

Solar radiation fluxes are hampered, most of the time, by persistent broken cloud fields, making it difficult to assess the direct aerosol radiative forcing. Analysis of a daily time series of global and direct solar radiation measurements, obtained from PSPs data at Skukuza, allowed the identification of the likeliest clear sky days during the daytime. Final validation and selection of the clear sky days, to avoid the contamination of high thin clouds, was made possible by scrutinising the daily video records obtained from total sky imager (TSI) and micro pulsar lidar (MPL) measurements.

The selected clear sky days were classified and grouped in terms of the optical state of the atmosphere (given the total amount of aerosols in the atmospheric column). This was made possible by using the AERONET Sun photometer data.

The ability to conduct combined instrumental data examination was facilitated after laboratory and field experiments had been undertaken at the Radiation and Climate Branch, NASA Goddard Space Flight Centre (Plate 2.2 and Plate 2.3) under the SMART group, and during the United Arab Emirates Unified Aerosol Experiment in year 2004.

Plate 2-2 Experimental process conducted at NASA Goddard facilities (to familiarise the author with radiometric measurements techniques and data handling) (January 2004).

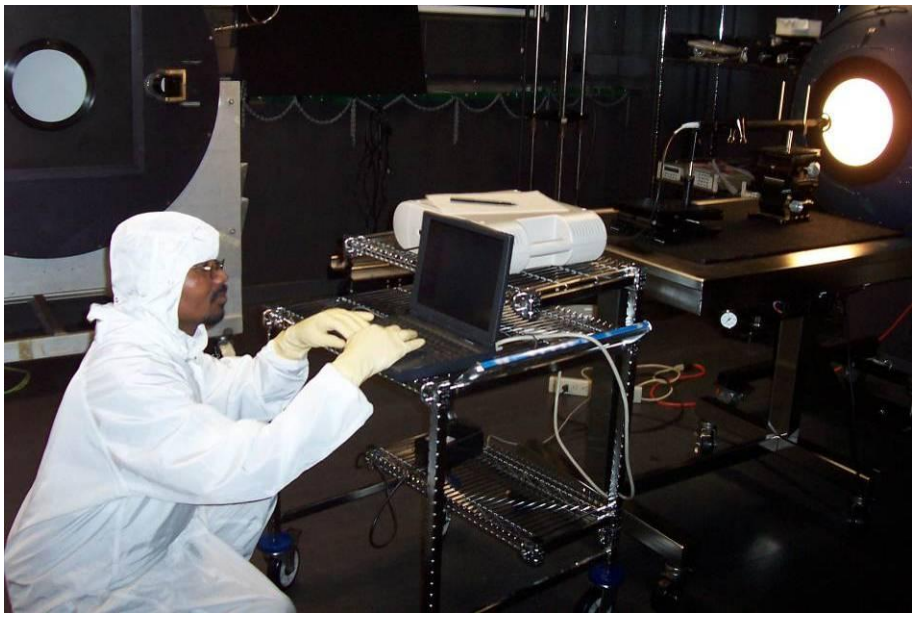

Plate 2-3 Experimental process conducted at NASA GSFC facilities' sphere laboratory (to familiarise the author with radiometric calibration methodology) (February 2004).

2.4.1 Direct aerosol forcing estimates for southern Africa

The Aerosol Robotic Network (AERONET) is a NASA leading programme providing physical and optical aerosol parameters for approximately 180 ground-based stations worldwide (http://aeronet.gsfc.nasa.gov/). AERONET has been in operation around the world for almost two decades. Recent AERONET development products include a set of estimates of direct solar effects (caused by atmospheric aerosols - mainly spectral and

broadband fluxes) and direct aerosol radiative forcing at bottom and top of atmosphere. For this study, the corresponding data sets for Mongu and Skukuza were selected for analysis and the results are presented in Chapter 5.

The calculations of direct solar effects and the direct aerosol radiative forcing at bottom and top of atmosphere were derived from the new radiative transfer module integrated into the AERONET Version 2 inversion code (Dubovik *et al*. 2006, Garcia *et al*., 2008). The model is described in more details in Chapter 1 (literature review).

The analysis of the daily direct aerosol forcing estimates was the first approach used for assessing the magnitude and variability of direct aerosol forcing at bottom and top of atmosphere in this region. Seasonal distribution and linkages were also investigated, with particular special attention given to the biomass burning and non-biomass burning periods.

The results for selected cloud free days, from surface solar measurements (discussed in more detail in Chapter 4), combined with the current results of direct aerosol radiative forcing analysis were used to improve the evaluation of the direct aerosol forcing in these region and to reduce uncertainties. Given that the selected cloud free days covered different aerosol loading magnitudes, which were exerting different forcing in the atmosphere, backward trajectory analysis was performed to better understand the air mass origins associated with each optical state.

To retain the regional perspective of these direct aerosol forcing estimates, the aerosol classes defined in Chapter 3 were cross-linked to identify the likeliest level of direct aerosol radiative forcing for the southern Africa region.

All data handling and analysis were supported by MATLAB computing programme and the detailed results on direct aerosol forcing analysis at Mongu and Skukuza in southern Africa are presented in Chapter 5.

2.4.2 Uncertainties associated with different data sets

The core data sets used in this research were mainly from CIMEL field direct measurements and AERONET derived products. The AERONET aerosol products are computed for three data quality levels: Level 1.0 (unscreened), Level 1.5 (cloud-screened), and Level 2.0 (cloud-screened and quality-assured) (http://aeronet.gsfc.nasa.gov). The AERONET data used in this study were taken from the highest quality level, i.e. 2.0.

The calibration of AERONET field instruments was performed by a transfer of calibration from reference CIMELs, which are calibrated by the Langley plot technique at Mauna Loa Observatory (Hawaii). Typically, the total uncertainty in spectral aerosol optical depth for a field instruments varies from 0.01 to 0.02 under cloud-free conditions for air mass equal one (Eck *et al*., 1999), with the highest errors (0.02) associated with the ultraviolet wavelengths. For the sky radiance measurements, calibration is performed by comparing to a reference integrating sphere with an accuracy of ±5% or better at the NASA Goddard Calibration Facility (Holben *et al*., 1998). Additional information on other field instruments and computational tools used in this study is provided in Table 2.1.

Table 2-1 List of instruments, tools, derived quantities and accuracy level

Instruments/Tools	Quantity	Accuracy
CIMEL Sun Photometer	Aerosol optical thickness	0.01-0.02 (Eck et al., 1999; Schmid *et al*.,1999)
	Single scattering albedo	0.03 (Dubovik *et al*., 2000)
	Asymmetry parameter	3-5% (Dubovik *et al*., 2006)
	Precipitable water	10% (Schmid *et al*., 2001)
Eppley (Precision Spectral Pyranometer)	Total shortwave flux and Diffuse shortwave flux	Eppley temperature dependence: ±1% over range from -20° to + 40°C Eppley linearity: ±5% over range from 0 - 2800 W m-2 Eppley cosine response: ±1% over 0° to 70° range ±3% over 70° to 80° range (Campbell Scientific, 2001, Application note 2RA-A)
Eppley (Normal Incidence Pyrhelometer)	Direct shortwave flux	±2% (Vignola & Lin, 2010)
Micro Pulsar Lidar (MPL)	Aerosol extinction coefficient	15-20% (Schmid, *et al*., 2006; Welton *et al*., 2002)
HYSPLIT_4 model	Air mass trajectory model	20 – 30% typical position error (Stohl, 1998)
AERONET solar flux estimates	Integrated total shortwave flux	+9±12 W m^{-2} (García *et al*., 2008)

****

The methodology and sources for data collection have been outlined. Data analysis procedures and the tools employed in this study have been discussed in detail. The results of the aerosol optical properties data analysis are presented in the next chapter.

Chapter 3.

Chapter 3 describes the climatology of aerosol optical properties over southern Africa; spatial and seasonal variation of the main aerosol parameters (aerosol optical thickness, Ångström exponent, size distribution and single scattering albedo) are analysed in detail. Additional analysis of aerosol optical properties in Middle East are presented and compared with southern Africa. Separate analyses of the coarse and fine size modes are discussed. Long-term trends of aerosol loadings in southern Africa and the Middle East will be explored.

3 Climatology of Aerosol Optical Properties over Southern Africa

A thorough understanding of the optical properties of aerosols (aerosol optical thickness, Ångström exponent, single scattering albedo, size distribution) and their spatial and temporal distribution is required before accurate evaluations can be made of aerosol effects in the climate system (Hsu *et al*., 2000).

Monitoring of aerosol parameters in southern Africa has been conducted since the middle of the 1990s by the AERONET programme. Long-term data is available of measurements of aerosols (in southern Africa) from two sites: Mongu in Zambia (15º 15' S; 23º 09' E; elev. 1107 m) and Skukuza in South Africa (24º 59' S; 31º 35' E; elev. 150 m) (Figure 3.1). Mongu is located in the centre of biomass burning activity in southern Africa and far from industrial sources. Skukuza is located in the Kruger National Park, in middle of the South African Highveld, quite far from both the industrial sources and the advected maritime aerosols from the Indian Ocean.

The two sites provide the basis for comparing the aerosol optical properties between tropical and subtropical sub regions. The aerosol types in southern Africa include predominately smoke, dust, industrial-induced pollution and sea salt particles. During the dry season period, from August to October, the predominant aerosol type over the study region is smoke, generated from biomass burning on land, and these aerosols are transported over the adjacent southern Atlantic and Indian Oceans (Ichoku *et al*., 2003; Eck *et al*., 2003; Haywood *et al*., 2003).

The existing long-term data from AERONET measurements represents valuable information and provides a good opportunity for defining the climatology of aerosol optical properties; in turn improving the understanding of direct radiative forcing by aerosols in this region. The aerosol data used for this analysis cover two periods: June 1995 to June 2007 for Mongu and July 1998 to June 2008 for Skukuza.

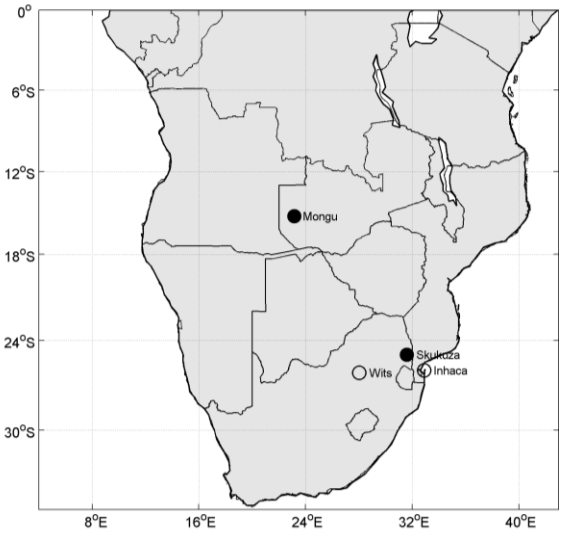

Figure 3-1 Geographical positions of Mongu, Zambia and Skukuza, South Africa (black dots). The positions of Inhaca Island on the east coast of southern Africa and Wits University, in the metropolitan area of Johannesburg, South Africa are indicated (open circles).

3.1 Variability of Aerosol Optical Thickness over Southern Africa

3.1.1 Seasonal variation of multi-year monthly mean aerosol optical thicknesses at Mongu and Skukuza

The seasonal variation of monthly average aerosol optical thickness at 500 nm — AOT (500 nm) — depicts a strong seasonal cycle, with maximum values observed in the months of August, September and October (ASO) for both sites (Figure 3.2). This seasonal peak occurs during the second half of the dry and the beginning of the wet season in southern Africa (spring and early summer) and is associated with high biomass burning activity during this period. Compared with the biomass burning season in South America, which reaches an annual maximum for approximately two months during August and September, the burning season in Southern Africa is longer, lasting three to four months (Holben *at al*., 2001).

The multi-year annual means of AOT (500 nm) are 0.28 and 0.21 for Mongu and Skukuza respectively. Monthly mean values ranged from 0.09 (April) to 0.62 (September) in Mongu

and from 0.15 (February, March and May) to 0.34 (September) in Skukuza. The onset of the biomass burning season begins one month earlier at Mongu than at Skukuza; however, the highest levels of AOT at both sites were recorded between August and October. During the nine month season at Mongu and the eight month Skukuza season (November – July), monthly mean values were below the annual means (0.28 and 0.21 for Mongu and Skukuza respectively).

Over southern Africa, aerosol loading is mainly influenced by seasonal biomass burning aerosols. These aerosols are primarily caused by uncontrolled savanna and forest fires, and inefficient agricultural practices (slash and burn). The loading occurs mostly in late dry season (Holben *et al*., 2001; Eck *et al*., 2003; Swap *et al*., 2003; Ito *et al*., 2007). Additionally, the absence of rain, as the primary removal process, and the associated weak convective transport during the dry season, because of the presence of persistent stable layers and upper level subsidence, causes high AOT in this region (Garstang *et al*., 1996; Cosijn & Tyson, 1996).

The contribution of biomass burning to the total aerosol loading is very significant, in particular at Mongu were about 52 % of the total annual aerosol load is released within the three months above the average (ASO). A slightly lower contribution is observed at Skukuza, with about 38 % of the total aerosol load within the same of three month period (ASO). This explicitly shows biomass burning to be a large source of aerosols in southern Africa. According to Giglio *et al. (*2006), Africa alone accounts for about 44% of the fires (and there are millions) that occur on the entire planet every year. Figure 3.3 shows the satellite observations of fire counts observed by Moderate Resolution Imaging Spectroradiometer (MODIS) collection 4 fire product in the recent decade.

A summary of seasonal averages of aerosol optical thickness at 500 nm is given in Table 3.1. Low aerosol loadings values ranging from 0.11 to 0.17 were observed from December to May (DJFMAM); values ranging from 0.20 to 0.27, were observed during June, July and August (JJA); high values ranging from 0.30 to 0.46, were observed during September, October, November (SON). These results highlight the large differences in aerosol loadings along the timeline of the yearly cycle (seasonal scale) and also between the two sub regions represented by Mongu and Skukuza (spatial scale).

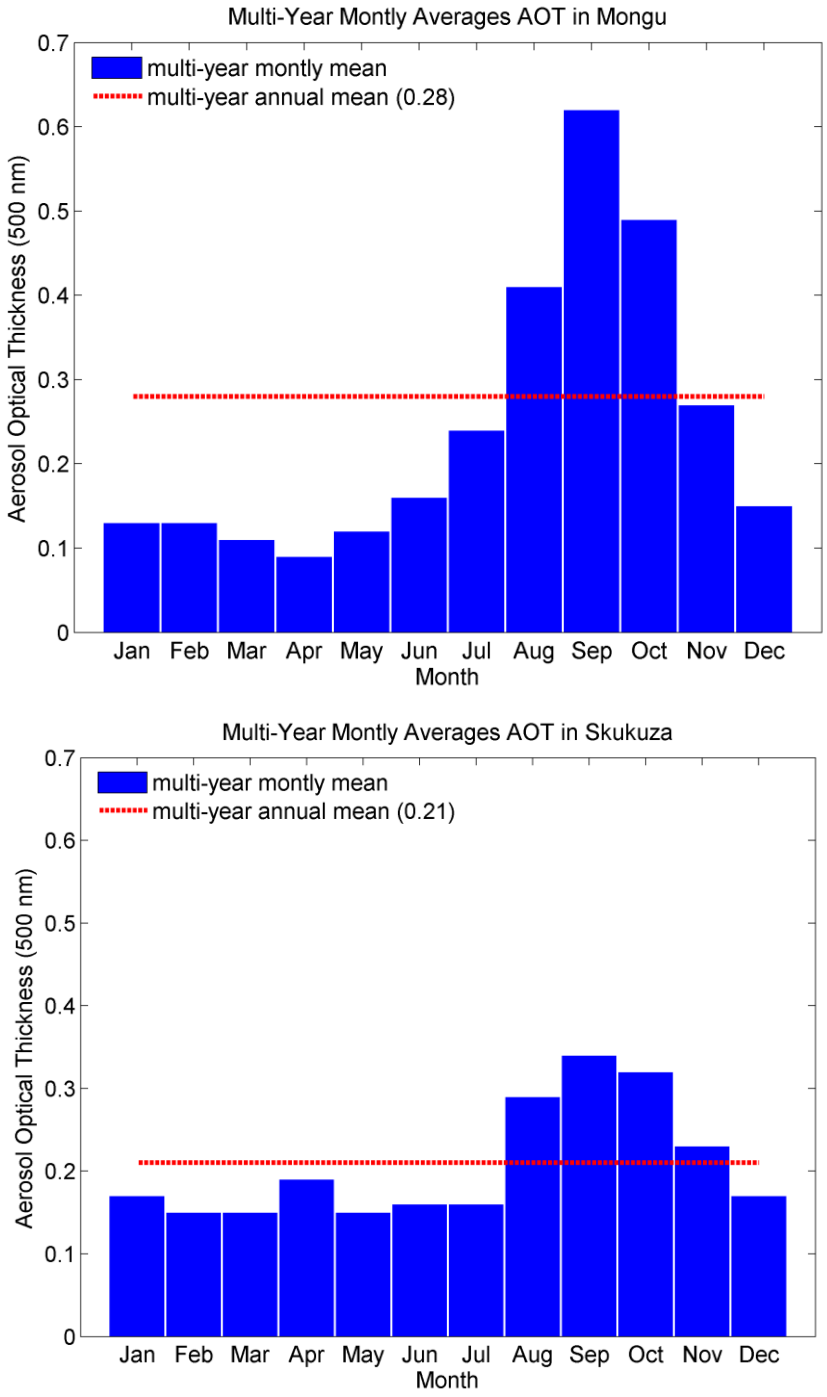

Figure 3-2 Seasonal multi-year monthly mean of aerosol optical thicknesses (computed from 1995 to 2007) in Mongu (upper panel) and (from 1998 to 2008) in Skukuza (lower panel).

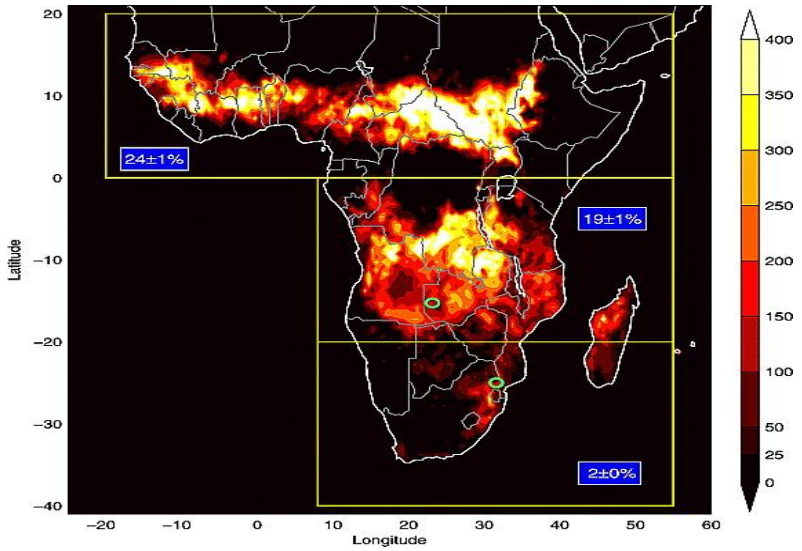

Figure 3-3 Annual fire counts in Africa averaged from 2001 to 2006 using measurements from the MODIS satellite instrument (collection 4). The numbers in the blue boxes are the mean (±standard deviation of the 6-year mean) contribution of the particular yellow-boxed regions to global annual fire counts. The green circles are the two AERONET sites Mongu, Zambia and Skukuza, South Africa. The color bar units are numbers of fires per year in per 0.5° latitude by 0.5° longitude grid box (After Magi *et al.*, 2009).

Table 3-1 Seasonal averages of aerosol optical thickness in Mongu and Skukuza.

Site	Seasonal Averages of AOT (500 nm)				Annual Average
	DJF	MAM	JJA	SON	
Mongu	0.14	0.11	0.27	0.46	0.28
Skukuza	0.17	0.17	0.20	0.30	0.21

Figure 3.4 gives the temporal variability of the seasonal and spatial differences of AOT magnitudes in this region. The aerosol magnitudes within a particular season fluctuate from year to year on both sites. The degree of variability is more observed in SON followed by JJA; during the same months the differences on aerosol magnitudes between the two sites are also more pronounced. From December to May both sites exhibit low interannual variability and the aerosol magnitudes are within a narrow range.

It can also be noted that, from June to November, aerosol loading magnitudes at Mongu are well above those of Skukuza; from December to May, however, the opposite occurs with aerosol values at Skukuza slightly higher than for Mongu. Kirkman *et al. (*2000), using airborne measurements, reported that the existing aerosol gradient in southern Africa reverses from biomass burning to non-biomass burning seasons. Ground based measurements also support this premise and will be investigated in more detail in further sections

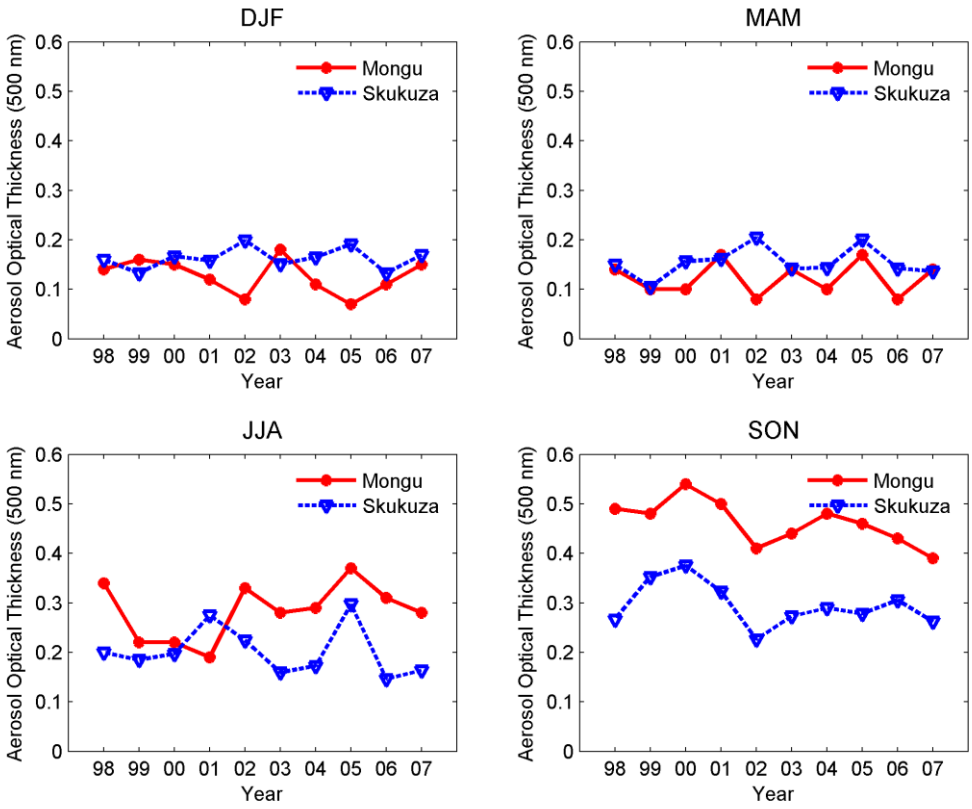

Figure 3-4 Interannual variability of aerosol optical thickness in Mongu (upper panel) and Skukuza (lower panel) showing changes of aerosol loading across different years.

Analysis of interannual variability and the likely trends of aerosol optical thickness will be discussed in next section.

3.1.2 Monthly interannual variability and likely aerosol trends in aerosol optical thickness at Mongu and Skukuza

Monthly interannual variability of AOT (500 nm) shows significant seasonal cycles of the aerosol content at both sites (Figure 3.5). The seasonal cycles follow the onset of biomass burning (end of dry season) and the offset of biomass burning at the beginning of the wet season. The cycles are defined by the levels of aerosol washout and the higher or lower availability levels of flammable fuels). The maximum monthly values occur consistently in September for Mongu but may vary between August and October for Skukuza.

The total aerosol content and the maximum monthly values vary from year to year. In some years a relative abundance of aerosols can be observed, for instance: years 2000 and 2001 at Mongu (Figure 3.5, upper panel) and years 1999, 2000 and 2001 at Skukuza (Figure 3.5, lower panel). In years 2002 and 2003 a relative reduction of the aerosol amount was recorded at both sites.

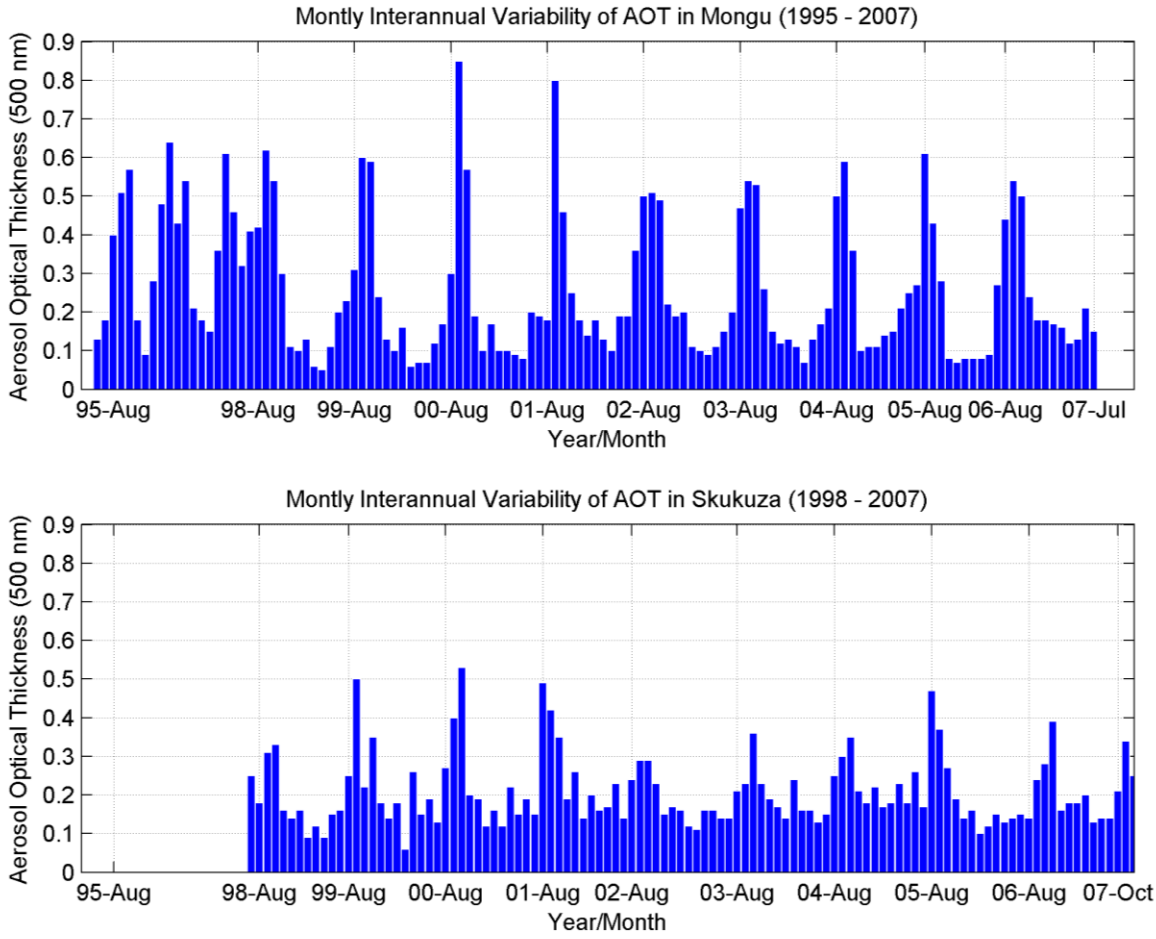

Figure 3-5 Monthly interannual variability of aerosol optical thickness in Mongu (upper panel) and Skukuza (lower panel) showing changes of aerosol loading across different years.

This variability is likely to be linked to the global or regional perturbation in patterns of atmospheric and oceanic circulation and the associated rainfall levels. The most well documented cause of this variability is the El Niño Southern Oscillation (ENSO). ENSO causes warmer and drier than average conditions in the wet season over the most southern Africa in its warm phase (El Niño) and relatively cold and wet conditions in its cold phase (La Niña). Evidence of an association between ENSO and rainfall in southern Africa has been documented in many studies (Miron & Tyson, 1984; Lindesay 1988, Rocha & Simmonds, 1997; Richard *et al*, 2000; Reason *et al*., 2000; Reason & Jagadheesha, 2005). The rainfall variation associated with ENSO in southern Africa affects (among other factors) vegetative production, the accumulation of bio fuel loads and the resultant biomass burning emissions (Anyamba *et al*., 2003; Shugart *et al*., 2004; Nemani *et al*., 2003).

According to the Ocean Nino Index (commonly used to classify ENSO phase in southern Africa) the years 1999, 2000 and 2001 were classified cold phase, i.e. La Niña, and the years 2002 and 2003 were reported as warm phase, i.e. El Niño. The two full data records in Figure 3.5 show a significant increased amount of AOT during the reported La Niña and a noticeably reduction for 2002/2003 El Niño. However this may not lead to a definitive conclusion on relationship between ENSO phases and the annual amounts of aerosols in southern Africa. In essence, further investigation across a longer time series will be required to validate such a conclusion.

Detection of aerosol trends

The results presented in Figure 3.5 depict clearly the inter-annual variability of total aerosol content in the atmosphere of southern Africa, as computed from multi-year monthly means. However, one crucial question under current debate by the aerosol community is whether or not overall atmospheric aerosols concentrations are increasing.

A simple linear model, using chi-square error minimisation, was applied to these aerosol data sets for estimation of trends. This linear model allows a simple approximation of the direction and magnitude of any major trends in the data (Yoon *et al*., 2011).

Let Y be the monthly AOT values, which are calculated with daily AOTs in a month. The linear trend model is given by Eq. 3.1, where B is a constant term, A is the direction and magnitude of the trend per year, X is independent variable associated with month index and ε is the data noise, which for practical purposes will be neglected.

$$Y = B + AX + \varepsilon \qquad (3.1)$$

The results of the linear regression gave a magnitude of change (slope of the regression line) nearly zero, i.e. - 0.001 for Mongu and - 0.0002 for Skukuza.

Both slope signs are negative, indicating a possible decrease in the trend. However the magnitude is too small to validate any possible change. Therefore the search on possible aerosol trend in southern Africa will continue through exploring published results dedicated to aerosol trend analysis at both the global and regional levels.

In recent years a growing number of studies on global and regional trends of AOT, using different data sources and methodologies, have been published. Many previous studies also

have adopted the simple model for AOT trend analysis. In order to analyse accurate trends, the simple model needs to be analysed with respect to AOT variability (Zhao *et al*., 2008).

Many data sources from satellite sensors, e.g. AVHRR, TOMS/OMI, ATSR, MISR and MODIS, have been used to trace global and regional aerosol trends, because these sensors have continuous and long-term observation histories (Yoon *et al*., 2011). In addition, ground based AERONET data have been crucial to validate the space aerosol measurements and site specific trends.

Several results from aerosol trends analysis consistently indicate a negative trend in global tropospheric AOT in the last decade (Mishchenko & Geogdzhayev, 2007; Zhao *et al*., 2008; Zhang & Reid, 2010; de Meij *et al*., 2010; Xia, 2011). At the regional level, negative trends of AOT were observed in the regions influenced by emissions from industrialized countries, i.e. a large part of Europe and Northeast America, and positive trends in the regions influenced by emissions from fast developing countries or smoke from biomass burning, i.e. Indian Bay of Bengal, east coast of Asia and Arabian Sea. The magnitudes of the changes in these studies are slightly different.

Of particular interest in this study are the southern Africa regional trend and, more specifically, the direction of loading at the two sites (Mongu and Skukuza). Yoon *et al*. (2011), using data from AERONET spectral measurements, reported temporal increase in fine AOT over regions dominated by emerging economy or slash burn agriculture in both East Asia and Southern Africa. He pointed out that positive trends of fine AOT are +1.76% a^{-1} at Mongu and +0.75% a^{-1} at Skukuza. In addition to this finding, Yoon also mentioned that the increase of AOT at Mongu and Skukuza are most likely affected by the strong seasonal cycle of biomass burning (Mishchenko & Geogdzhayev 2007; Zhao *et al*., 2008).

De Meij *et al*. (2010), using MODIS and MISR data, indicated an average negative trend for the African continent, with the cautionary note that these negative trends are not statistically robust because of the limited number of ground stations used for comparison.

More recently, Xia (2011), using aerosol data from 79 AERONET stations worldwide, investigated the trends on AOT and Angstrom wavelength exponent (AE). The Xia study gives more detailed information of the 79 AERONET stations, including Mongu and Skukuza in southern Africa. The map below (Figure 3.6) summarizes the results by site

station. In particular, he concluded that the AOT at Mongu and Skukuza had decreased, but the trends were small and were not significant. On the other hand, AE at these two sites increased significantly in recent decades, indicating an increased emission of fine particles into the atmosphere. A qualitative comparison reveals that the findings of the current study are consistent with those of Xia (2011). It is also important to emphasise that the aerosol trend analysis methodology within high seasonal aerosol variability areas like southern Africa needs to be further investigated.

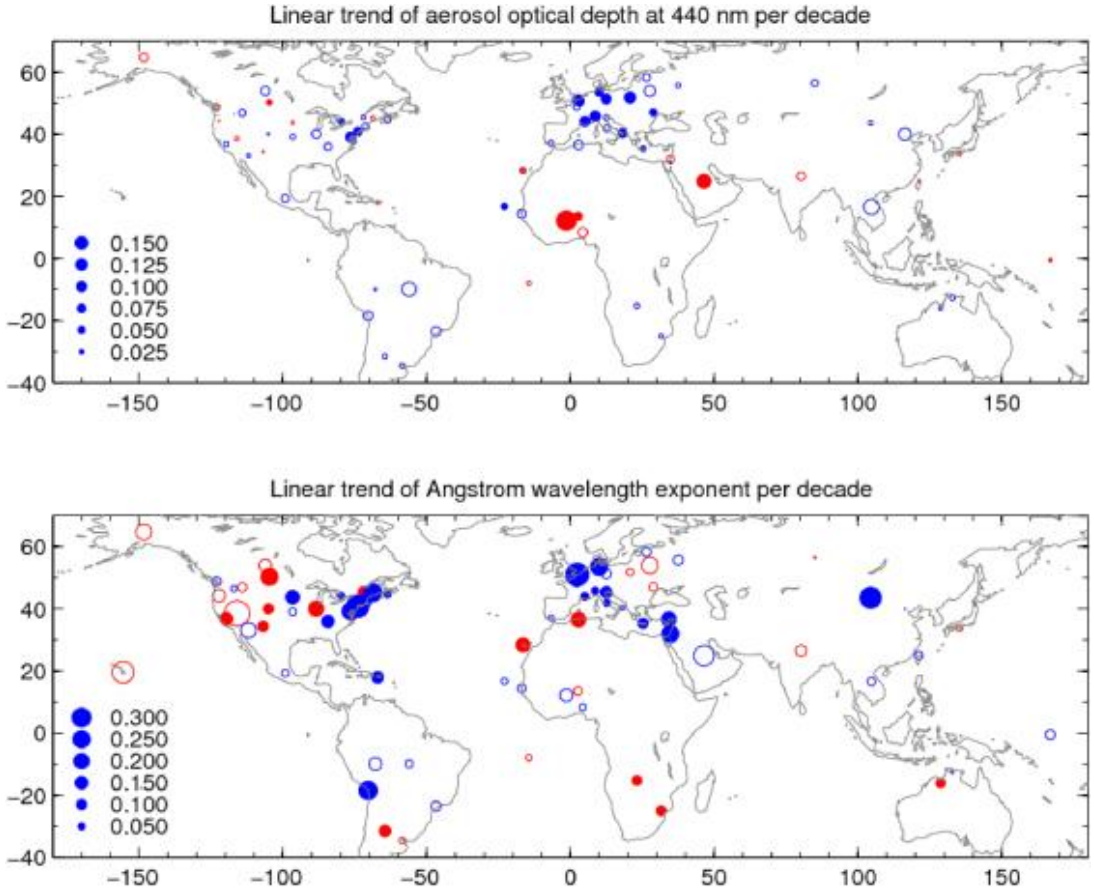

Figure 3-6 Linear trend for AOT at 440 nm and AE (per decade). The blue and red circles represent that the trends are negative and positive, respectively. The solid circles represent trends that are significant at a 95% level (Adapted from Xia, 2011). The trends over Mongu and Skukuza can be viewed by small blue circles (upper panel), indicating slight decrease for AOT and solid red circles (lower panel), indicating noticeable increase on fine particles given by AE (After Xia, 2011).

3.1.3 Aerosol loading classification in southern Africa

Given the magnitude of the climatological values of AOT and their seasonal variability, it is reasonable to suggest a classification grade of the state of the atmosphere in southern Africa based on aerosol loading. This study suggests five grades of AOT at 500 nm,

namely: ‘Very low’; ‘Low’; ‘Medium’, ‘High’ and ‘Very High’. Table 3.2 gives the relationship between the specific category and the quantitative AOT range at 500 nm.

The association of aerosol loading magnitude and category level may aid the aerosol research community in southern Africa to assess the state of atmospheric turbidity more quickly and thereby understand the possible radiative effects. The proposed classification will be used in the next sections and chapters, to build links with other aerosol parameters (especially direct forcing by aerosols in this region).

Table 3-2 Aerosol loading classifications in southern Africa (AOT at 500 nm).

AOT range at 500 nm	Aerosol loading classes
< 0.1	Very Low
0.1 – 0.2	Low
0.2 – 0.3	Medium
0.3 – 0.5	High
> 0.5	Very High

3.1.4 Day to day variability of aerosol optical thickness: Mongu and Skukuza

Daily averages of AOT (500 nm) ranged from 0.02 to 1.7 at Mongu and 0.01 to 1.4 at Skukuza over the entire monitoring period. The overall averages for the entire period of observations were 0.28 and 0.21 for Mongu and Skukuza respectively. A high degree of day-to-day optical variability was evident at both sites, with Mongu showing episodes of very high turbidity (AOT > 0.5) which were more common than at Skukuza (Figure 3.7). This variability was largely attributed to the diverse contributions of aerosol and varying meteorological conditions influencing the tropospheric columns above Mongu and Skukuza. The two aerosol columns were likely to include particles from a range of common sources (local and transported wind-blown dust; emissions from domestic biofuel usage; local and transported biomass burning) and one source (related only to Skukuza) the long-range transport of industrial emissions from the South African Highveld. Previous studies on air mass transport climatology from the industrial South African Highveld revealed that the transport to the east, off shore to the Indian Ocean, accounted for 70% of the fine mode particles (Freiman & Piketh, 2003). This air pathway passes over Skukuza and is likely to carry particles from the main Highveld industrial sources.

One of the atmospheric features that drew particular attention was the extremely high AOT daily values recorded by the sun photometers network, in early September 2000, during SAFARI 2000. This high AOT was associated with the widespread haze exiting off-shore towards the Indian Ocean. This phenomenon was named the River of Smoke (Annegarn *et al*., 2002). A massive thick plume of smoke was advected from central Zambia, southeast over southern Africa, exiting the subcontinent over Inhaca Island, Mozambique (Eck *et al*., 2003; Schmid *et al*., 2003).

This an unusual atmospheric transport pattern over southern Africa, observed during SAFARI 2000, was later confirmed to be associated with strong coupling mechanism between the subtropical circulation systems and the mid-latitude westerly flows; this coupling was likely to have been enhanced by the strong La Niña event of 1999/2000 (Kanyanga, 2008).

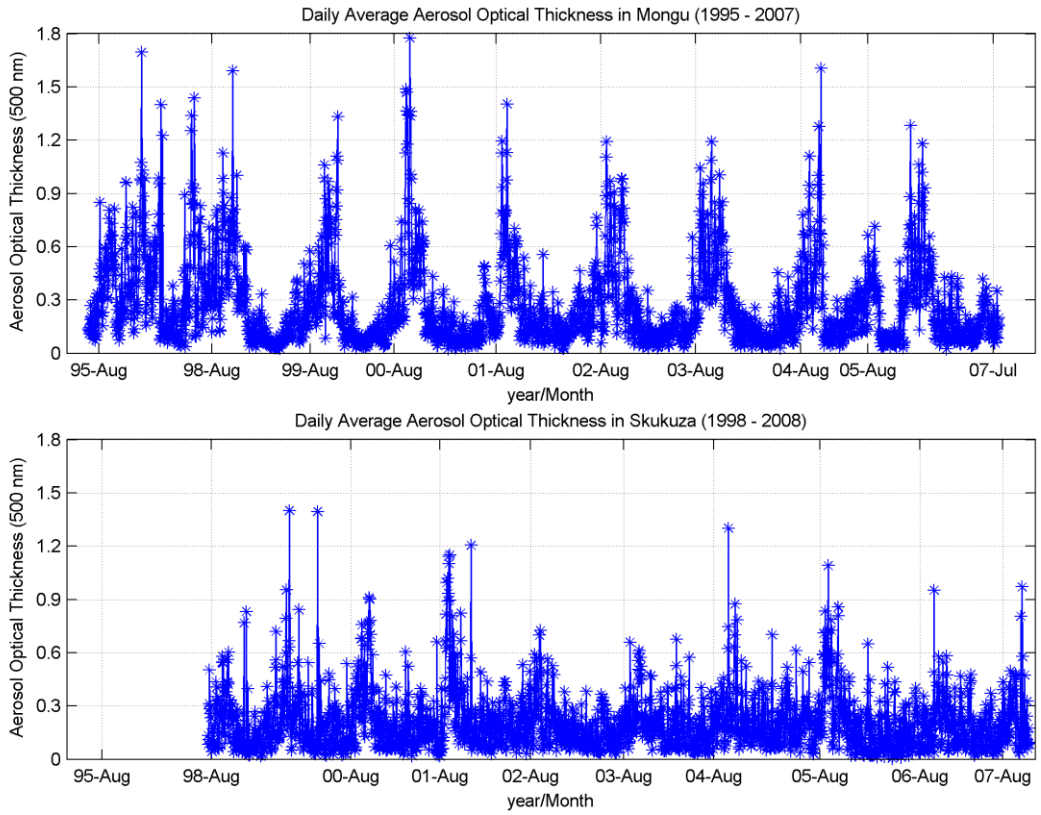

Figure 3-7 Day to day variability of aerosol optical thickness from 1995 to 2007 in Mongu (upper panel) and from 1998 to 2008 in Skukuza (lower panel).

As previously noted, aerosol loadings in southern Africa are characterised by low values from December to May; medium values in June to August and high to very high during September and November. For a better understanding of the day-to-day variability of AOT

values in these three distinct periods, the time series under investigation were separated into two main seasons. The first season covered the peak of biomass burning (August, September and October) and the second the dry non-biomass-burning season outside the rainy season (April, May and June).

During the biomass burning seasons, daily values of AOT (500 nm) varied from 0.03 to 1.7 at Mongu, and from 0.02 to 1.4 at Skukuza (Figure 3.8); the overall averages were 0.50 and 0.31 respectively. In contrast, during non-biomass-burning dry season periods, the AOT (500 nm) varied between 0.02 – 0.49 at Mongu, and from 0.01 to 0.65 at Skukuza (Figure 3.9). The overall averages for this period were 0.14 and 0.17 respectively. The AOT values presented above revealed that episodes of extremely high AOT, greater than 1 at 500 nm, occurred at both sites only in the biomass burning periods. Once again this demonstrated the strength of the biomass burning source. It was also noted that, within the biomass-burning period, there were low episodes of aerosol loading occurring, and, during non-biomass burning periods, high aerosol loading episodes were observed. The combined effects of the instrument measurement error resulted in a total uncertainty of ~ 0.010–0.021 in computed AOT for field instruments, which uncertainty was spectrally dependent with the higher errors evident in the UV (Eck *et al*., 1999).

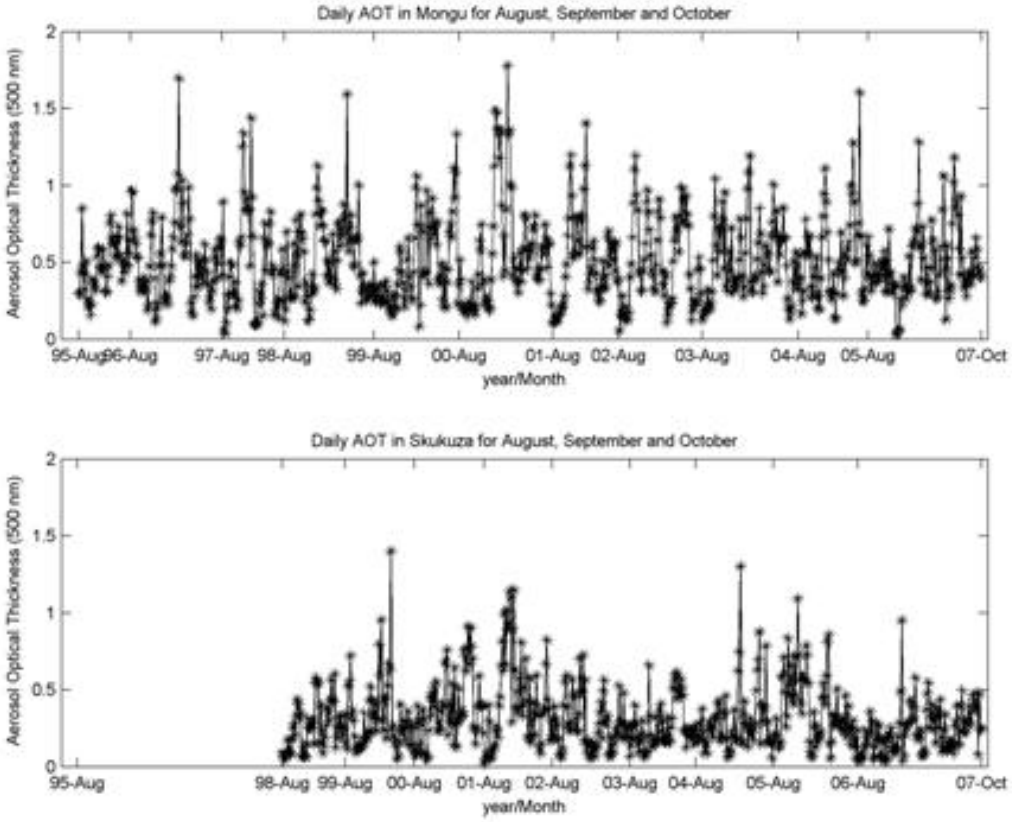

Figure 3-8 Day to day variability of aerosol optical thickness for Mongu and Skukuza during the biomass-burning season in southern Africa, i.e. August, September and October.

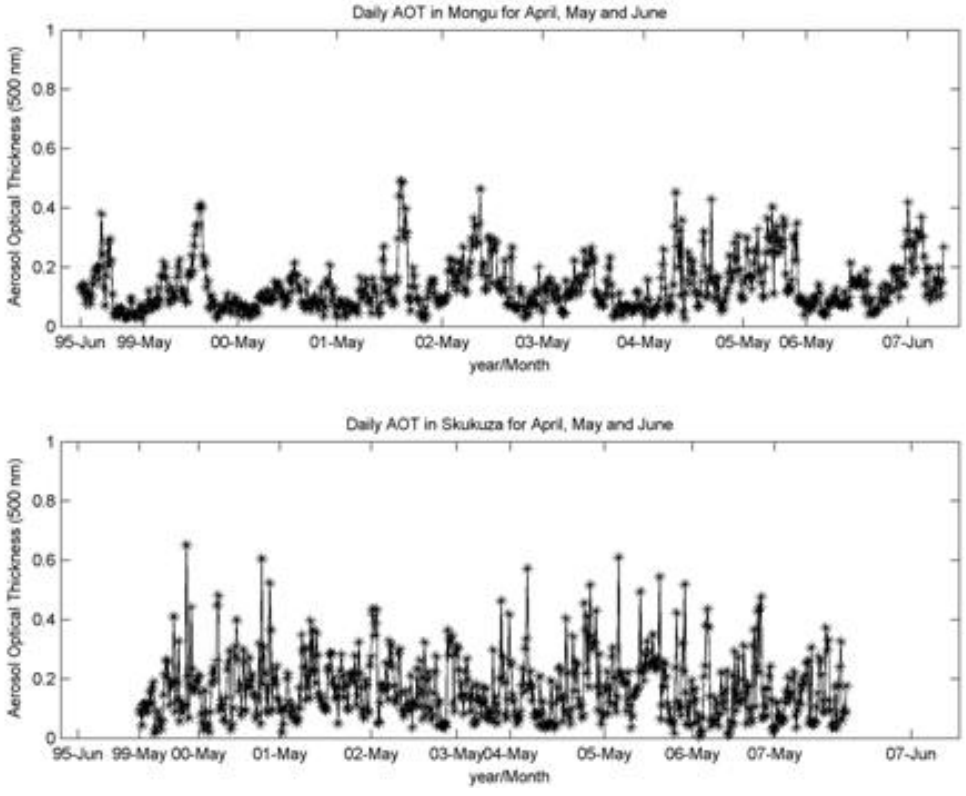

Figure 3-9 Day to day variability of aerosol optical thickness for Mongu and Skukuza during the non-biomass burning dry season in southern Africa, i.e. April, May and June.

Frequency distribution of the aerosol optical thickness

The frequency distribution calculates how frequently individual values occur within a range of values. The results allow for evaluating the probability that a certain range of AOT magnitude occurred for each site. The frequency of occurrence histograms of AOT (500 nm) for all data recorded at Mongu (1995-2007) and Skukuza (1998 – 2008) are presented in (Figure 3.10); both sites showed typical AOT skewed distributions (O'Neill *et al*., 2000b).

The mode values were 0.06 and 0.05; median values were 0.19 and 0.17 at Mongu and Skukuza respectively. The difference between the mean and median at Mongu (0.28 and 0.19) was significant when compared with the equivalent difference at Skukuza (0.21 and 0.17). These differences indicated that the AOT values at Skukuza were more normally distributed than at Mongu. It was also evident from this distribution that episodes of very high AOT, i.e. AOT (500 nm) > 0.5), were more frequent in Mongu than at Skukuza. More detailed analysis in different aerosol loading classes and different seasons will be discussed in the next section.

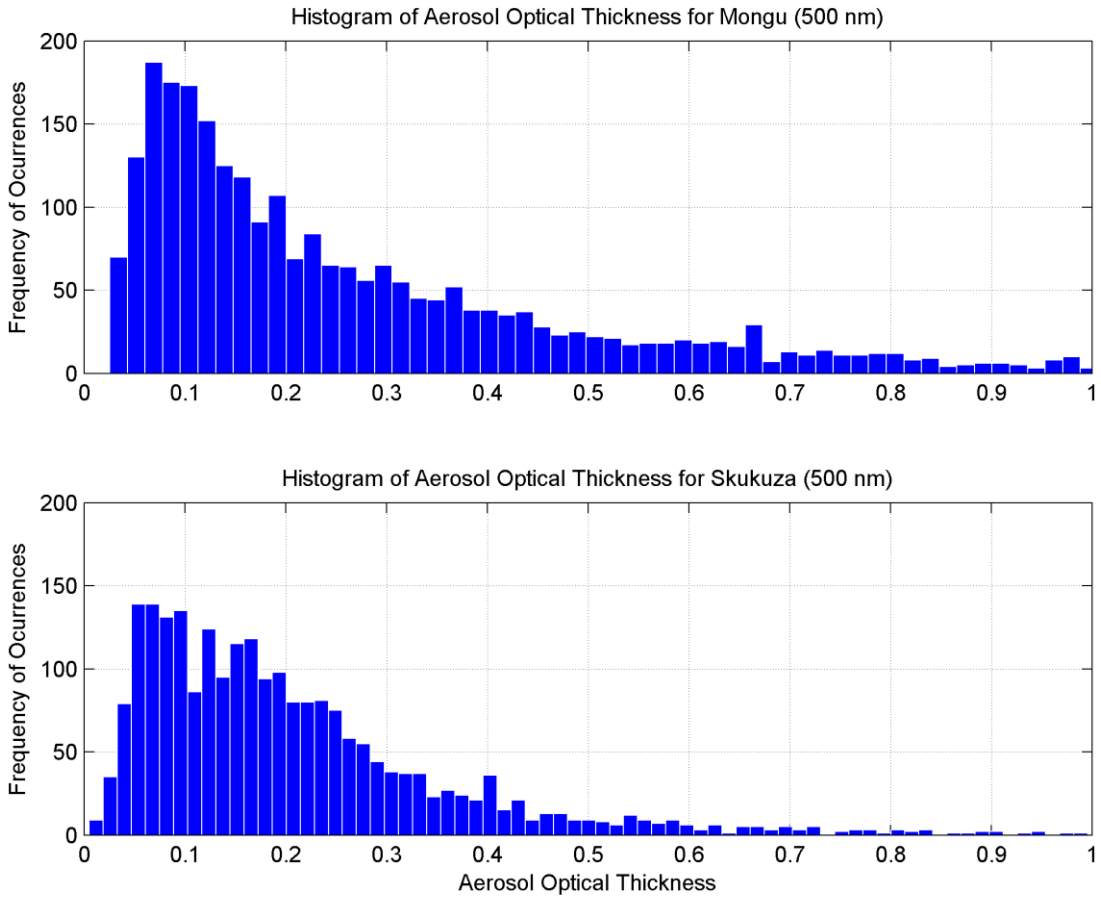

Figure 3-10 Frequency distribution of aerosol optical thickness for Mongu in Zambia (upper panel) and Skukuza in South Africa (lower panel).

Based on the wide range of daily averages of AOT, and their high variability in southern Africa, it is important to understand the frequency distribution of AOT within the classes, as suggested previously in section 1.1.3. The results show all five proposed classes i.e. 'Very low'; 'Low'; 'Medium', 'High' and 'Very High', occurred at both sites in an almost proportional manner, with the exception of the very high loading (AOT > 0.5) where the turbidity levels were significantly higher for Mongu. Given the strong seasonal cycle of AOT magnitudes in southern Africa, the frequency distribution analysis will be extended to look, in particular, at the biomass burning and non-biomass burning periods.

Table 3.3 summarises the probability of occurrences of aerosol optical thickness values within the defined aerosol classes above Mongu and Skukuza throughout the year (all data points) and during the biomass burning (ASO) and non-biomass burning (AMJ) periods. Under the extremes of optical classes defined in previous sections (Table 3.2), the probability that AOT (500 nm) values would fall below 0.1 is 23.7% for Mongu and 27.8%

for Skukuza; the probability that AOT values would rise to levels greater than 0.5 is 16.4% for Mongu and 5.8% for Skukuza.

Table 3-3 Probability of occurrences of aerosol optical thicknesses values within different classes for all data points and the biomass burning (ASO) and non-biomass burning (AMJ) periods at Mongu and Skukuza.

Aerosol loadings classes	AOT range	Probability within the range (%)					
		Mongu			Skukuza		
		All data points	ASO	AMJ	All data points	ASO	AMJ
Very Low	< 0.1	23.7	1.2	44.7	27.8	12.0	33.7
Low	0.1 – 0.2	26.7	7.6	37.2	31.9	23.8	34.5
Medium	0.2 – 0.3	15.7	14.4	12.0	20.7	23.5	20.4
High	0.3 – 0.5	17.4	33.1	6.1	13.8	24.9	10.1
Very High	> 0.5	16.4	43.7	0	5.8	15.8	1.3

The results on Table 3.3 outline the likely distribution of AOT levels within different classes and different times in the year. Between the biomass burning versus non-biomass burning period, a huge optical contrast was observed, with significant changes in column aerosol loading between one season and another. This can be explained by looking at the data from Mongu where, during the biomass burning period, the probability that the AOT will be beyond the 'very high' class (AOT > 0.5) is greater than 40%; on the other hand the probability is nearly zero for AOT > 0.5 within the non-biomass burning period. Similar contrasts can be observed for Skukuza; nevertheless Skukuza has shown a smaller optical contrast when compared with Mongu.

Another particular divergence observed between Mongu and Skukuza is that, during the biomass burning period, the AOT magnitudes are bigger at Mongu than at Skukuza (north-south gradient of AOT); on the other hand, during the non-biomass burning period, the AOT magnitudes are bigger at Skukuza than Mongu (south-north gradient of AOT).

The north-south gradient was demonstrated by high values of probability within the 'high' and 'very high' classes for Mongu when compared with Skukuza; meanwhile the south-north gradient was depicted by low values of probabilities within the 'low' and 'very low' classes for Skukuza when compared with Mongu. In other words, Mongu tends to be cleaner than Skukuza during the non-biomass burning period. These results sustain the hypothesis of the reversal gradient within the two sub regions already raised in Section 1.1.1. In addition the results corroborate the early findings, from airborne measurements,

by Kirkman *et al. (*2000) that an aerosol gradient exists over southern Africa; that it reverts between the biomass burning and non-biomass burning seasons.

Earlier studies, using the same source of ground based data, always highlighted that AOT decreases from north to south, following the north-south gradient in the regional precipitation (Eck *et al.*, 2001, 2003; Queface *et al.*, 2003; Barenbrug, 2003). However, this study demonstrates that there are seasonal changes in the direction and intensity of the AOT gradient in southern Africa. These changes of AOT gradient direction and intensity may have significant implications for radiative forcing potential over the subcontinent at a seasonal level.

3.2 Particle size

3.2.1 Analysis of Ångström exponent over Mongu and Skukuza

The Ångström exponent (α) parameter provides qualitative information about the aerosol size distribution. The α values presented in this study were computed from 440-870 nm wavelengths. When $\alpha < 0.75$, coarse particles dominate; when $\alpha > 0.75$, fine mode particles exert the greatest influence (Eck *et al.,* 1999; O'Neill *et al*., 2000a; Eck *et al*., 2005).

Analysis of histograms obtained from the frequency distribution and probabilities calculations were used to investigate the particle size given by the Ångström exponent (α). The histograms of the Ångström exponent indicated a wide range of particle sizes, with median Ångström exponent values of 1.73 and 1.41 in Mongu and Skukuza respectively (Figure 3.11). These results indicate that size particles at Mongu are primarily dominated by strong fine mode particles sources; at Skukuza a mixture of coarse and fine particles sources are evident. The tropospheric aerosol loading data indicate both sites have a diverse number of contributing sources. However, the dominant range, given by the median Ångström exponent well above unity, indicated that the aerosol particle size was dominated, for the most part (and to a larger extent in Mongu than in Skukuza), by fine particles.

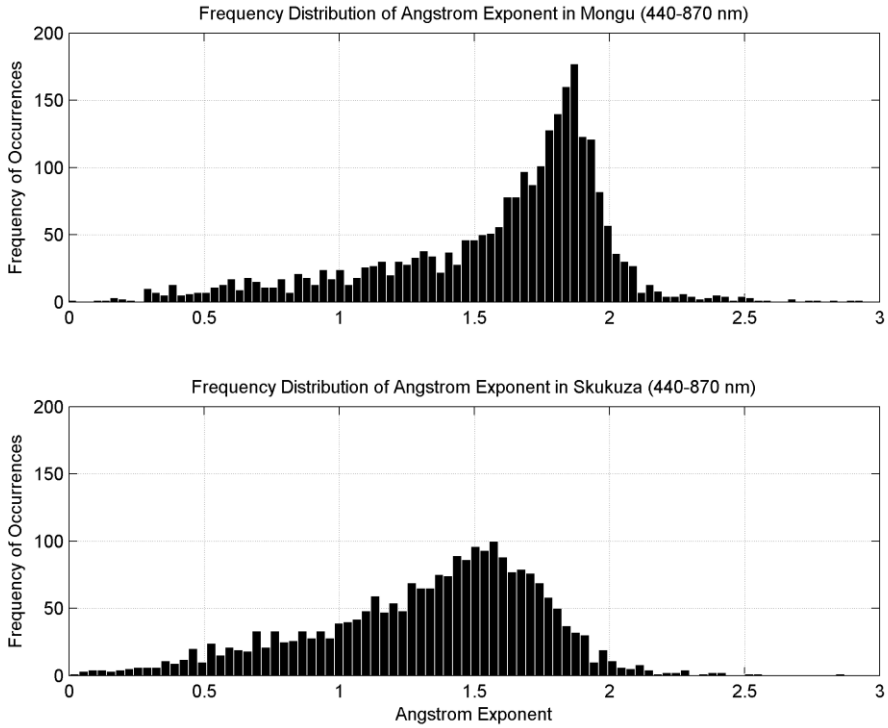

Figure 3-11 Ångström exponent distribution showing the frequency of occurrences for a given size mode of particles. Particle size are dominated by fine mode to a larger extent in Mongu than in Skukuza.

Table 3.4 gives more detailed information about the α-value classes and the probability they will lie within a given class. Ångström exponent values in the class (1.5 – 2.0) accounted for ~ 60% of the aerosol loading at Mongu, indicating that very fine particles were dominant at this site. Coarse particles, probably from airborne dust or the aerosol aging process, were also found in small concentrations. By contrast Ångström exponent values in the class (0.5 – 1.5) represented ~ 50% at Skukuza, indicating a well-balanced mixture of coarse and fine particles at this site. The predominance of each component (coarse or fine) is investigated in detail in the next section.

Table 3-4 Ångström exponent ranges and their probabilities within a given range.

Ångström exponent	Probability within the range (%)	
	Mongu	Skukuza
< 0.5	2.6	4.6
0.5 – 1.0	9.2	16.1
1.0 – 1.5	18.6	39.6
1.5 – 2.0	62.4	37.5
> 2.0	7.2	2.2

3.2.2 Analysis of fine and coarse mode optical thickness

Atmospheric aerosols are rarely mono-modal and often exhibit a bimodal distribution. Hence, the recognition that the aerosol particle size distribution is effectively bimodal, enables researchers to exploit the spectral curvature information ln τ_a versus lnλ to extract the elemental optical parameters of each mode (O'Neill *et al*., 2003). The total aerosol optical thickness (τ_a) can be represented as the sum of fine and coarse mode optical thickness ($\tau_a = \tau_f + \tau_c$).

The separation of the aerosol optical thicknesses into two distinct components, τ_f and τ_c, yields aerosol optical statistics which allow the understanding of atmospheric optical events whether dominated by fine or by coarse mode particle size distribution. Recently AERONET started providing aerosol optical data in these two separate components, generated from the latest version of the spectral de-convolution algorithm developed by O'Neill *et al*. (2006).

Seasonal variation of the fine and coarse mode aerosol optical thickness in Mongu and Skukuza

Atmospheric aerosol loads are dominated by fine mode particles throughout the year (with monthly averages of AOT (500 nm) for fine mode particles) ranging between 0.07 - 0.57 and 0.11 - 0.28, at both Mongu and Skukuza (Figure 3.12, upper panels). Remarkable increases in fine particles levels were observed from July to November at Mongu and from August to November at Skukuza. In contrast, the coarse mode at both sites remained at low AOT values (0.02 – 0.06) throughout the year, with the lowest values registered during the early part of the dry season and slightly increasing towards the wet season (Figure 3.12, lower panels).

To assess the contribution of each component to the total aerosol optical thickness, the percentages (for Mongu and Skukuza) of the fine and coarse modes are presented in Figure 3.13. White and black bars represent the fine and coarse mode percentages respectively. The general picture confirmed that fine particles dominate the atmospheric loadings at these sites, with an average percentage of approximately 78%.

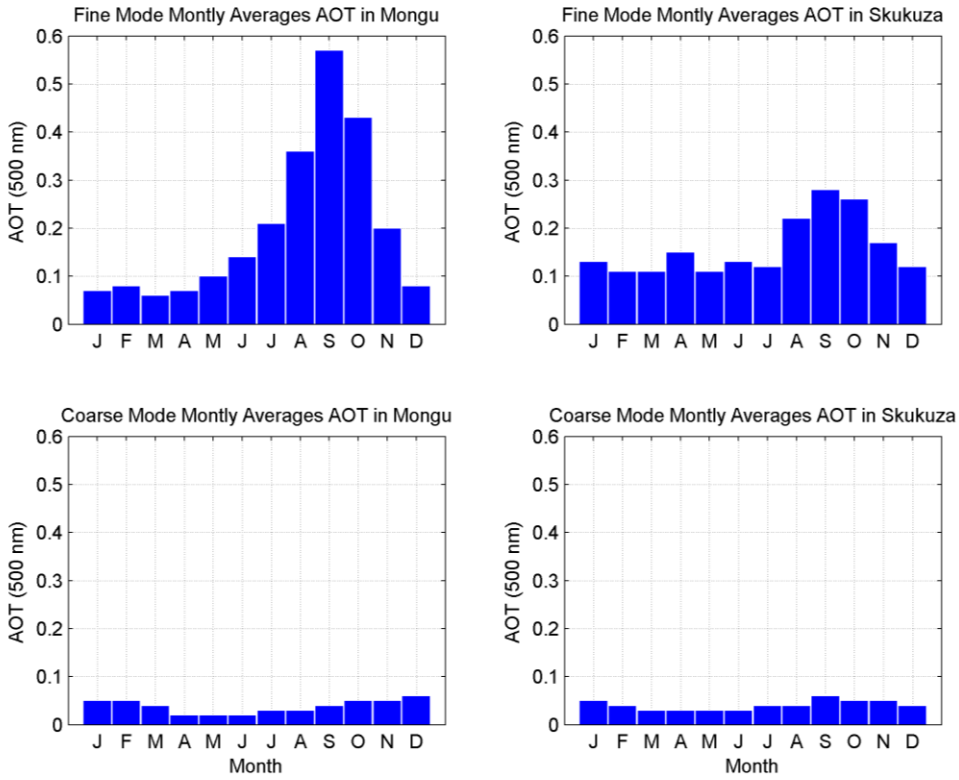

Figure 3-12 Seasonal variations of fine and coarse mode components of aerosol optical thicknesses at 500 nm at Mongu and Skukuza. Fine mode components are shown in the upper panels; coarse mode components in the lower panels.

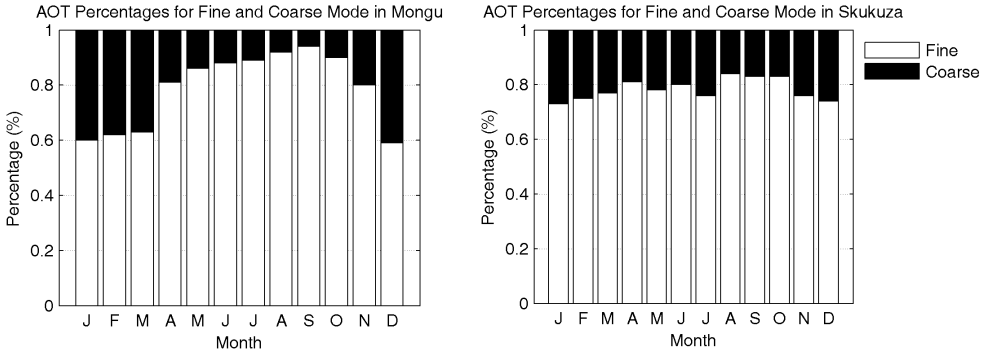

Figure 3-13 Monthly percentages of the distribution of fine and coarse mode aerosol particles in Mongu and Skukuza. White bars represent the fine mode and black bars the coarse mode percentages.

At Mongu, the presence of fine mode particles was significant from August to October, with the level of contributions falling between 90% and 94%. During the wet period, from December to March, the fine particles percentage decreased to ~ 60%; the coarse mode contributions showed complementary increments. These results are good indicators of the strong contribution from biomass burning to the fine particles, at the end of the dry season, in this region.

At Skukuza the contribution of biomass burning to the fine mode was observed, particularly from August to October, with monthly average percentages of ~ 83%. However, the strength of the fine particles sources was also significant outside the peak periods of biomass burning, with the lowest level for fine mode particles at 73%, i.e. well above the lower value for Mongu (60%). These results suggested that fine mode particle sources affecting the atmosphere of Skukuza were not limited to biomass burning but were likely include industrial and other fossil fuel combustion sources from the South African Highveld. Maenhaut *et al*. (2002), using PIXE technique, analysed the chemical composition of aerosol samples collected by SDI cascade impactor at Skukuza during the SAFARI 2000 dry season campaign (August – September 2000). He found mainly fine particles of sulphur (S), potassium (K) and silicon (Si). Fine S at the Skukuza site probably originates predominantly from industrial emissions from the Highveld, i.e. within the Mpumalanga province. Fine K is an indicator for biomass burning (pyrogenic) emissions, and fine Si originates from soil dust.

The summary of seasonal averages of the fine and coarse mode aerosol optical thickness and their percentage distribution is given in Table 3.5. By applying the same aerosol loading classification used in previous sections, aerosol optical thickness of the coarse component can be seen to fall within the limits of the 'very low' class (AOT at 500 nm < 0.1), in comparison with the wide range of optical classes covered by the fine components (very low, low, medium and high).

Table 3-5 Seasonal averages of AOT at 500 nm and percentages distribution of the fine and coarse mode in Mongu and Skukuza.

Period	Seasonal averages for fine and coarse modes							
	Mongu				Skukuza			
	Fine	Coarse	(%) of Fine	(%) of Coarse	Fine	Coarse	(%) of Fine	(%) of Coarse
DJF	0.08	0.05	60	40	0.12	0.04	74	26
MAM	0.08	0.02	77	23	0.13	0.03	79	21
JJA	0.24	0.03	90	10	0.16	0.04	80	20
SON	0.40	0.05	88	12	0.24	0.06	80	20

From December to May, aerosol loadings for the fine component at Mongu were less than 0.1; in this same period values between 0.1 – 0.2 were observed at Skukuza. During winter (JJA) and the early biomass burning season, both sites showed an increase in the presence of fine mode components, with the highest values registered during SON. The changes of

aerosol loadings were more pronounced in Mongu than in Skukuza, where the values fluctuated between 0.1 and 0.3 ('low' and 'medium' classes).

3.2.3 Monthly interannual variability and likely trends of the fine mode aerosols optical thickness over southern Africa

Results outlined in previous sections have shown that the coarse component of the aerosol loading did not change significantly and did not contribute to the very high aerosol loadings in the region. For this reason, further analysis will be concentrated on the fine mode components.

Figure 3.14 shows the monthly inter-annual variability of the fine mode aerosol optical thickness in Mongu and Skukuza. The strength of biomass burning as source of fine particles in the atmosphere can be better evaluated by observing the higher magnitudes of AOT at Mongu when compared to Skukuza. By combining the information (shown in Figure 3.14 and the previous Table 3.5), it is reasonable to conclude that, from December to May, southern Africa experiences a relatively clean atmosphere, followed by a transition period (June to August) of a moderately turbid atmosphere. Finally, from September to October, the atmosphere is laden with high levels of biomass burning aerosols.

The search on the possible trend of the fine mode component, by using the linear regression, shows a very small magnitude of change – i.e. nearly zero, (- 0.0003 for Mongu and - 0.0002 for Skukuza). The slope of regression lines are both negative, indicating possible decreased trend; however this is statistically not sufficiently significant to validate any possible trend. Similarly this result corroborates the previous findings in section 1.1.2.

The separation of the fine component from the total AOT clearly indicates that the inter-annual fluctuations are mainly associated with the variation of aerosol amounts released during the biomass burning season. Assuming that most of the fine particles sources (including forest and savanna fires) were from those most related with human activities, positive changes in human behaviours and practices are possible in the future, thereby significantly reducing the amount of tropospheric aerosols in this region and leading to better air quality. However, the socio-economic implications of the necessary changes required to make a positive impact on the air quality are far reaching and will need independent investigation.

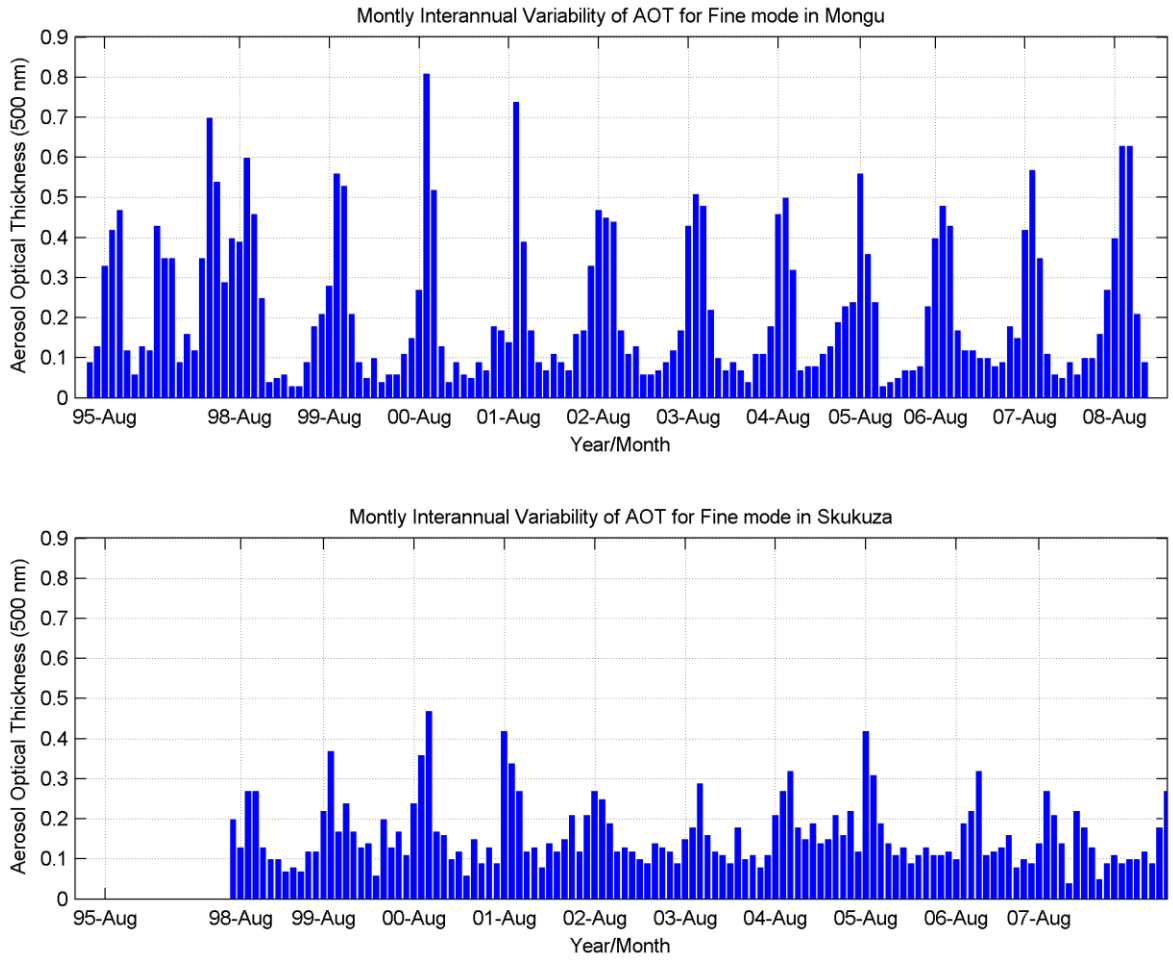

Figure 3-14 Inter-annual variability of the fine mode AOT in Mongu (upper panel) and Skukuza (lower panel).

3.2.4 Analysis of the volume size distribution

The volume size distribution gives the relative concentrations of aerosol particles present in the atmosphere, sorted according to size. The current sun photometer retrieval algorithm for volume size distribution (Dubovik & King, 2000) has shown good agreement with other independent aircraft measurements within southern Africa (Haywood *et al*., 2003). Aerosol size particles in southern Africa cover a wide range of sizes, with typical bio-modal size distribution. Figure 3.15 shows retrieved aerosol volume size distribution in different seasons for Mongu (upper panel) and Skukuza (lower panel). The aerosol mode concentrations vary significantly along the year. From December to May (with average AOT between 0.11 to 0.17), the concentrations of aerosol particles were quite low (less than 0.03 $\mu m^3 \mu m^{-2}$, blue and pink lines in Figure 3.15) and well balanced between both coarse and fine modes concentrations at both sites (Mongu and Skukuza). The winter period and the early stage of biomass burning activities were characterised by the increase

in fine particle concentrations; this increase continued and reached high values during (SON) the peak of biomass burning season.

Changes in concentrations of fine mode particles, from the non-biomass burning periods to the peak of biomass burning periods, were clearly observed at both sites; Mongu showing a higher contribution (by a factor of four) in comparison with Skukuza (by factor of only two). From this perspective, it was clear that biomass-burning in southern Africa is a significant source of fine particles that interact efficiently with the solar radiation and can noticeably affect the radiation budget of the region. The magnitude of the direct forcing associated with biomass burning period at Mongu and Skukuza were discussed and assessed in Chapter 5.

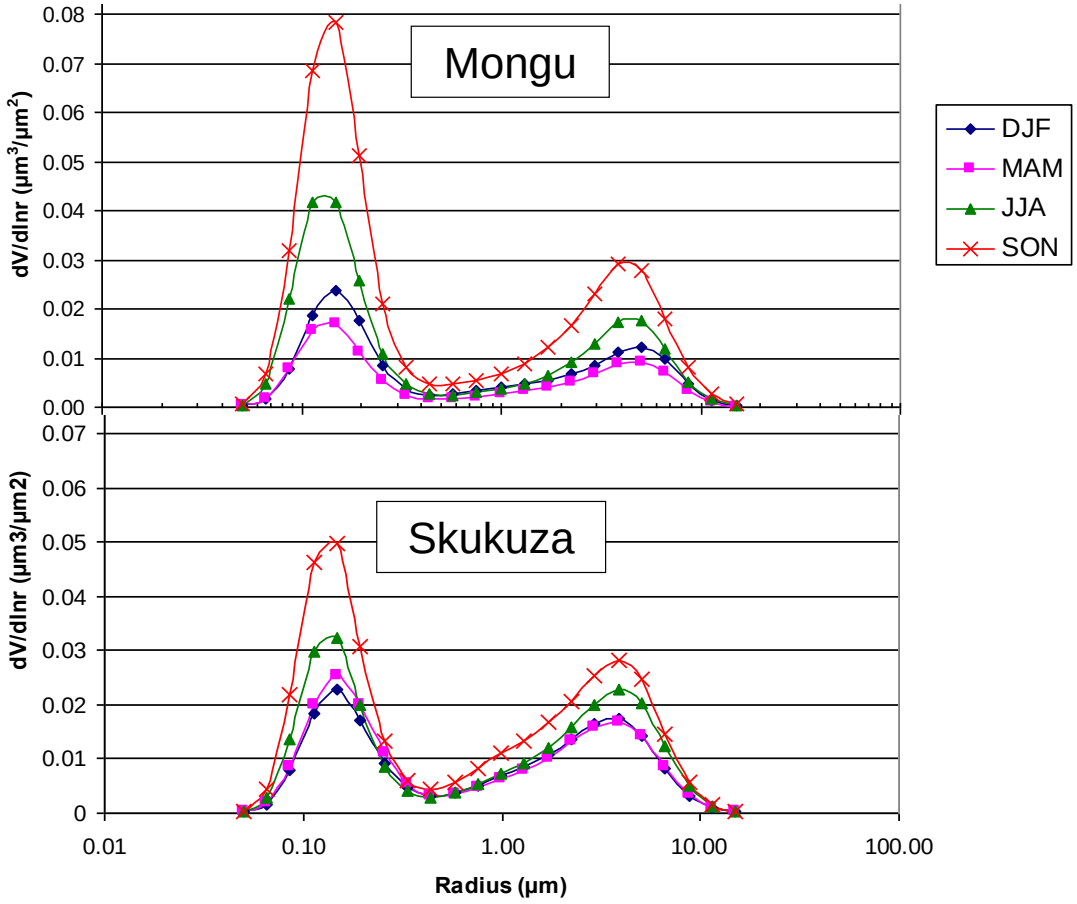

Figure 3-15 Volume size distributions retrievals for different seasons in Mongu (upper panel) and Skukuza (lower panel).

3.3 Column-integrated aerosol single scattering albedo

The single-scattering albedo (SSA) is an important parameter specifying the impact of aerosols on radiative forcing, particularly for absorbing aerosols such as those generated from biomass burning (Kaufman *et al.*, 1997). Previous analyses of the accuracy of SSA

retrievals from AERONET data have shown the combined systematic uncertainty to be ~ 0.01 (Eck *et al*., 2001; Leahy *et al.*, 2007).

Figure 3.16 shows the spectral dependence of SSA between 440 and 1020 nm of wavelength. Single scattering albedo decreased with wavelength at both sites and differences in magnitudes were also observed in all wavelengths. Decreased SSA with wavelength is characteristic of the absorption by small black carbon (BC) particles in a mixture of non-absorbing particles (Eck *et al*., 2001; Dubovik *et al*., 2002).

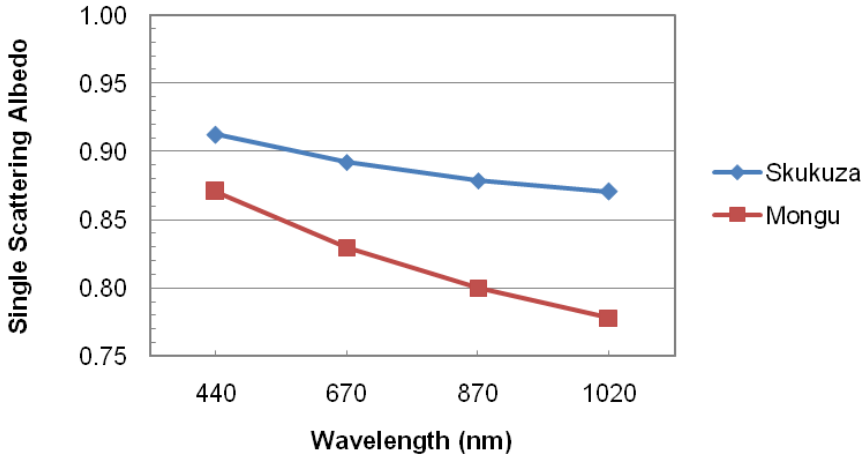

Figure 3-16 Average single scattering albedo throughout the year in Mongu and Skukuza. SSA decreased with wavelength indicating absorption features of the aerosols in southern Africa.

Single scattering values between the two sites show that Mongu has lower values when compared with Skukuza. The high degree of absorption observed over Mongu, i.e. low SSA, is associated with much more black carbon (produced by flaming phase combustion of savanna grass in Zambia) (Ward *et al*., 1996; Eck *et al*., 2003). In general, biomass burning aerosols are known as to be an absorbing aerosol, with high concentrations of black carbon produced by combustion. However, the highest absorption (lowest SSA) is observed for African savanna biomass burning when compared to the Amazonian tropical forest in South America and the boreal forests in North American and Canada (Dubovik *et al*., 2002). Low SSA values may induce additional warming (because of absorption) in the tropospheric column, which then may have implications in the local and regional atmospheric thermodynamics, i.e. increased atmospheric stability and reduced convection.

Special attention was given to the magnitude of the SSA in the visible range (440 to 670 nm), to allow comparison with early studies. In this study, SSA values varied between 0.91 and 0.89 at Skukuza at 440 and 670 nm respectively; at Mongu the values varied between 0.87 and 0.83 at the same wavelengths. Previous radiative forcing studies for southern

Africa have debated the values used for SSA in this region. Ichoku *et al. (*2003) suggested using 0.88 and 0.84 within the same wavelength range (440 and 670 nm) instead of the constant value of 0.90 derived from Brazilian smoke during the SCAR-B experiment. Recently Leahy *et al.* (2007) used (SSA = 0.85 ± 0.02) for this regions. This study suggests that (SSA = 0.85 ± 0.02) is the most representative for the northern region (the area most affected by biomass burning emissions). On the other hand these SSA values are not appropriate south of 20º S, where a different value (showing less absorbing aerosols) would be more realistic for Skukuza, i.e. SSA = 0.90 ± 0.01.

Given the high seasonal variation of biomass burning activity in southern Africa it was reasonable to look more closely to discover what happened to the SSA values within the peak of biomass burning and the non-biomass burning seasons. The results show that, during the peak of biomass burning season, i.e. August, September and October, the SSA values were closer at the two sites; i.e. the percentage amount of absorption increased over Skukuza and remained unchanged over Mongu (Figure 3.17 upper panel).

For the non-biomass burning period and outside the rain season, i.e. April, May and June, the SSA values became more divergent between the two sites; i.e. the percentage amount of absorption decreased significantly over Skukuza (SSA value increased from average value of 0.90 ± 0.01 to 0.93 ± 0.01). For Mongu a small decrease of absorption was observed (SSA value as increased from average value of 0.85 ± 0.02 to 0.86 ± 0.02) (Figure 3.17 lower panel).

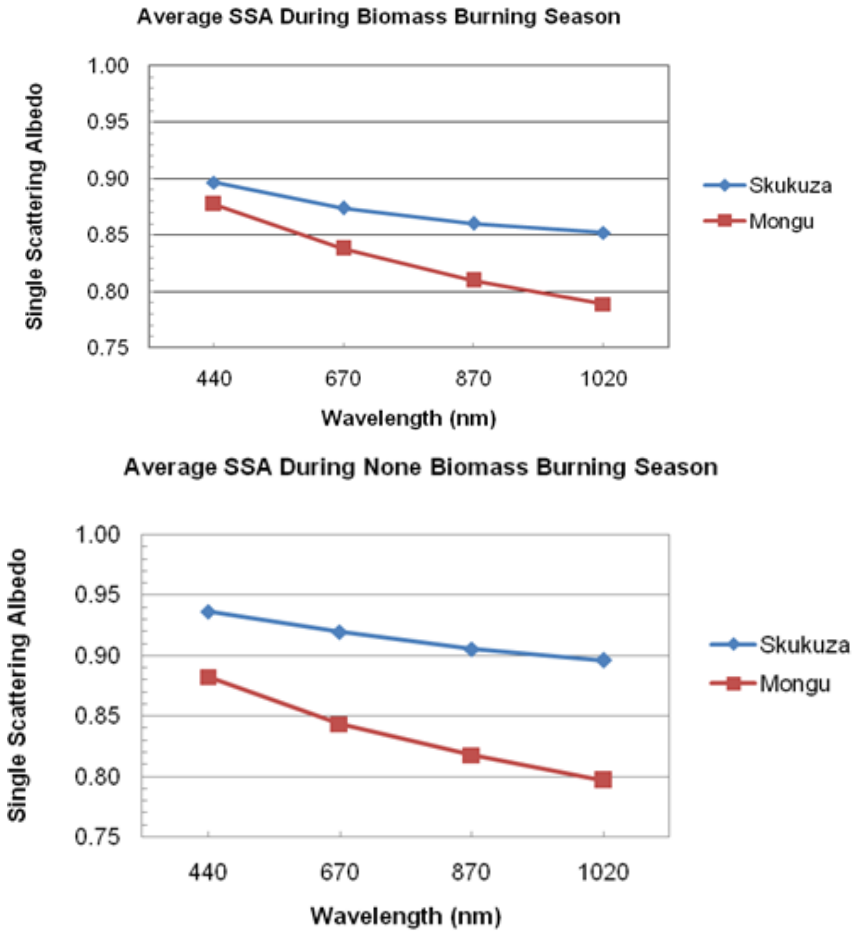

Figure 3-17 Average single scattering albedo over Mongu and Skukuza during the peak of biomass burning season (August, September and October) (upper panel) and none biomass burning season (April, May and June) (Lower panel). Significant change in percentage amount of absorption can be observed over Skukuza.

These results point out that, south of 20º S, the aerosol chemical composition between the non-biomass burning season and the biomass burning season changes significantly. During the biomass burning season, the aerosol composition south of 20º S is a mixture of BC and non-absorbing particles. On the other hand, during non-biomass burning, non-absorbing particles such as sulphates are dominant.

The previous sections of this chapter outlined and discussed the aerosol optical properties in Southern African based on long-term measurements at Mongu in Zambia and Skukuza in South Africa. The main findings can be summarised as following:

- Aerosol optical thicknesses at 500 nm were characterised by low seasonal multi-month mean values (0.11 to 0.17) from December to May; medium values (0.20 to 0.27) between June and August; high to very high values (0.30 to 0.46) during September to November.

- The spatial distribution of aerosol loadings showed that the north had higher magnitudes of AOT than the south in the biomass-burning season and the opposite applied in the non-biomass burning season, i.e. there is a reversal gradient in AOT in this region.
- From the present aerosol data, no long-term discernible trends in aerosol optical thicknesses were observable in this region. However a slight decrease of AOT tended to be depicted by the linear regression analysis; which was statistically not significant for robust conclusion.
- Aerosol volume-size distribution was characterised by low concentrations in the non-biomass burning period and well balanced particle size contributions of both coarse and fine modes. In contrast, high concentrations were characteristic of the biomass burning period, combined with significant dominance of fine mode particles.
- Single scattering albedo values decreased with wavelength, revealing the absorption properties of small black carbon particles. SSA values changed significantly between non-biomass burning and biomass burning seasons, south of 20º S. Little or insignificant changes were observed north of 20º S.

The next section will outline and discuss the aerosol optical properties of different environment beyond southern Africa. In particular, this study will give a summary of the main characteristics of aerosol optical properties in Middle East based on AERONET measurements in Saudi Arabia and United Arab Emirates (UAE) and will discuss how these compare with southern Africa.

3.4 Analysis of aerosol optical properties in Middle East

For a better understanding of the aerosol optical properties for different environments and geographical locations, a secondary region of study in Middle East was selected. The interest in this region was engendered by the fact that Middle East is located at similar geographical latitudes to those of southern Africa (but in the northern hemisphere) and also represents an environment quite different from southern Africa. Additionally, the Climatology Research Group (CRG) at Wits University, under which this study has been conducted, have been an active part of the aerosol research teams in the Middle East since

starting in 2004, i.e. the United Arab Emirates Unified Aerosol Experiment (UAE^2). The detailed science plan of this experiment was described by Reid *et al*. (2004).

The Middle East region selected as a secondary study area is bounded by latitudes 6^o to 36^o N and longitudes 32^o to 72^o E (Figure 3.18). The aerosol environment in this region includes strong regional desert dust sources of predominately coarse mode size particles, maritime sources, intermediate size, and fine mode pollution particle sources from petroleum extraction and processing facilities (Eck *et al*., 2008). The primary area of study for this research, the southern African region, is correspondingly bounded by latitudes 6^o to 30^o S and longitudes 5^o to 45^o E. For this secondary region of study three sites were selected: Solar Village, Saudi Arabia; Dhadnah and Hamin, UAE.

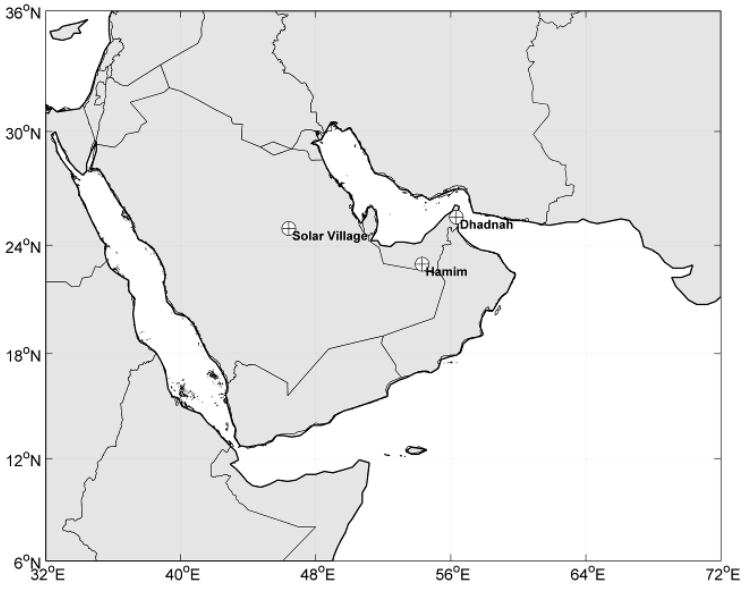

Figure 3-18 Middle East region showing the geographic positions of Solar Village in Saudi Arabia, Dhadnah and Hamin in United Arab Emirates. The three locations are AERONET sites in this region.

3.4.1 Seasonal averages of aerosol optical thickness in Middle East

The three sites in Middle East (Solar Village, Dhadnah and Hamin) have the longest record of ground based aerosol measurements provided by AERONET programme in this region. The data used for this analysis covered the periods of 1999 - 2008 for Solar Village in Saudi Arabia; 2004 - 2007 for both Hamin and Dhadnah in United Arab Emirates (UAE). Analysis of seasonal means of AOT at 500 nm for different size components (total, fine and coarse) are summarised in Table 3.6.

The annual means of AOT for the two sites in the UAE. i.e. Hamin — inland desert, located ~125 km inland from the Gulf, and Dhadnah — coastal, located near the coast of

the Gulf of Oman, have higher values (0.37 and 0.39) than the inland desert site in Saudi Arabia (Solar Village with annual mean of 0.32). The values in all three Middle East sites are significantly higher when compared with the annual means for Mongu — 0.28 and for Skukuza — 0.21 in southern Africa.

Examination of the data, for both fine and coarse components in the Middle East, revealed that the AOT of the coarse component has similar magnitude of annual averages at all three sites, ranging between 0.22 and 0.23. Noticeable differences can be observed for the fine component, with AOT magnitudes of 0.14 and 0.16 for Hamin and Dhadnah respectively, and 0.11 for Solar Village. The coastal site of Dhadnah is likely to be influenced by fine mode pollution particle sources from petroleum extraction and processing facilities (Eck *et al*., 2008). However coarse aerosols (desert dust) are still the largest size fraction at all three sites.

Table 3-6 Seasonal averages of AOT at 500 nm and percentage distribution of the total (T), fine (F) and coarse (C) mode components in Solar Village, Hamin and Dhadnah.

Period	Seasonal averages of AOT and percentages distributions for fine and coarse															
	Solar Village					Hamin					Dhadnah					
	T	F	C	% F	% C	T	F	C	% F	% C	T	F	C	% F	% C	
DJF	0.22	0.08	0.13	38	62	0.25	0.12	0.13	48	52	0.25	0.14	0.11	56	44	
MAM	0.43	0.10	0.33	23	77	0.36	0.10	0.26	28	72	0.39	0.12	0.27	31	69	
JJA	0.40	0.13	0.27	33	67	0.56	0.17	0.39	30	70	0.57	0.20	0.37	35	65	
SON	0.25	0.12	0.13	48	52	0.29	0.15	0.14	52	48	0.36	0.20	0.16	56	44	
Ann.	0.32	0.11	0.22	33	67	0.37	0.14	0.23	38	62	0.39	0.16	0.23	41	59	

Aerosol seasonal variation

Seasonal variability of the AOT indicated lower aerosol content in Autumn (SON) and Winter (DJF) in this region of the northern hemisphere. By contrast, aerosol content was significantly higher in Spring (MAM) and Summer (JJA). At all three sites the peak of AOT was associated with the increase of coarse particles occurring in May in Saudi Arabia (Solar Village), and July (for both Hamin and Dhadnah) in the UAE. These results corroborate the findings of (Sabbah & Hassan, 2008; Eck *et al*., 2008), which showed that high AOT magnitudes during spring are because of the increase in wind speed and with the 'haboob' events (strong surface winds as a result of thunderstorm outflow) observed frequently in Summer.

Conversely, in the Middle East, from September to February, the aerosol content was observed to be relatively low; from March to August, the aerosol content was relatively high. The main source of coarse particles in this region is more likely to be wind-blown desert dust (Sabbah & Hassan, 2008; Eck *et al*., 2008).

Frequency distributionn of fine and coarse components

The frequency distribution of fine and coarse components clearly indicated that coarse fractions dominate in this region. On average, the coarse component accounted for 67% at Solar Village; 62% at Hamin and 59% at Dhadnah. These results highlight the source strength of coarse particles in Middle East. During Spring (MAM), the coarse component was between 69% and 77% for the three sites and during Autumn (SON), the coarse component is reduced to 52% at Solar Village, 48% at Hamin and 44% at Dhadnah.

3.4.2 Comparisons of aerosol loads in Middle East and southern Africa

Given the aerosol loading classification (as determined for southern Africa in Section 3.1.3) the frequency distribution of the AOT magnitudes in Middle East were assessed (Table 3.7). If the threshold value of AOT is established as being equal to 0.3 at 500 nm; the probability that the total AOT would be greater than the 0.3 was 46% at Solar Village, 54% at Hamin and 63% at Dhadnah. These percentages, when compared with southern Africa (Mongu (33.8%) and Skukuza (19.6%), are significantly higher at the given threshold. However, during the biomass burning period in southern Africa, aerosol loading levels were comparable to Dhadnah (in the case of Mongu) and to Solar Village (in the case of Skukuza).

Table 3-7 Probability of occurrence of different aerosol modes at selected sites in the Middle East and southern Africa.

Aerosol loadings classes (reference to southern Africa)	AOT range	Probability within the range (%)				
		Solar Village	Hamin	Dhadnah	Mongu	Skukuza
Very Low	< 0.1	7.3	2.1	2.9	23.7	27.8
Low	0.1 – 0.2	18.0	18.9	14.1	26.7	31.9
Medium	0.2 – 0.3	28.1	25.1	20.1	15.7	20.7
High	0.3 – 0.5	31.4	36.3	36.8	17.4	13.8
Very High	> 0.5	15.2	17.6	26.1	16.4	5.8

The high levels of aerosol loading in Middle East are associated with coarse particles from desert dust (Sabbah & Hassan, 2008; Eck *et al*., 2008); in southern Africa high episodes of

AOT are associated with fine particles mainly from biomass burning or biofuel combustion (Holben *et al*., 2001; Eck *et al*., 2003; Swap *et al*., 2003).

Low levels of aerosol loadings (AOT < 0.2) are infrequent in Middle East when compared to levels experienced in southern Africa. AOT values of less than 0.2 accounted for about 20% in Middle East, whereas in southern Africa the equivalent levels were higher than 50%. These differences in aerosol loading levels, and the dominant size particle and composition, lead to significant differences in the optical properties of these two environments.

3.4.3 Inter-annual variability and trends of fine and coarse mode aerosols optical thickness in Middle East

The inter-annual variability of AOT in Middle East is presented in the next section by evaluating the deviation from multi-year monthly means of AOT for both fine and coarse components. The aerosol long term trends were also assessed and compared with southern Africa.

Solar Village

Departures from multi-year monthly means of the fine and coarse mode aerosol components show smooth and significant inter-annual variability for the fine and coarse aerosols respectively (Figure 3.19). Long-term trends on the fine mode component were not discernible. However, an increasing trend was observed in the coarse component (Figure 3. 19, lower panel), notable between 2003 and 2008, by positive deviations. Xia (2011), also using a time series of monthly anomalies from AERONET data, reported a strong and significant increasing trend of AOT (0.17 per decade). He also demonstrated that increased AOT goes with a decreased Ångström exponent, indicating increased dust activities over this site.

Hamin and Dhadnah

The inter-annual variability and trends of AOT at Hamin in UAE were similar to those from the Solar Village site in Saudi Arabia. The inter-annual variability and trend was more pronounced for coarse components in comparison with the fine mode. For the coastal site of Dhadnah, the results showed more pronounced inter-annual variability for coarse components when compared to the fine mode (Figure 3. 20). However in terms of trends, the fine mode also showed a positive trend when compared with the other two sites (Table 3.8). de Meij, *et al. (*2010), using both MODIS and MISR showed positive trends of AOT

in Dhadnah without explicitly mentioning the particle size. The existence (or otherwise) of this observed trend should be reviewed in the future, because the current data period used in this study is short (only five years) and a longer period of data collection would result in a better and more accurate assessment of any possible trend.

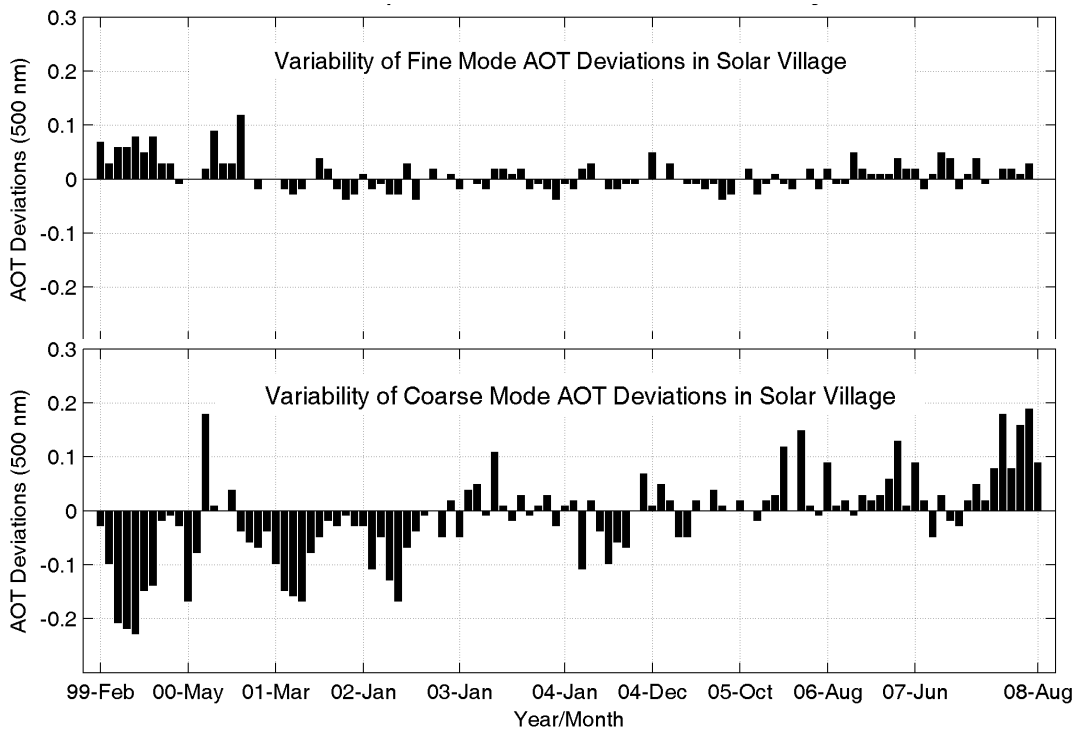

Figure 3-19 Deviations of aerosol optical thickness for fine and coarse modes in Solar Village, showing that an upward (increasing load) of aerosols are mainly in the coarse mode fraction (lower panel).

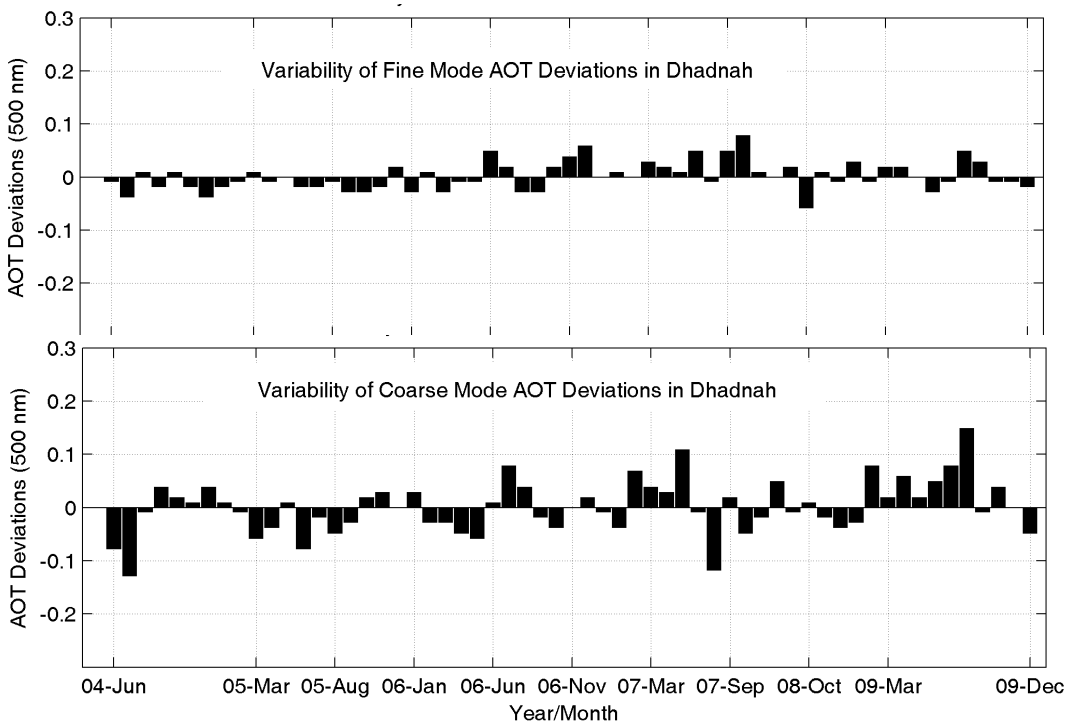

Figure 3-20 Deviations of aerosol optical thickness for fine and coarse modes in Dhadnah, with the coarse component showing an increasing trend.

Table 3.8 summarises the trend analysis, using the slope of regression line (where positive or negative values indicate possible increased or decreased trend) at all three sites in the Middle East plus the two sites in southern Africa. The positive sign and magnitude of the slope of regression line demonstrated an increasing trend for coarse particles (dust) for both the inland desert sites of Solar Village in Saudi Arabia and Hamin in UAE. The increased trend (positive slope) is also observed in Dhadnah; however the fine component is likely more increased than coarse component.

In southern Africa no discernible trend was identified, yet a negative slope was observed, but this is not statistically robust enough to draw a convincing conclusion. The reasons associated with the possible increase of aerosols in Middle East do not form part of this study.

Table 3-8 Aerosol trends within the observation period given by the slope of linear regression in different sites across Middle East and Southern Africa.

Aerosol Modes	Slope of linear regression				
	Solar Village	Hamin	Dhadnah	Mongu	Skukuza
Total	+0.0014	+0.0014	+0.0010	-0.001	-0.0002
Fine	-0.0002	-0.0003	+0.0004	-0.0003	-0.0002
Coarse	+0.0020	+0.0020	+0.0001	-0.0001	-0.0001

3.4.4 Analysis of Ångström exponent, volume size distribution and single scattering albedo over Solar Village, Hamin and Dhadnah

Ångström exponent

Table 3.9 shows the frequency distribution of Ångström exponent (α) within different classes. The α-values presented in this table were computed from 440 to 870 nm wavelengths. The dominant size range was below one; indicating that the aerosol particle size was mainly coarse mode (to a larger extent in Solar Village than in Hamin and Dhadnah). The probability that particle sizes would be within the coarse fraction was above 70% in all sites. Though the fine fraction was consistently the smaller fraction of the total aerosol loading, it occurred more in Dhadnah than in Hamin and Solar Village. These results reinforced the previous findings that Solar Village and Hamin are predominately dominated by dust particles with very little fine particles, while at Dhadnah a mixture of coarse (dust) and fine particles from petrochemical extraction and processing is significant (Eck *et al*., 2008).

Table 3-9 Ångström exponent classes and their probabilities for selected sites in the Middle East.

Ångström exponent	Probability within the range (%)		
	Solar Village	Hamin	Dhadnah
< 0.5	40.4	31.9	20.7
0.5 – 1.0	43.3	42.2	47.3
1.0 – 1.5	13.8	23.2	27.9
1.5 – 2.0	1.4	2.4	3.8
> 2.0	0	0.3	0.1

Volume size distribution

The multi-year seasonal volume size distribution for Solar Village and Dhadnah is presented in (Figure 3.21 and Figure 3.22). Size distribution was almost uni-modal (coarse) for Solar Village and bi-modal for Dhadnah, yet the concentration of fine mode was significantly lower when compared to coarse mode. For the entire year, concentrations of coarse particles dominated in both sites, with a mean radius around 15 µm.

The variation in aerosol volume size distribution is clearly noticeable within the coarse mode, while the fine mode remains relatively stable. The magnitudes of the volume size distribution of the coarse mode were high during Spring (MAM) and Summer (JJA) and low during Winter (DJF) and Autumn (SON). The peak concentrations at Solar village occur within MAM and JJA for Dhadnah. These results confirm that Spring was dustier than Summer in Solar Village (Sabbah & Hasan, 2008) and also shows that Summer was dustier than Spring in Dhadnah.

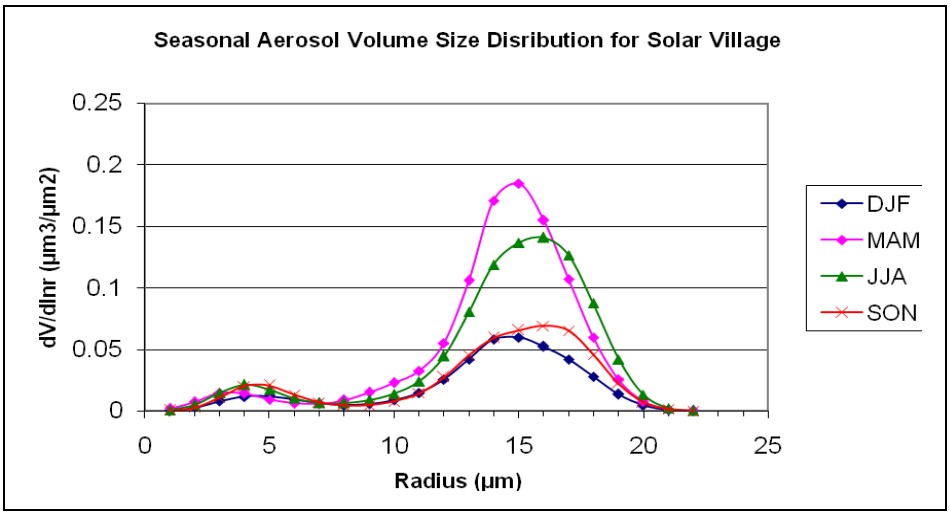

Figure 3-21 Volume size distributions retrievals for different seasons in Solar Village, showing that coarse particles were the main source of aerosols in this site.

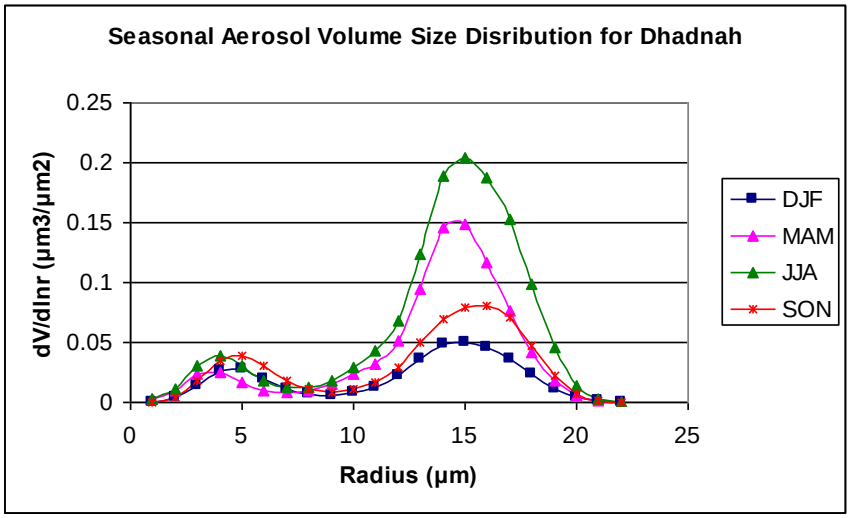

Figure 3-22 Volume size distributions retrievals for different seasons in Dhadnah.

Single Scattering Albedo

The single scattering albedo (SSA) in the Middle East increased with wavelength (as shown in Figure 3.23) and is consistent with a number of dust aerosols (Dubovik *et al*., 2002). SSA for dust increases with wavelength in the range of 0.3 to 1.0 µm. This is because of significantly higher absorption in the UV and visible wavelengths (less than ~ 0.6 µm - because of electronic bands) and lower absorption at longer solar wavelengths (675-1020 nm) (Bergstrom *et al*., 2002; Eck *et al*., 2008).

The magnitude of the SSA in the visible range (440 to 670 nm) varied between 0.89 to 0.94 at Solar Village and 0.93 to 0.94 at Dhadnah. Differences in SSA magnitudes were evident for shorter wavelengths (small particles were relatively more abundant in Dhadnah); interaction with solar radiation (shorter wavelength) was more efficient when compared with the coarse particles dominating at Solar Village. The frequent presence of small particles from petrochemical facilities over the coastal site of Dhadnah increased the SSA compared to the inland desert site of Solar Village. Eck *et al. (*2008) reported higher single scattering albedo for the pollution-dominated events over the Gulf than at the desert inland site. Additional analysis on the variation of the single scattering albedo in the different seasons was also conducted. The results showed no significant changes of SSA values in these two sites.

In southern Africa the SSA, in the visible range, behaved in different manner, i.e. the SSA decreased with wavelength and the absorption was even higher at longer wavelengths (675-1020 nm) when compared to the less absorbing dust in Middle East (Eck *et al*., 2008).

The percentage amount of absorption was higher for aerosol particles in southern Africa (dominated by biomass burning) compared to Middle East (dominated by dust particles).

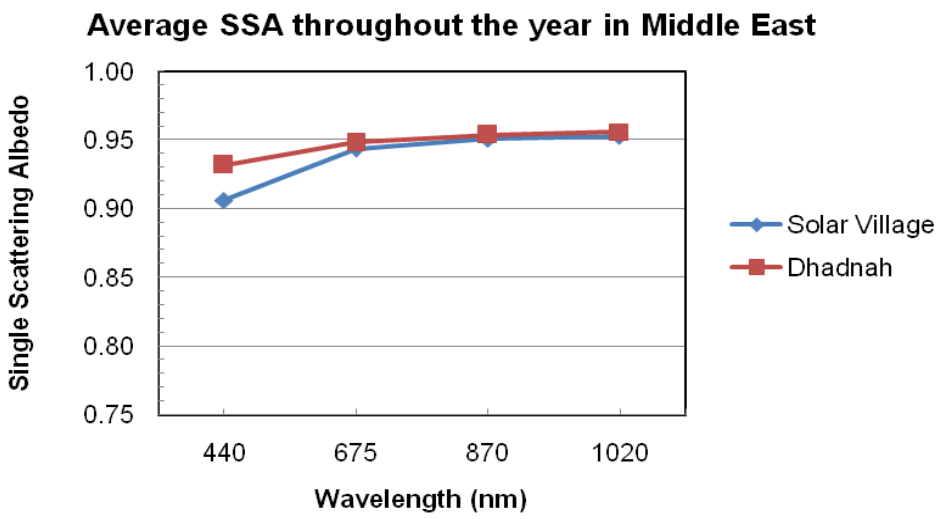

Figure 3-23 Average single scattering albedo throughout the year in Solar Village and Dhadnah. SSA increased with wavelength indicating absorption features of a number of dust aerosols.

The current analysis of the aerosol optical properties in the Middle East allowed defining main differences between Middle East and Southern Africa as follows:

- Aerosol loading levels in Middle East were higher than Southern Africa;
- Aerosol size particles in Middle East were dominated by coarse particles (desert dust), in contrast fine particles (mainly from biomass burning) dominated in Southern Africa;
- Aerosol volume size distribution was clearly bimodal in Southern Africa: primarily almost uni-modal (coarse) over the inland desert sites in Middle East;
- Single scattering albedo in visible range, increased with wavelength in Middle East, whereas this decreased in Southern Africa. The percentage amount of absorption is high for aerosol particles in southern Africa (dominated by biomass burning) compared to Middle East (dominated by dust particles). In addition dust particles are less absorbing at longer wavelengths (675 - 1020 nm) compared to biomass burning aerosols.
- The aerosol optical properties differences observed in these two environments demonstrate the need to characterise aerosols at regional scale or less, and improve the quantity and quality of measurements.

****

Long-term measurements of aerosol optical parameters over southern Africa provided valuable data to compile a picture of the climatology of aerosol optical properties. Statistical analyses on temporal and spatial variation of aerosol optical thickness; the Ångström exponent; size distribution and single scattering albedo were presented. Analysis was also extended to include separate size modes, i.e. coarse and fine. Similar analysis of aerosol optical properties was performed for secondary study region in Middle East. This allowed comparisons of the aerosol radiative properties between southern Africa and the Middle East. The next chapter will discuss the solar radiation flux measurements and the aerosol forcing assessment during SAFARI 2000.

Chapter 4.

This chapter presents the surface solar fluxes measurements at Skukuza during SAFARI 2000; identifies and describes the clear sky days from combined instruments; discusses the air mass back trajectory of the selected clear sky days for better understanding the aerosol origins and the associated optical properties. The influence of aerosols in radiation fluxes changes at the surface is accessed.

4 Solar Radiation Fluxes Measurements and Aerosol Radiative Forcing Assessment

Aerosols modify the Earth-atmosphere energy budget through various atmospheric processes e.g. the direct effect by scattering and absorption of the solar and Earth's radiation (Charlson *et al*., 1992); the semi-direct effect by changing atmospheric thermodynamics and cloud formation (Koren *et al*., 2004) and the indirect effect by changing cloud microphysics (Rosenfeld & Lensky, 1998). The addition of anthropogenic aerosols to the atmosphere may change the radiative fluxes at the top-of-atmosphere (TOA), within the atmospheric column and at the bottom of atmosphere (BOA), and hence perturb the energy balance of all climate systems.

The impact of aerosols on the Earth´s energy budget can be quantified in terms of aerosol radiative forcing (ARF) - defined as the difference between atmospheric radiative fluxes when aerosols are present and when they are absent (Vogelmann *et al*., 2003). In this regard, the ability to measure accurately the global and diffuse solar fluxes near the Earth's surface in cloud-free conditions is fundamental for assessing the ARF and for testing aerosol models being used to calculate radiative forcing of climate (Kaufman *et al*., 2002).

During the SAFARI 2000 experiment, a set of instruments were deployed at Skukuza to measure the global, direct and diffuse solar fluxes. In addition, a total sky imager (to assess the cloud cover fraction in atmosphere) was also deployed and the amount of atmospheric aerosols were quantified by ground based sun photometers from AERONET (positioned in different locations across Southern Africa) (Holben *et al*., 1998). Detailed explanations of the instruments used to measure the above mentioned parameters during SAFARI 2000 were given in Chapter 1, under the literature review section (1.2.4).

4.1 Radiation fluxes measurements during SAFARI 2000

Three parameters of surface radiation fluxes were measured at Skukuza: global, direct and diffuse. The global radiation fluxes were measured by a precision spectral pyranometer (PSP); direct radiation fluxes were measured by a normal incidence pyrheliometer (NIP) and the diffuse radiation was measured by a precision spectral pyranometer (shaded).

The measurements were taken every one minute, for the period 17 August to 16 September 2000. Figure 4.1 presents the time series of global, direct and diffuse solar radiation measurements taken at Skukuza. During the measurement period, distinct cycles of radiation fields, characterising different states of atmosphere, were observed. In some cases, an increase in the diffuse radiation was followed by a reduction in the direct solar radiation, suggesting strong attenuation of the solar radiation because of the presence of clouds or aerosols in the atmosphere. The instantaneous values of daily global solar radiation reached maximum values of about 1000 W m^{-2} and minimal values of ~200 W m^{-2} (Figure 4.1, upper panel); the maximum value of diffuse solar radiation was often below 200 W m^{-2}. However this level can reach as high as 500 W m^{-2} (Figure 4.1, lower panel).

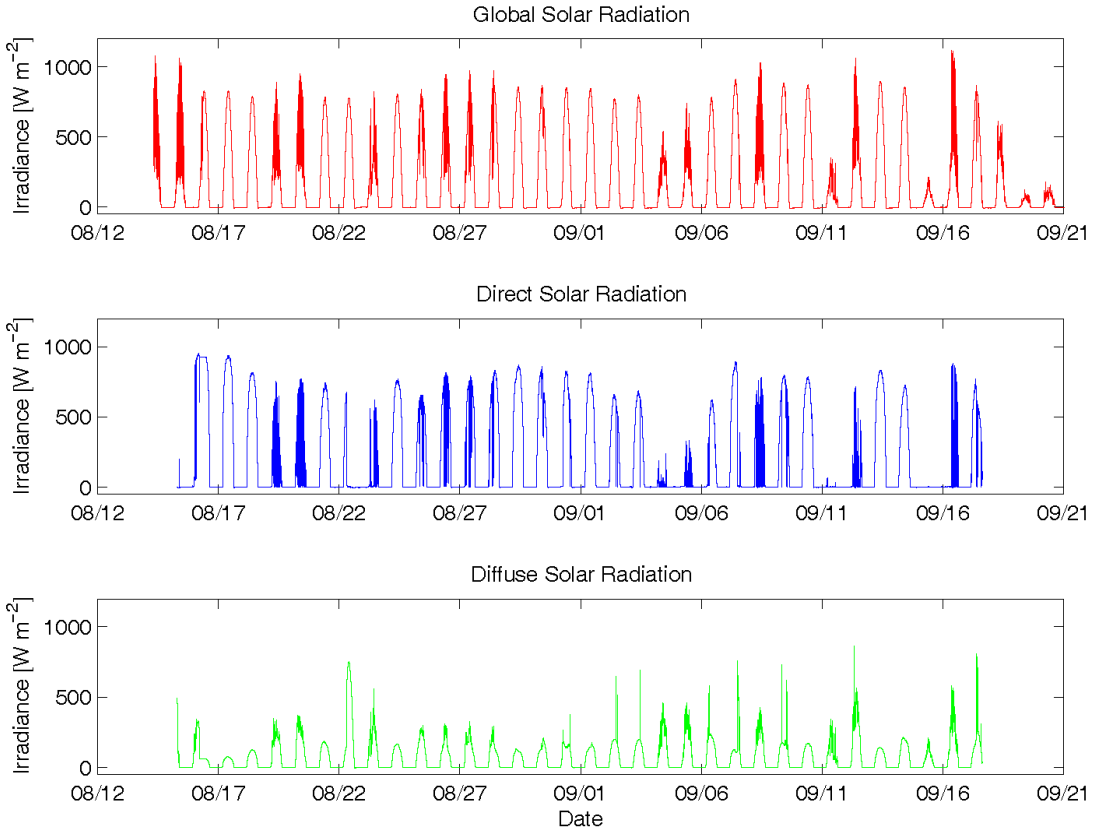

Figure 4-1 Time series of the global, direct and diffuse solar irradiances as measured by solar radiometers at Skukuza from 17 August to 16 September 2000.

By fitting the regression line between the global radiation component and the sum of direct and diffuse components, the linear relationship can be confirmed, i.e. global = direct + diffuse, as represented in Figure 4.2. It is important to mention that three independent instruments (one for each component) were used to generate the measurement data. The current instantaneous solar fluxes data were examined to identify cloud free days and used to investigate the changes of solar fluxes associated with the variation of aerosols concentrations in the atmosphere. This will be discussed in the next sections.

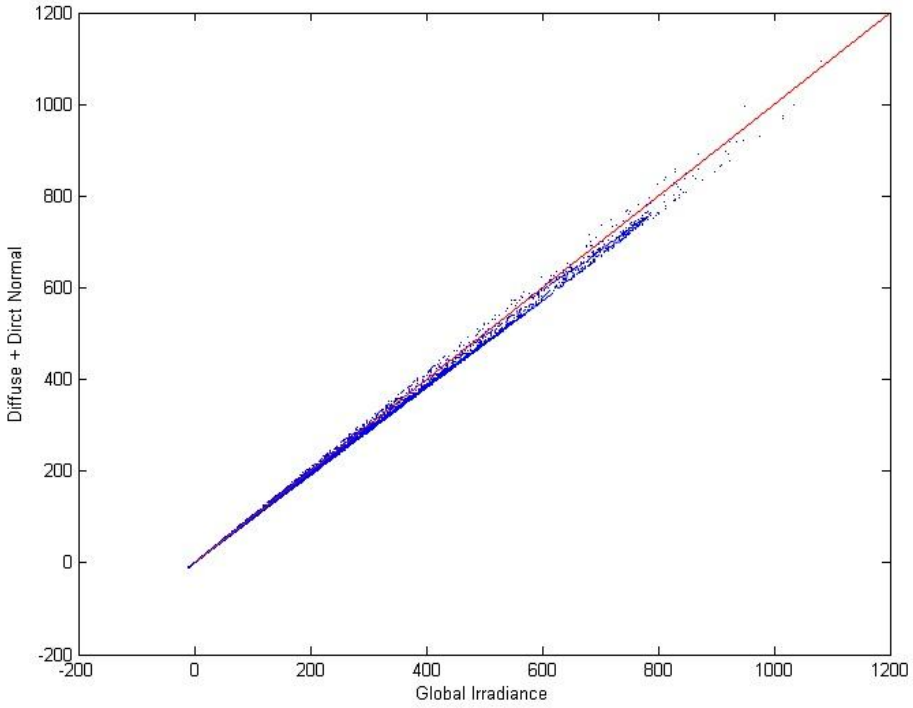

Figure 4-2 Linear relationships between the global solar component and the sum of direct normal and diffuse components. Blue points represent measured solar flux data and the red line, the linear fitting.

4.2 Radiation Fluxes Measurements and Clear Sky Identification

Solar radiation flux measurements are hampered by persistent (and frequent) broken cloud fields, making it difficult to assess the aerosol radiative forcing. Accurate assessment of the real state of the atmosphere is fundamental to understanding the forcing elements in the atmosphere.

The radiative forcing by aerosols in the atmosphere can be better assessed without the presence of clouds (which are present most of the time making assessments more difficult). Therefore accurate identification of clear sky conditions is essential for studying aerosol radiative forcing and this exercise may require the use of multiple instruments.

The acquired radiation fluxes at Skukuza (presented in Section 4.1) were screened to distinguish cloudy or cloud free days. From the measured radiation fluxes it is possible, in principle, to identify the state of the atmosphere, particularly on a cloud free day. By observing the time series plot of daily instantaneous radiation measurements given by the precision spectral pyranometer (PSP), it is possible to distinguish typical patterns observed in cloudy or cloud free measurements.

Figure 4.3 (upper panel) shows a typical pattern given by global solar flux measurement for both a cloudy and a cloudless day. A noisy time series can be observed for a cloudy day (12 September 2000); conversely, a smooth curve is characteristic of a cloud-free day (e.g. 13 September 2000).

To improve the accuracy of the identification of cloud free days during the measurement period, additional instruments were used. The pictures from the total sky imager (TSI) and the vertical profile of the Micro Pulse Lidar (MPL) were analysed. For example, the previous two days, shown as cloudy or cloudless days respectively, were checked for confirmation. 12 September 2000 was a cloudy day, while the following day, 13 September, was cloudless (Figure 4-3, middle and lower panels).

4.3 In Depth Analysis of the Selected Cloud Free Days

The previous methods for selecting cloud-free days, i.e. by observing the plotted instantaneous global or direct fluxes for each day and checking the processed pictures from the TSI and MPL, gave confidence in the selection of cloud-free days.

The screening results for cloud free days confirm that solar radiation fluxes are hampered most of the time by persistent broken cloud fields. For example, during the 31-day measurement period from 17 August to 16 September 2000, only eight days were cloud-free days at Skukuza (Table 4.1 first column). In addition, the period of measurement (August and September) fell outside the summer rain season in southern Africa.

On cloud free days, the attenuation of solar radiation can be rightfully attributed to the aerosols and gas constituents of the atmosphere; the changes of radiation fluxes from one cloud free day to another can be mainly attributed to changes on aerosol loading in the atmosphere.

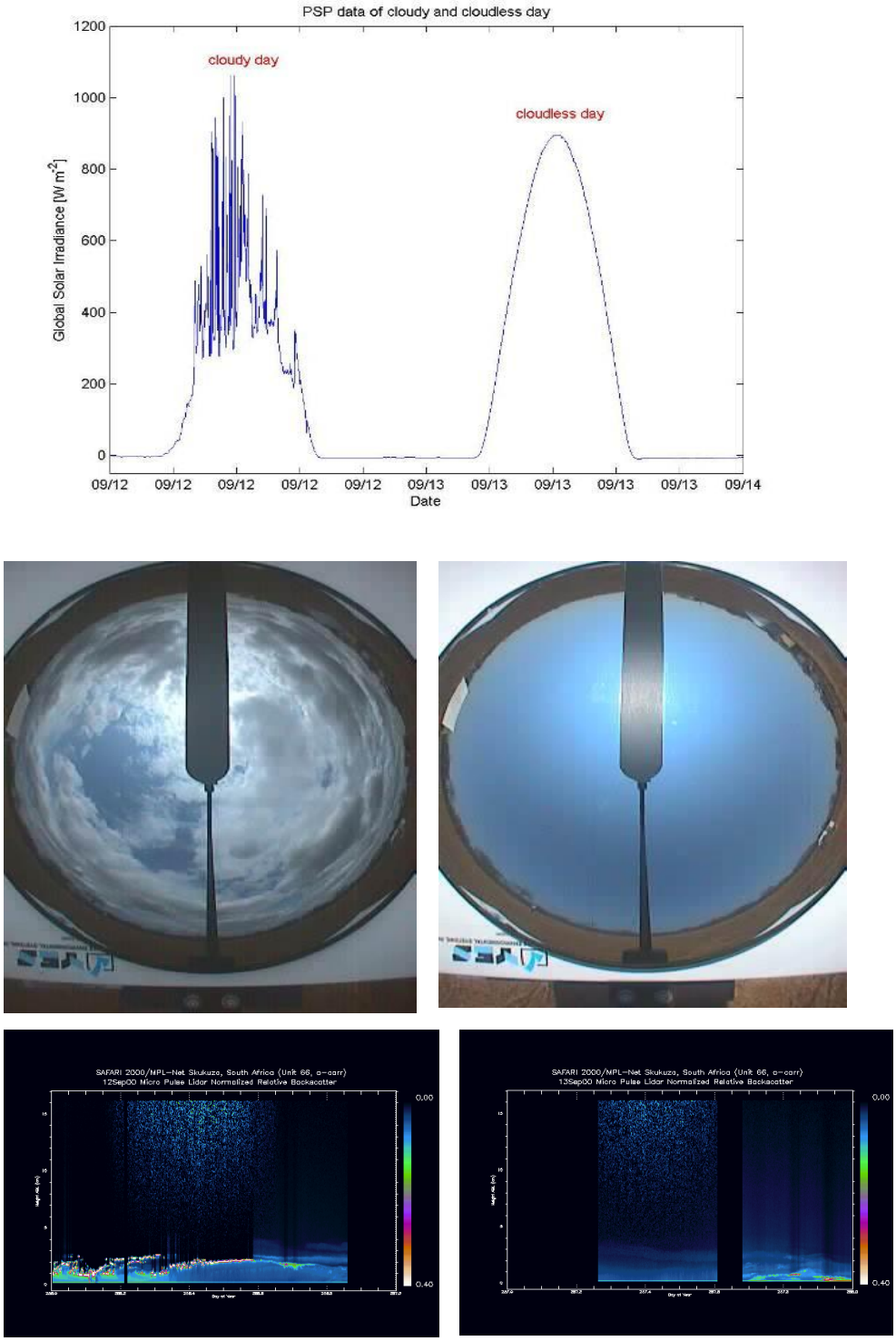

Figure 4-3 Typical patterns associated with different sky conditions, for a cloudy or a cloudless day, recorded by different instruments: PSP (upper), TSI (middle) and MPL (lower). From PSP measurements, a noisy time series was observed on a cloudy day—12 September 2000; a smooth curve was associated with a cloud-free day —13 September 2000.

Table 4.1, gives the qualitative and quantitative descriptions of the state of the atmosphere of each cloud free day by cross linking specific aerosol optical properties, such as the diurnal variation of the AOT and the daily average of the Ångström exponent. This analysis also allowed linking each selected cloud free day with the aerosol load classification given in Chapter 3. The amount of maximum direct and diffuse fluxes is also presented.

The collection of parameters given in Table 4.1 facilitates the understanding of the variation of aerosol concentrations in the atmosphere as direct influences in both the atmospheric turbidity and the amount of direct and diffuse solar fluxes reaching the ground. For instance, cloud free days, with low content of aerosols, have high maximum direct fluxes and low maximum diffuse fluxes. The inverse occurs with increased aerosol concentrations.

Table 4-1 Qualitative and quantitative description of the state of atmosphere for each cloud-free day. The eight cloud-free days covered different aerosol loadings magnitudes, from very low aerosol loading to very high loadings. In addition, random changes of aerosol loadings during the day can be observed.

Date	Likely state of the atmosphere	Daily average Ang. Exp.	Diurnal AOT range at 500 nm	Aerosol loading classes	Maximum Direct Flux ($W\ m^{-2}$)	Maximum Diffuse Flux ($W\ m^{-2}$)
17 Aug	Very clear day and very low aerosol loading	1.55	0.05 – 0.09	Very Low	930	75
18 Aug	Cloudless, hazy early morning otherwise clear late morning and afternoon	1.76	0.22 – 0.26	Medium	817	124
21 Aug	Cloudless, but very hazy all day	1.99	0.4 – 0.6	High to Very High	740	185
24 Aug	Cloudless, very hazy in the morning	1.83	0.30 – 0.45	High	758	167
29 Aug	Cloudless, hazy in the morning to moderate clear in the afternoon	1.83	0.20 – 0.28	Medium	862	126
01 Sep	Cloudless, clear in the morning and very hazy in the afternoon, possible smoke or very high cirrus clouds	1.63	0.25 – 0.75	Medium to Very High	807	172
13 Sep	Cloudless and hazy almost all day	1.60	0.26 – 0.30	Medium	830	140
14 Sep	Cloudless and hazy almost all day	1.54	0.45 – 0.61	High to Very High	715	212

An important output from this analysis is that the eight cloud-free days selected at Skukuza, covered almost all aerosol loading classes from 'Very low' to 'Very High'. This diverse state of the atmosphere in cloud free days served as 'golden dates' for assessing the direct forcing by aerosols at Skukuza and was also applied in final calculation of direct forcing at Mongu (Section 5.4 in Table 5.6).

4.3.1 Analysis of air mass transport to Skukuza for the selected cloud free days

For better understanding the aerosol dynamics associated with the selected cloud free days, air mass transport to Skukuza within a limited number of days will be discussed. Three days backward trajectories from midnight (24H00) for each selected day was performed using the trajectory model HYSPLIT_4 (HYbrid Single-Particle Lagrangian Integrated Trajectory) model Version 4 (Draxler *et al*., 2009). The backward trajectories were simulated at three different levels of the atmosphere (850, 700 and 500 hPa).

The simulated trajectories were assumed to be responsible for advecting aerosols over southern Africa in general (and to Skukuza in particular), therefore the analysis will give information on possible aerosol origins (and the likely particle size) by combining the Ångström exponent values and retrieved size distribution. The following analysis for each cloud free day has been grouped according to the aerosol loading classification given in Table 4.1.

Transport under very low aerosol loading conditions

From the selected eight days, it was possible to identify only one day (17 August 2000) as having close to pristine conditions, when it was characterised by very low AOT values, ranging between 0.05 to 0.09, a relatively low average of Ångström exponent (1.55) and low maximum diffuse fluxes, 75 W m^{-2}, confirming the lower presence of aerosols, i.e. little scattered radiation. Consequently this day was used to represent, hypothetically, the tropospheric condition "*without aerosols*" in the calculation of changes in surface radiation fluxes under the selected cloud free days and different aerosol concentrations (next sections).

The three days back trajectory simulation from 17 August 2000 shows a persistent maritime flow (Easterly flow) to Skukuza for all three atmospheric levels at 850, 700 and 500 hPa (Figure 4.4, left panel). In addition the volume size distributions confirmed the low concentrations of aerosols and the dominance of the coarse mode on this day (Figure

4.4, right panel). In this sense, it is reasonable to say that the observed very low aerosol loading conditions and low attenuation of solar radiation are closely associated with clean coarse mode maritime aerosols.

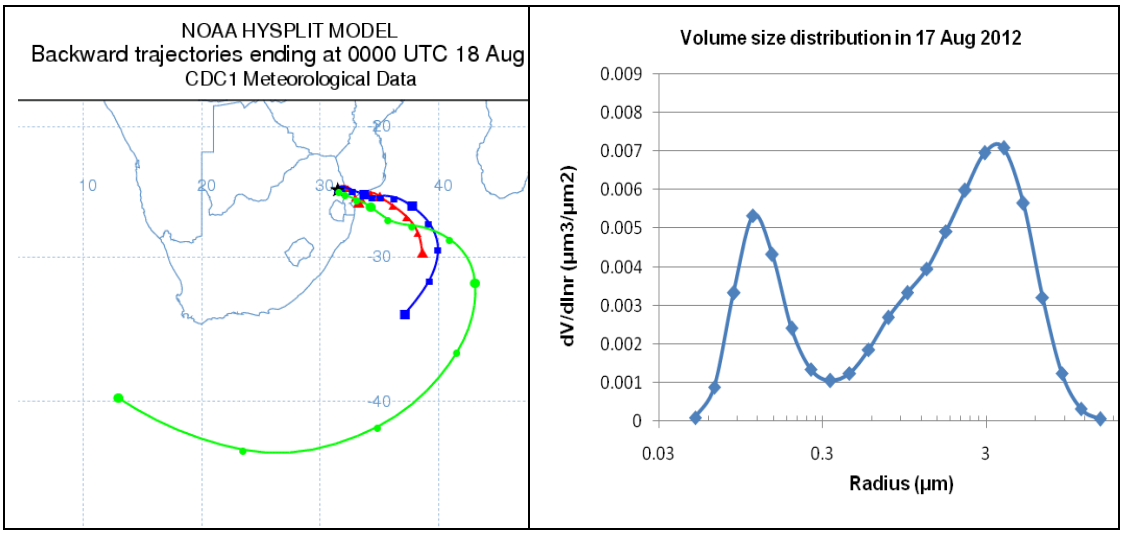

Figure 4-4 Three-day back trajectories from 17 August 2000 (midnight), under very low aerosol loading conditions showing persistent maritime flow to Skukuza at 850 hPa (red), 700 hPa (blue) and 500 hPa (green), left panel. On the right panel the volume size distribution is presented.

Transport under the medium aerosol loading conditions

Three of the eight selected days fell in the range of medium aerosol loading (0.2 < AOT <0.3) and, for illustration purposes only, two days were selected for discussion (18 and 29 August 2000). On both days back trajectory simulations show that air mass transport to Skukuza was mainly characterised by a mixture of maritime and sub continental flows; however differences on flow direction may be noted at different levels (Figure 4.5, upper blocks).

The air mass transport to Skukuza, arriving on 18 August 2000, with a relatively small diurnal AOT range (0.20 – 0.26), was dominated by maritime transport (easterly flow) at low levels (850 and 700 hPa) and a sub continental transport (westerly flow) at high level (500 hPa) (Figure 4.5, upper blocks, left panel). Also, with approximately the same AOT range (0.20 – 0.28), on 29 August 2000 a sub continental southwest flow dominated the air transport in low levels (red and blue trajectories lines); at high level (green trajectory line), a maritime southeast flow was observed (Figure 4.5, upper blocks, right panel).

Analysis of the volume size distribution showed lower aerosol concentrations (dV/dlnr < 0.01 $\mu m^3\ \mu m^{-2}$) on 18 August 2000 (dominated by maritime flow), with well balanced fine and coarse particles (Figure 4.5, lower blocks, left panel). Conversely the sub continental

flow on 29 August 2012 had particularly higher aerosol concentrations of fine mode particles (dV/dlnr ~ 0.05 μm^3 μm^{-2}), with large differences between fine and coarse mode (Figure 4.5, lower blocks, right panel).

Given the variability on air transport directions observed in this aerosol class interval, the conclusion can be drawn that the medium aerosol class interval cannot be associated to a specific air transport direction. However it can be concluded that sub continental flows enhance aerosol concentration (particularly the fine mode); conversely the maritime flow was characterised by low aerosol concentration dominated by coarse aerosols particles.

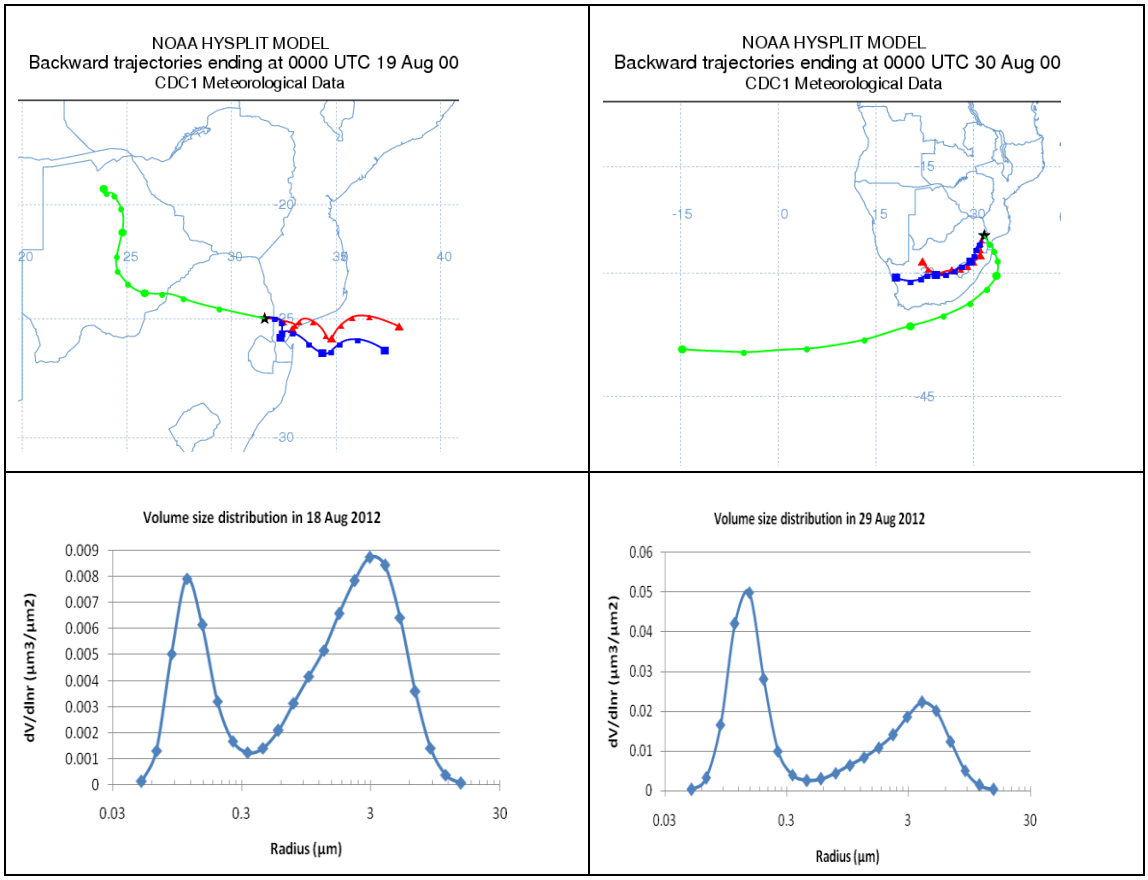

Figure 4-5 Three-day back trajectories from 18 and 29 August 2000, midnight (upper blocks), under the medium aerosol loading class at 850 hPa (red), 700 hPa (blue) and 500 hPa (green). In the lower blocks the retrieved volume size distribution for the same days are presented. The trajectories were started at midnight of the following day (to cover completely the targeted day) plus the two previous days.

Transport under the high aerosol loading conditions

Two of the eight cloud free days fell in the range of high aerosol loading class (0.3 < AOT <0.5) - the 24 August and 14 September 2000. Air mass transport arriving on 24 August 2000 at Skukuza was sub continental, with southwest and westerly flows (Figure 4.6, upper blocks, left panel); on 14 September 2000 an anticyclonic (anticlockwise) air mass

trajectory with clear recirculation pattern was observed (Figure 4.6, upper blocks, right panel). The air mass recirculation patterns and their consequences on the length of aerosol residence time over southern Africa have been discussed in different studies (Tyson *et al*., 1996; Garstang *et al*., 1996; Freiman & Piketh, 2003).

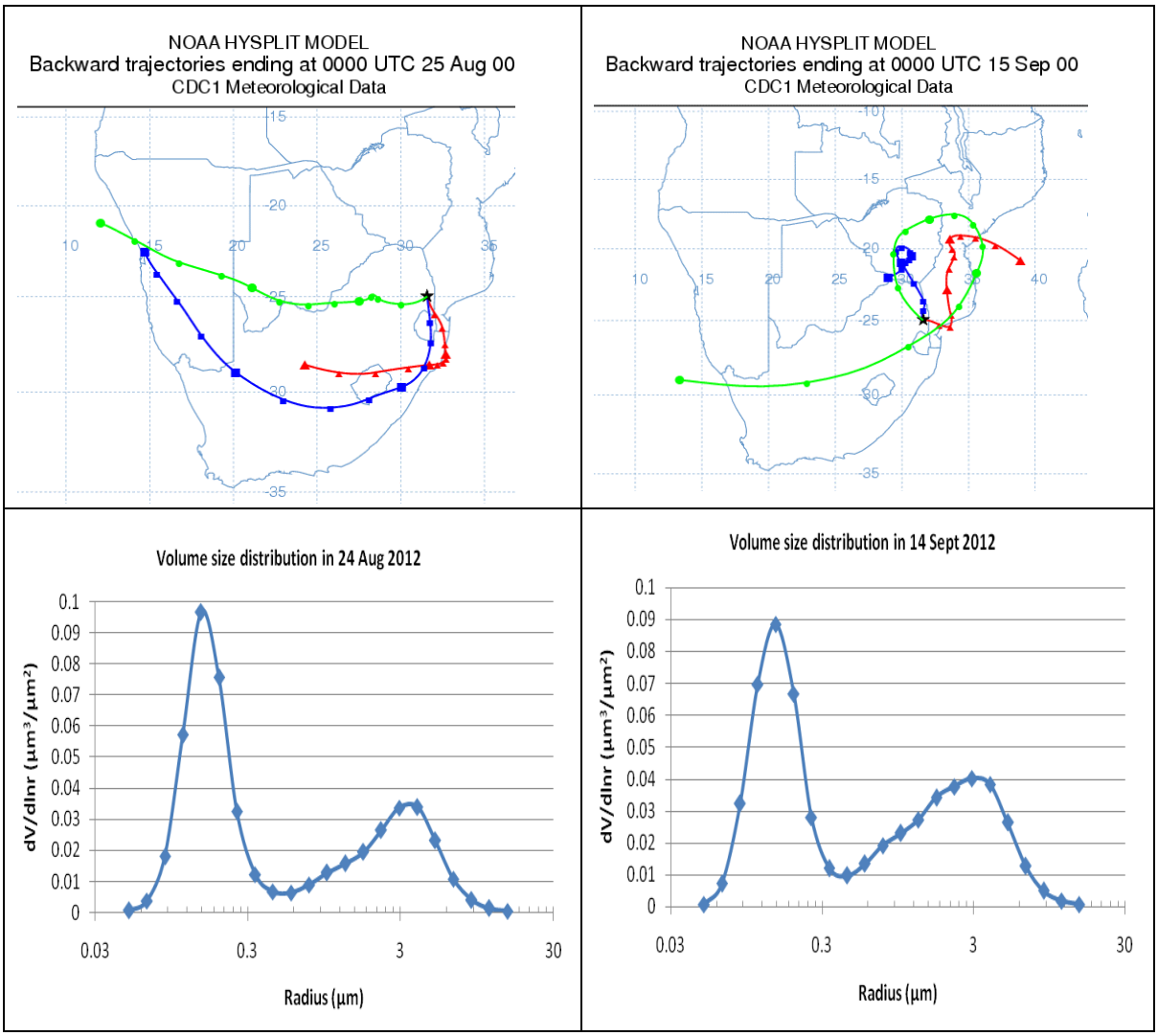

Figure 4-6 Three-day back trajectories from 24 August and 14 September 2000, midnight (upper blocks), under the high aerosol loading class at 850 hPa (red), 700 hPa (blue) and 500 hPa (green); below the volume size distribution showing high concentration of fine particles is presented (lower blocks).

The volume size distribution on both these study days was clearly bi-modal, with a high concentration of fine particles (dV/dlnr ~ 0.1 $\mu m^3 \mu m^{-2}$) and a relatively low concentration of coarse particles (dV/dlnr ~ 0.04 $\mu m^3 \mu m^{-2}$).

Relative differences of particle size between the two days can be viewed by way of the daily average values of the Ångström exponent; on 14 September there was more of the

coarse particles present - as expected when associated with the small contribution of maritime air mass at 850 hPa (red) and 500 hPa (green); consequently the Ångström exponent was relatively small (1.54) if compared to 24 August (1.83).

Transport under the very high aerosol loading conditions

Two of the eight selected days fell within the class of very high aerosol loading (AOT > 0.5), the 21 August and 1 September 2000. The air mass transport to Skukuza, arriving on 21 August 2000, was dominated by an anticyclonic flow at low levels (850 and 700 hPa) (probably originating from the industrial Highveld) and a remote westerly flow at high level (500 hPa) (Figure 4.7, upper blocks, left panel). On 1 September 2000, a northwest flow likely originated from high biomass burning areas, dominating the air transport in low levels; an additional contribution at high level was revived from a southwest flow (Figure 4.7, upper blocks, right panel). On both days air mass transport arriving at Skukuza was characterised by very slow moving air (almost stagnant) at low levels (850 and 700 hPa) and a fast movement at high level (500 hPa).

The volume size distribution on both days was clearly bi-modal with a high concentration of fine particles ($dV/dlnr \sim 0.1\ \mu m^3\,\mu m^{-2}$) and a relatively low concentration of coarse particles, peaking between $0.04 – 0.06\ \mu m^3\,\mu m^{-2}$. The Ångström exponent on 21 August 2000 indicated very fine particles (1.99) associated with industrial aerosols transported from the South African Highveld; on 1 September 2000, the Ångström exponent was relatively small (1.63), but also indicated fine particles possibly transported from high biomass burning area.

The relative differences on the Ångström exponent values within the same size fraction (fine mode) allowed distinctions to be made between aerosols associated with the industrial Highveld (non-hygroscopic) and the biomass burning aerosols, which grow as they take up water vapour (hygroscopic).

The eight selected cloud free days, in association with their optical properties, i.e. aerosol optical thickness, volume size distribution and Ångström exponent, well represented the aerosol loading classes defined in Chapter 3, namely: ‘Very low’; ‘Low’; ‘Medium’, ‘High’ and ‘Very High’ aerosol loadings. The information obtained in this analysis, together with the climatology of aerosol optical properties, will be used in the next chapter to promote a better understanding of the aerosol radiative forcing in the region.

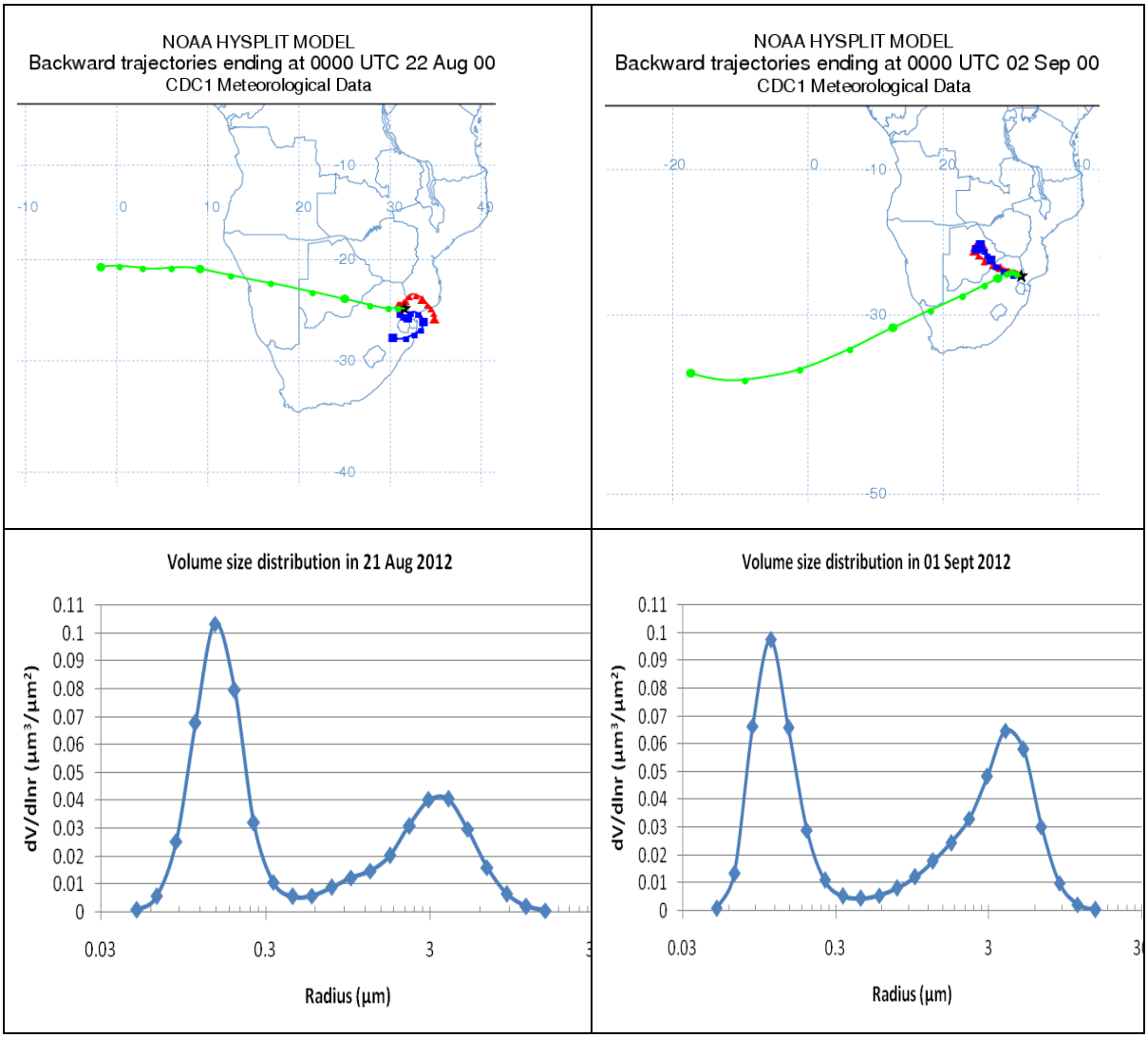

Figure 4-7 Three-day back trajectories from 21 August and 01 September 2000, midnight (upper blocks), under the very high aerosol loading class, showing very slow moving air (almost stagnant) at low levels (850 and 700 hPa, red and blue respectively) and a fast movement of air at high levels (500 hPa, green). The volume size distribution (lower blocks) shows high concentration of fine particles and a relatively small concentration of the coarse fraction.

4.4 Changes in surface radiation fluxes attributed to the variation of aerosol loadings in the atmosphere

The presence of aerosols in the atmosphere reduces the amount of solar radiation reaching the ground through scattering and absorption (attenuation). The amount of solar radiation attenuated by aerosols is proportional to the amount of aerosols measured on the total atmospheric column and expressed as aerosol optical thickness (AOT); therefore the variation of aerosol loadings in the atmosphere should be reflected in the changes of radiation fluxes reaching the ground.

By using the measured surface radiation fluxes and the aerosol optical thickness at Skukuza for the selected cloud-free days presented in section 4.3, the relationship between the changes of surface radiation fluxes attributed to the variation of aerosol optical thickness can be demonstrated. This analysis, based on measurements, represents a rough assessment of the aerosol radiative forcing at the surface and helps to understand the limitation of the instrumental measurements on aerosol forcing estimates. The interpretation of the aerosol forcing cannot be explained only by measurements because the instrumentation has limitations in that one measurement can only represent one condition (either clean or loaded atmosphere). Therefore, the results of both a clean atmosphere and a loaded atmosphere cannot be contained within one measurement. Furthermore, the clean atmosphere is hypothetical - to simulate this condition a model is used, and the assumption is made that no aerosols are present.

For the current analysis using the selected cloud free days (Table 4.1 in section 4.3), the very clear day on 17 August 2000, with AOT < 0.1, was assumed as a reference day (hypothetically without any aerosols). Subsequently the changes in radiation fluxes have been computed as the difference, for specific zenith angles, between the radiation flux on any given day and the radiation flux on the reference day. Two components of measured radiation fluxes (direct and diffuse) in different zenith angles (given as time of the day) were evaluated.

For the direct component, as represented in Figure 4.8, the changes of solar fluxes (difference between the radiation flux at given day and the reference day), were negative. This negative value indicates that aerosols present in atmospheric column reduce the amount of solar energy reaching the ground. The results showed that days with a relatively low amount of aerosols in atmosphere, i.e. medium and below, had a relatively low magnitude of change in radiation fluxes (on 18 August; 29 August and 13 September); high aerosol loadings were associated with high magnitudes of changes (on 21 August; 24 August and 14 September). Diurnal changes could also be depicted (as noted on 1 September), ranging from medium aerosol loading in the morning to very high in the afternoon. These results also revealed that days with a small diurnal range of aerosol loadings also had a small diurnal range of direct solar fluxes; days with large diurnal changes in aerosol loading also had a large diurnal range of direct solar fluxes.

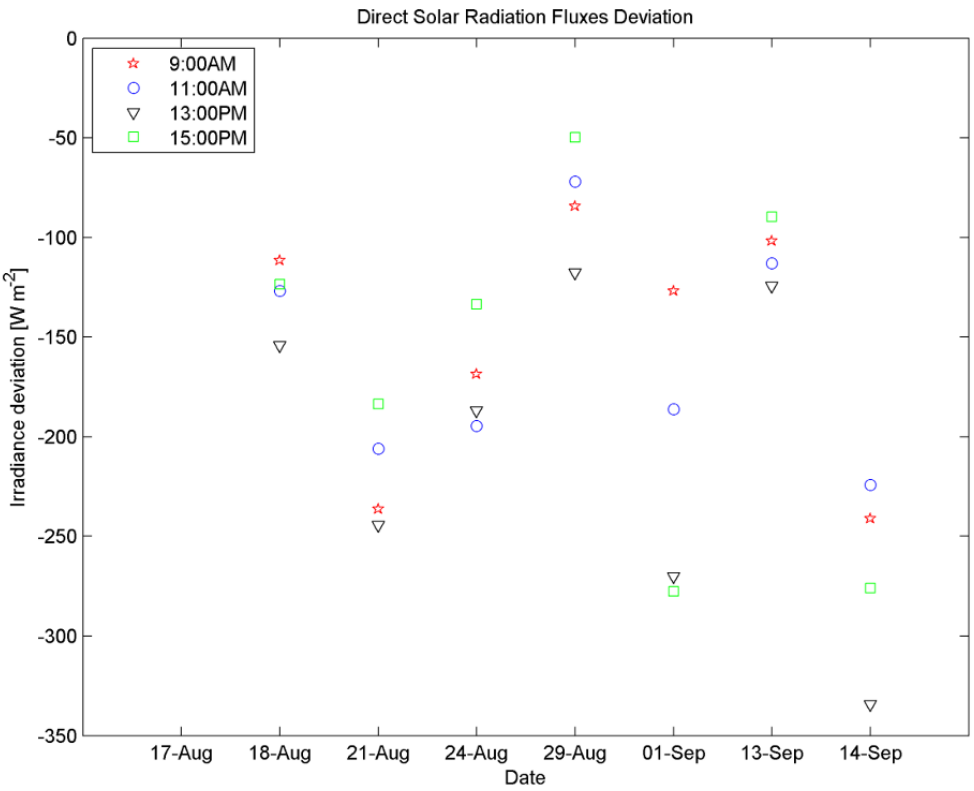

Figure 4-8 Computed changes of surface direct solar radiation fluxes for the selected cloud free days at Skukuza (year 2000). The changes in radiation fluxes were computed as the difference between the radiation flux for the given day and the reference day (very clear day, 17 August 2000) for specific zenith angles given as time of the day.

For the diffuse component (Figure 4.9), the changes of solar fluxes (difference between the radiation flux at given day and the reference day), were positive. The changes in diffuse solar fluxes also followed a pattern similar to the direct component. Low values were associated with low aerosol loadings and vice versa. However, it is important to note that the amplitude of change was lower for diffuse radiation than for direct radiation.

The above computed changes on surface radiations fluxes, associated with the variation of the aerosol loadings, demonstrate how the addition of aerosols as measured by AOT magnitude may affect the radiation budget in the Earth's system. One important aspect arising from this analysis is the limitation of the instrumental measurements; however the cloud free conditions remain the pre-requisite for accurate evaluation of the influence of aerosol in direct forcing. It is difficult to estimate the aerosol forcing for specific day or time without support of simulation of models. The following chapter will discuss the aerosol radiative forcing computed from model estimates.

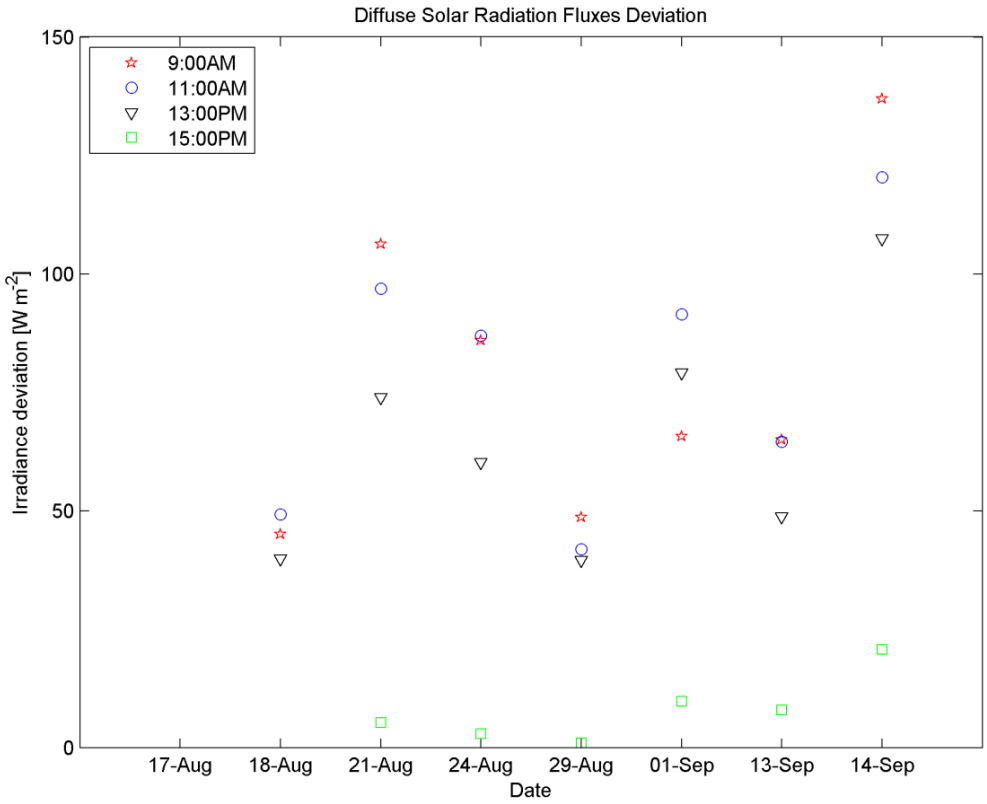

Figure 4-9 Computed changes of surface diffuse solar radiation fluxes for the selected cloud free days at Skukuza.

****

The surface solar fluxes measurements combined with other observations taken at Skukuza during SAFARI 2000 were used to assess and describe the real state of the atmosphere. These parallel measurements, from a total sky imager or micro pulsar Lidar, allowed the reduction of the uncertainty in identifying data corresponding to the clear sky periods (crucial to validating the aerosol radiative forcing calculations). Back trajectory analysis and particle size distribution were used to explore links between different aerosol loading classes and aerosol source origins. The direct aerosol forcing in southern Africa will be described in the next chapter.

Chapter 5.

Long-term direct aerosol forcing estimates in two core sites in southern Africa will be studied (first assessment) to quantify the direct aerosol forcing magnitude and temporal variation for bottom of atmosphere and top of atmosphere. Aerosol radiative forcing for the selected cloud free days will be used as best case study to assess the linkages between aerosols load classes and aerosol forcing magnitudes. The results of Chapter 3 and Chapter 4, together with the current chapter, will be combined to give a final assessment of direct aerosol forcing in southern Africa.

5 Direct Aerosol Radiative Forcing over Southern Africa

The radiative forcing concept was introduced in literature to account for changes in the solar radiation fluxes due to changes in the atmospheric constituents. Consequently, the direct aerosol radiative forcing, denoted as ΔF, is defined as the difference in the energy flux between a situation where aerosols are present, F^A, and a situation where these atmospheric particles are absent, F^C. These values can be estimated at the bottom of atmosphere (BOA) and the top of atmosphere (TOA).

Thus, radiative forcing can be defined at these two levels as:

$$\Delta F_{BOA} = F_{BOA}{}^{\downarrow A} - F_{BOA}{}^{\downarrow C} \quad \text{and} \quad \Delta F_{TOA} = F_{TOA}{}^{\uparrow C} - F_{TOA}{}^{\uparrow A}$$

where the arrows indicate the direction of the solar global fluxes: $\downarrow \equiv$ downward flux and $\uparrow \equiv$ upward flux. Negative values of ΔF at the BOA and at the TOA are associated with an aerosol cooling effect; a warming effect is because of positive values of ΔF at the BOA and at the TOA. The radiative forcing is measured in energy per unit area [W m^{-2}].

Accurate estimates of direct radiative forcing by aerosols in southern Africa are necessary to improve the knowledge of changes in radiative forcing and climate parameters. In this context, the Aerosol Robotic Network (AERONET) provides an extended set of physical and optical aerosol parameters (for about 180 ground-based stations) which form the key information for estimating aerosol radiative effects. At present AERONET also provides a set of estimates of direct solar effects caused by atmospheric aerosols (spectral and broadband fluxes, aerosol radiative forcing).

5.1 Estimates of direct aerosol radiative forcing (ARF) in southern Africa

The AERONET Version 2.0 inversion algorithm (Dubovik *et al*. 2006) recently incorporated a new radiative transfer module into operational inversion code (more details are described in Chapter 2). This module provides estimates for spectral and broadband fluxes at the bottom and top of atmosphere, direct aerosol radiative forcing and aerosol radiative forcing efficiency (available for any of ~ 180 ground-based AERONET stations) (Garcia *et al*., 2008).

The recent information on direct solar effects computed from the AERONET long term measurements, combined with the climatology of aerosol optical properties in southern Africa (see Chapter 3) and the radiation fluxes measurements from SMART group during SAFARI 2000(see Chapter 4), forms the key information used in this study to assess the direct aerosol forcing and reduce the uncertainties in the direct aerosol forcing estimates within southern Africa.

The following two sections, will discuss the direct aerosol radiative forcing from AERONET model estimates at two core sites in southern Africa for bottom and top of atmosphere respectively.

5.1.1 Daily direct aerosol radiative forcing at bottom of atmosphere (BOA) at Mongu and Skukuza

Figure 5.1 shows daily averages of direct ARF at Mongu and Skukuza between 1995 to 2007 and 1998 to 2007 respectively. Daily values varied between (-4 to ~ -200 W m^{-2}) for Mongu and (-2 to ~ -170 W m^{-2}) for Skukuza. The mean direct ARF computed from multiannual data provided by AERONET at the BOA was estimated to be -53.34 W m^{-2} for Mongu and -36.63 W m^{-2} for Skukuza. Strong seasonal cycles in direct aerosol forcing magnitudes following the seasonal variability of AOT patterns in southern Africa were observed.

The direct ARF exerted at BOA was negative, thus reducing the amount of solar radiation reaching the ground. The amount of attenuated energy is proportional to the amount of aerosols in the atmosphere as demonstrated in Chapter 4, Section 4.4.

In general, the results showed aerosols exerted strong negative forcing at Mongu when compared with the Skukuza aerosols. However, the high seasonal variation of the radiative

forcing magnitudes indicated the need for further investigation to better depict the aerosol forcing intensity in both sub-regions.

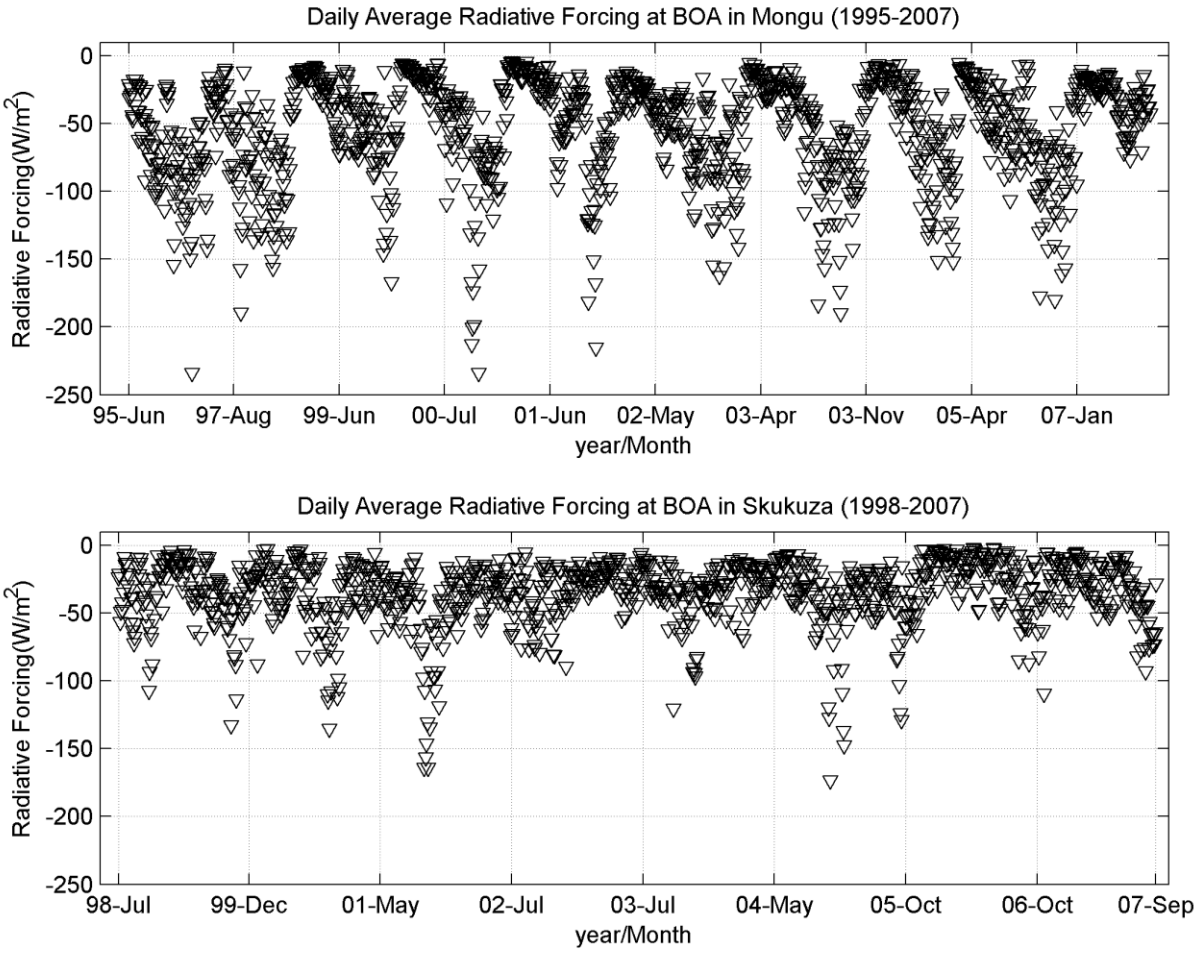

Figure 5-1 Daily averages of direct aerosol radiative forcing at BOA atmosphere from 1995-2007 for Mongu (upper panel) and 1998 -2007 for Skukuza (lower panel).

5.1.2 Daily direct aerosol radiative forcing at the top of atmosphere (TOA) at Mongu and Skukuza

The direct ARF exerted at TOA was also negative but of small magnitude when compared with BOA. In Figure 5.2 it can be seen that the daily direct aerosol radiative forcing at TOA varies between 0 and 50 W m^{-2} and the multi-year mean values were of the same magnitude — -11 W m^{-2} — over both Mongu and Skukuza.

The influence of the seasonal variability of AOT because of biomass burning in the region was not limited to the BOA, but was also noted at TOA. High values of direct ARF were observed during the biomass burning periods at both sites. The results also suggested the existence of strong sources of aerosols other than biomass burning in the southern part of this region; for instance at Mongu, direct ARF values above -20 W m^{-2} (in absolute value)

were only registered during the peak of biomass burning season (ASO); at Skukuza these values were observed both during and outside the biomass burning season. In the next sections a detailed analysis on temporal variation of the direct aerosol radiative forcing will be evaluated.

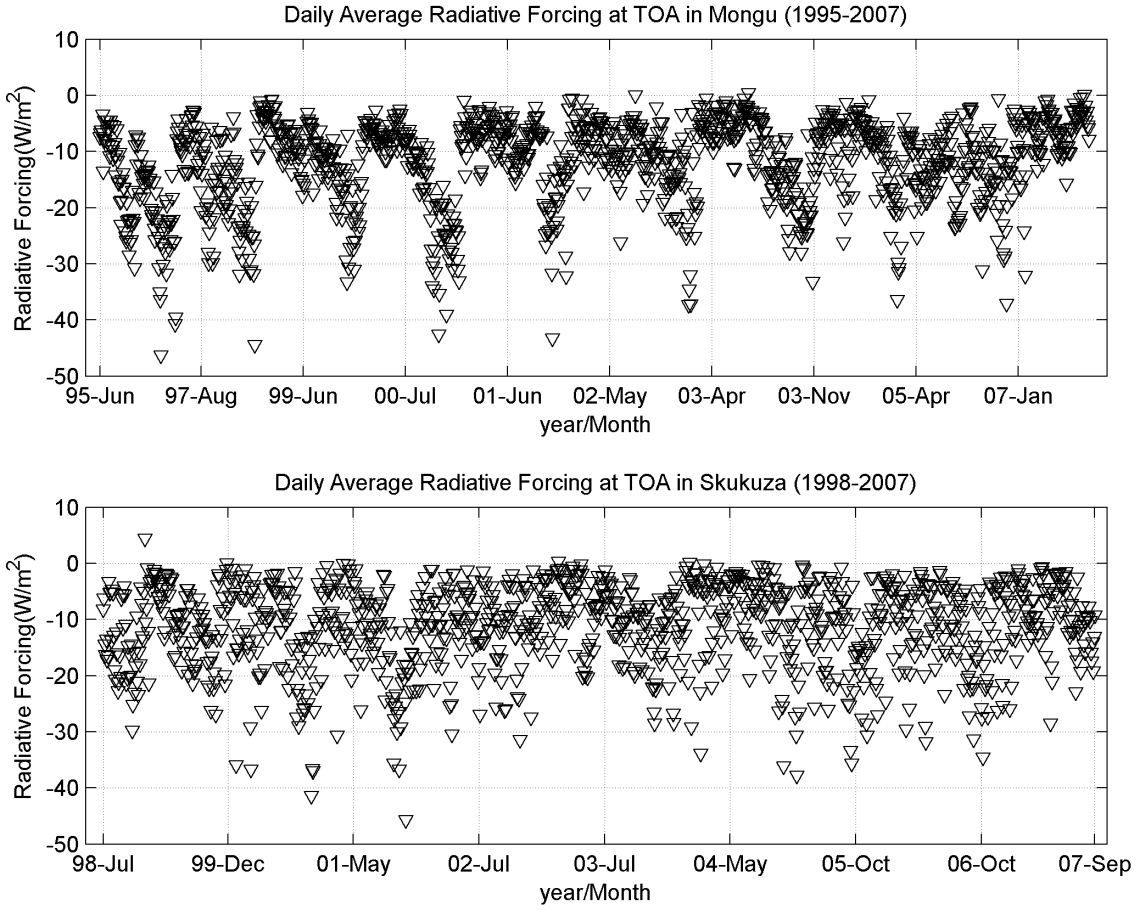

Figure 5-2 Daily averages of direct aerosol radiative forcing at TOA atmosphere from 1995-2007 for Mongu (upper panel) and 1998 -2007 for Skukuza (lower panel).

The above results demonstrate that aerosols exerted less forcing at TOA than at BOA, and in terms of averaged magnitude, direct ARF at BOA was up to four times higher than at TOA. The recorded daily averages clearly show how the tropospheric aerosols influence the radiation budget of the Earth system.

In order to evaluate the seasonal variation of the aerosol radiative forcing magnitudes, associated with both the biomass burning and non-biomass burning periods, the probabilities of occurrences within different classes of direct ARF and different periods of the year are described below.

Table 5.1 gives the probabilities of occurrence of direct aerosol forcing magnitudes at BOA throughout the year for all data points, and during the biomass burning (ASO) and non-biomass burning (AMJ) periods.

In general, direct ARF magnitudes covered a wide range of intervals (from 0 to -200 W m^{-2}) throughout the year at both sites. The results also indicated the forcing magnitude at Mongu was higher than at Skukuza. This was supported by observing that the forcing magnitude above -50 W m^{-2} (in absolute value) accounted for 43% at Mongu; for Skukuza it was just 20%.

There were significant seasonal differences in direct ARF magnitudes at BOA in southern Africa; during the biomass-burning season, direct ARF values were above -50 W m^{-2}, accounting for 84% and 43% for Mongu and Skukuza respectively. For the non-biomass burning season, and by using lower reference values of -25 W m^{-2}, direct ARF values above this reference level accounted for 42% and 48% for Mongu and Skukuza respectively.

From these results, it is reasonable to suggest that direct aerosol radiative forcing at the BOA over southern Africa should be characterised on a seasonal basis. The mean values do not depict the real month by month values and further analysis needs to be conducted.

Table 5-1 Probability distribution of direct radiative forcing values at BOA for all data points, the biomass burning (ASO) and non-biomass burning (AMJ) periods at Mongu and Skukuza.

Daily radiative forcing classes (W m^{-2})	Probability within the range (%)					
	Mongu			Skukuza		
	All data points	ASO	AMJ	All data points	ASO	AMJ
0 to -25	28.20	1.55	56.45	40.89	18.64	51.79
-25 to -50	29.96	14.86	30.64	40.64	39.04	42.09
-50 to -75	19.05	27.46	11.18	12.29	24.69	5.86
-75 to -100	13.96	28.50	-	3.79	10.58	0.26
-100 to -150	9.56	21.93	-	2.06	6.04	-
-150 to -200	1.93	4.84	-	0.33	1.01	-
-200 to -250	0.34	0.86	-	0.00	-	-

Similar estimates of probability of occurrences have been made for the TOA for the same periods. Table 5.2 shows the probability distributions for all data points and for selected quarters weres quite similar over Mongu and Skukuza. Slight differences were observed during the biomass-burning season, with Mongu indicating that aerosols exerted more

direct forcing when compared with estimates at Skukuza. A significant difference was observed during the non-biomass burning season where there was less direct aerosol radiative forcing at Mongu than at Skukuza. This difference, during the non-biomass burning period, was not noticeable at the BOA, but was observed at the TOA. These results emphasise the previous findings of reverse gradient on aerosol loading between biomass-burning and non-biomass burning, and supports the importance and need for accurate aerosol radiative forcing characterisation by seasons.

Table 5-2 Probability distribution of aerosol radiative forcing at TOA for all data points and the biomass burning (ASO) and non-biomass burning (AMJ) periods for Mongu and Skukuza.

Daily radiative forcing classes (W m^{-2})	Probability within the range (%)					
	Mongu			Skukuza		
	All data points	ASO	AMJ	All data points	ASO	AMJ
0 to -10	49.86	17.79	72.45	50.12	29.22	59.44
-10 to -20	34.66	46.80	26.59	35.37	44.58	32.91
-20 to -30	12.52	29.02	-	12.20	22.42	6.63
-30 to -50	2.82	6.39	-	1.98	3.78	1.02

5.1.3 Seasonal variation of multi-year monthly mean of direct aerosol radiative forcing in southern Africa

Monthly means of direct ARF revealed strong dependence on the aerosol optical thickness seasonal cycle in southern Africa. The highest values of direct ARF were observed during the peak of the biomass burning period (ASO); the lowest values were observed from December to May, (within the non-biomass burning season) (Figure 5.3). The impact of biomass burning on the aerosol forcing was not limited to the BOA, but also influenced the forcing at TOA. Forcing magnitudes during the biomass-burning period was almost double that of the non-biomass burning at both BOA and TOA.

Aerosol forcing results also confirmed the atmosphere above Mongu was cleaner than at Skukuza during the non-biomass burning season. These results add more evidence that the industrial complex on the South African Highveld is a significant contributing aerosol source for Skukuza and influences the forcing magnitude for both BOA and TOA in this sub region.

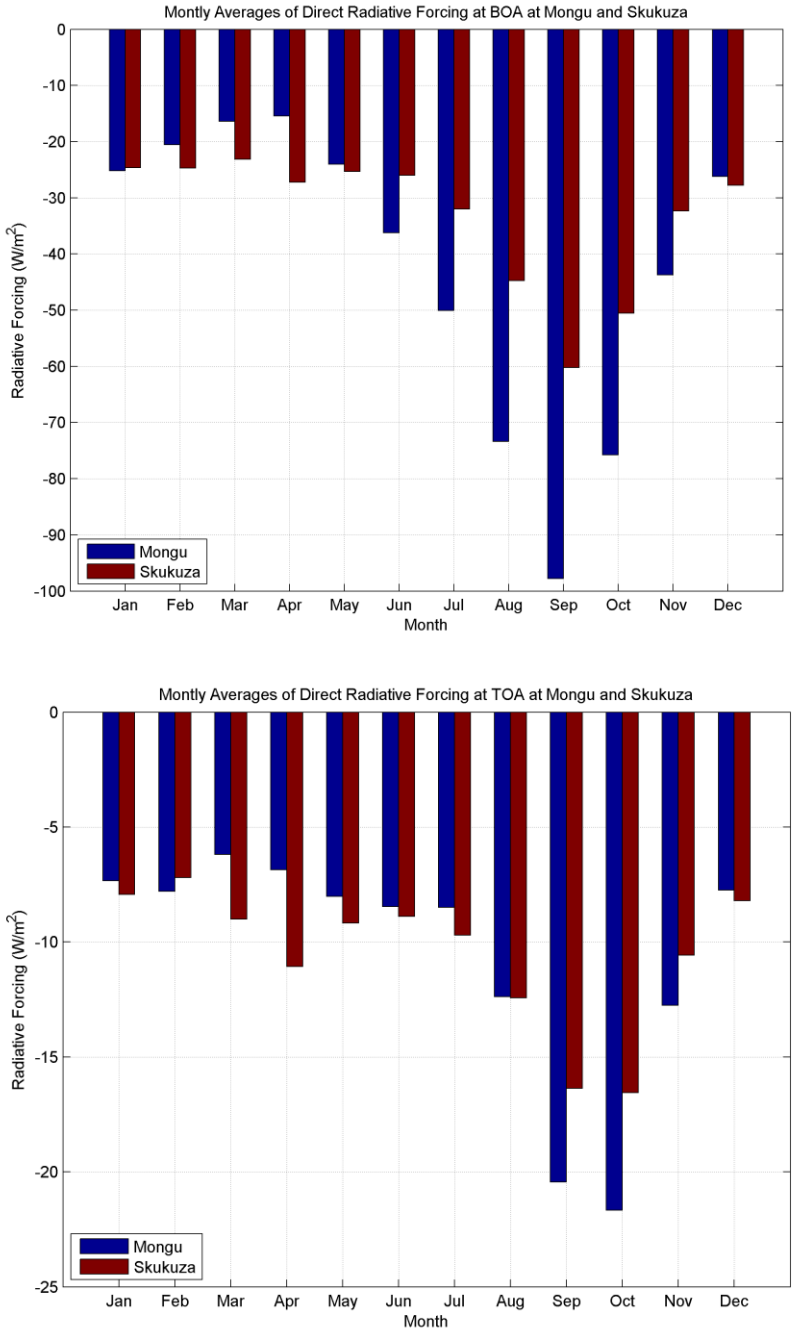

Figure 5-3 Seasonal multi-year monthly means of direct aerosol radiative forcing for Mongu and Skukuza at BOA (upper panel) and at TOA (lower panel).

The large negative forcing at BOA during the biomass burning season in conjunction with low single scattering albedo (results presented in Chapter 3), provides evidence of increase in solar radiation trapped in the atmospheric layer, because of aerosol absorption. This absorption produces an atmospheric temperature gradient contributing to the modification of atmospheric dynamic and cloud characteristics (aerosol semi-direct effect).

Previous results have demonstrated that direct ARF in southern Africa changes significantly from one season to other. To outline in more detail the differences between the seasonal variations, throughout the year, the probability distribution has been estimated for each month for both BOA and TOA. Table 5.3 and Table 5.4 give the direct ARF classes and the probability of occurrence within the specified ranges. For BOA, from January to May, direct ARF values were more frequently within the range of 0 to -25 W m^{-2}, with an average of ~ 70% for Mongu and ~60% for Skukuza. The remaining percentages fell within the range of -25 W m^{-2} to -50 W m^{-2}. The month of June can be considered the transitional month, i.e. the changeover towards higher values of forcing and the time at which the optical properties at Mongu begin to noticeably differ from Skukuza's properties.

From August to October forcing magnitudes were significantly different between the two sites. During this period, Mongu accounted for ~ 70% above -50 W m^{-2}; Skukuza was ~ 50% below -50 W m^{-2}. The month of November can also be regarded as a transitional month - towards lower values of forcing. The forcing characteristics in December were similar for both sites and the forcing values were uniformly distributed within two classes, 0 to -25 W m^{-2} and of -25 to -50 W m^{-2}.

These analyses allowed for reconfirmation of the reversal gradient of aerosol loads and aerosol radiative forcing. More specifically, the north – south gradient applies between June to November and the opposite applies between December and May.

Table 5-3 Direct aerosol radiative forcing classes at BOA and their monthly probability of occurrence

Direct aerosol radiative forcing classes (W m^{-2})		Probability within the range (%) for specific month											
		J	F	M	A	M	J	J	A	S	O	N	D
0 to -25	Mongu	64.7	73.7	71.4	84.9	61.7	29.9	17.4	2.1	1.4	0.8	20.0	42.9
	Skukuza	59.0	68.2	67.2	59.1	53.4	44.9	42.2	27.6	11.1	16.7	43.6	45.5
-25 to -50	Mongu	29.4	26.3	28.6	15.1	30.6	42.2	45.2	26.2	6.2	8.3	44.4	42.9
	Skukuza	39.3	25.0	27.6	33.3	41.6	48.6	46.9	40.0	35.4	42.6	48.4	54.6
-50 to -75	Mongu	5.9	------	------	------	6.7	24.1	22.4	27.9	23.8	32.6	22.2	7.2
	Skukuza	1.6	6.8	5.2	6.5	5.0	6.5	9.4	20.0	29.9	24.1	6.5	------
-75 to -100	Mongu				------	1.0	3.7	11.4	22.8	27.6	40.2	4.4	7.1
	Skukuza				1.1			1.6	6.9	13.2	12.0	1.6	
-100 to -150	Mongu							3.7	17.7	29.5	17.4	8.9	
	Skukuza								3.5	9.7	4.6		
-150 to -200	Mongu								3.4	9.1	0.8		
	Skukuza								2.1	------			
-200 to -250	Mongu									2.4			
	Skukuza												

Table 5-4 Direct aerosol radiative forcing classes at TOA and their monthly probability of occurrence

Direct aerosol radiative forcing classes (W m^{-2})		Probability within the range (%) for specific month											
		J	F	M	A	M	J	J	A	S	O	N	D
0 to -10	Mongu	76.5	57.9	85.7	84.9	71.5	64.2	73.5	33.3	9.1	3.8	37.8	71.4
	Skukuza	68.9	75.0	69.0	50.5	64.0	60.1	62.5	37.2	26.4	22.2	51.6	61.4
-10 to -20	Mongu	23.5	42.1	9.5	13.7	28.0	34.8	26.5	57.0	43.3	34.1	37.8	28.6
	Skukuza	23.0	15.9	25.9	37.6	28.6	34.8	34.4	44.1	43.8	46.3	37.1	29.6
-20 to -30	Mongu	----	----	2.4	1.4	0.5	1.1	----	9.3	37.1	51.5	17.8	----
	Skukuza	8.2	6.8	3.5	10.8	5.6	5.1	3.1	16.6	26.4	25.0	9.7	9.1
-30 to -50	Mongu	----	----	2.4	-----	-----	-----	----	0.4	10.5	10.6	6.7	----
	Skukuza	----	2.3	1.7	1.1	1.9	-----	-----	2.1	3.5	5.6	1.6	----

5.2 Analysis of direct aerosol radiative forcing for the selected cloud free days from Skukuza measurements during SAFARI 2000.

Solar radiation fluxes are usually hampered by persistent broken cloud fields; making it difficult to assess the aerosol radiative forcing. During the SAFARI 2000 dry season field campaign (August-September 2000), it was possible to identify, with more confidence, the cloud-free days. This was done by combining the measurements of the precision spectral pyrometer (PSP), the total sky imager (TSI) and the Micro Pulse Lidar (MPL) (See Chapter 4 for more details).

The results of direct aerosol forcing estimates derived from AERONET modelling on specific cloud free days, with their associated aerosol optical properties obtained from ground based measurements (see Table 4.1 in section 4.3) were used as best case examples to investigate linkages between certain levels of aerosol loading in the atmosphere with the related direct aerosol forcing.

By selecting the direct ARF computed from AERONET model for the eight cloud free days at Skukuza, the following findings (as illustrated in Figure 5.4) shown by BOA (red triangles) and TOA (blue circles) can be summarised thus:

(i) tropospheric aerosols influence the forcing on both BOA and TOA;

(ii) the magnitude of direct aerosol radiative forcing is proportional to the aerosol loading;

(iii) if aerosols are either not present or insignificant in the troposphere, direct aerosol radiative forcing at BOA and TOA is very small and almost of the same magnitude, e.g. on the selected reference day, 17 Aug 2000;

(iv) direct aerosol radiative forcing at the TOA is less sensitive to the changes of aerosol concentrations in the tropospheric column and is likely to be around -30 W m^{-2} for cloud free days;

(v) differences between forcing magnitudes at BOA and TOA increase with the amount of aerosols in the tropospheric column.

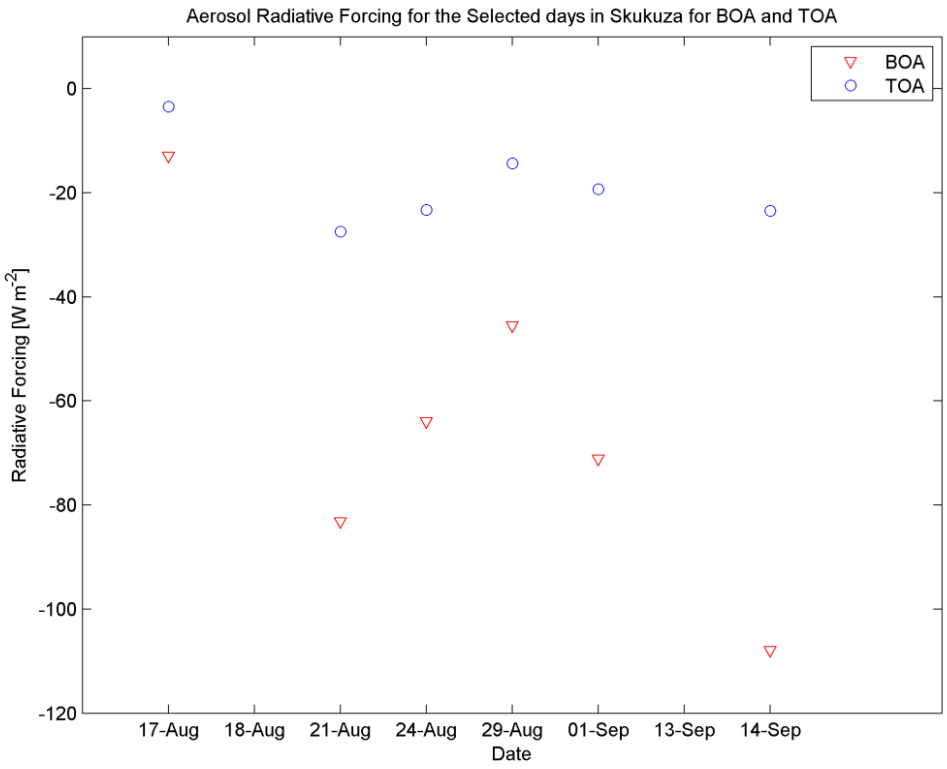

Figure 5-4 Top and bottom of atmosphere direct aerosol radiative forcing for the selected eight cloud free days at Skukuza during SAFARI 2000.

Furthermore the results from these best case analyses will be linked to the regional climatology of aerosol optical properties (given in Chapter 3) to depict the aerosol characteristics for the region; more importantly these results will help to reduce the uncertainty of direct aerosol forcing values extrapolated from model estimates.

5.2.1 Analysis of direct aerosol radiative forcing in southern Africa based on the correlation to the climatology of the aerosol optical properties.

From a regional climate perspective, estimating the overall direct radiative forcing of aerosols is the aim of this thesis; individual aerosol optical properties are intermediate objectives. For this reason, the following sections will build linkages of the previous site and time specific analyses to the regional perspective.

The climatology of aerosol optical properties in southern Africa makes the setting of aerosol loading classes possible, within the aerosol optical thickness range of 500 nm (Queface *et al.*, 2011). This aerosol loading classification, associated with the long-term direct aerosol radiative forcing estimates, together with the direct aerosol radiative forcing magnitudes obtained from the best case study (cloud free days), will form the tie point to outline the main direct aerosol radiative forcing features experienced in southern Africa.

The main underlying concept is: once the aerosol optical thickness at 500 nm is known, the direct aerosol radiative forcing at BOA and TOA can consequentially be estimated. The applicability of this concept is also based on the premise that aerosol optical thickness is one of the easiest measurable aerosol optical parameters; thus long-term measurements of this parameter are available.

Following the results of the best case study analysis (in Chapter 5.2), it is possible to correlate aerosol loading classes, based on climatology, with direct ARF magnitudes obtained from the best cloud free days. Table 5-5 illustrates the correlation of direct aerosol radiative forcing classes attributed to the different aerosol loading classes in cloud free conditions. The results show that direct aerosol radiative forcing at BOA varies between -20 to -100 W m^{-2}; at TOA the direct aerosol radiative forcing lies between -5 to -30 W m^{-2}. It is evident that changes in the aerosol amounts in the atmosphere have a significant influence on the magnitude of direct aerosol radiative forcing.

The use of the accurately assessed cloud free days (from Skukuza measurements) allowed the reduction in the wide range of variability initially observed from the model estimates. For instance: in previous analyses, based on model estimates, it was found that daily direct aerosol radiative forcing values were between -2 and -200 W m^{-2} for BOA and 0 and -50 W m^{-2} for TOA. These high values may have been because of cloud contaminations by high cirrus clouds. Such high or overestimated values are likely to be recalculated and their accuracy resolved by using the case studies of the cloud free days.

Table 5-5 Summary of direct aerosol radiative forcing magnitudes attributed to the different aerosol loading classes for cloud free days.

Aerosol loading classes	AOT range at 500 nm	Related aerosol RF magnitude (W m^{-2})	
		BOA	TOA
Very Low	< 0.1	[-20, 0]	[-5, 0]
Low	0.1 – 0.2	[-40, -20]	[-10, -5]
Medium	0.2 – 0.3	[-60, -40]	[-20, -10]
High	0.3 – 0.5	[-80, -60]	[-25, -20]
Very High	> 0.5	[-100, -80]	[-30, -25]

The mean direct ARF, as illustrated by medium aerosol loading conditions (0.2 <AOT< 0.3) was within -60 and -40 W m^{-2} for BOA and -20 and -10 W m^{-2} for TOA. By averaging

the two extreme values, reference values of -50 W m^{-2} for BOA and -15 W m^{-2} for TOA were obtained.

The general outcome from this averaging of results suggested: if AOT (500 nm) values were below 0.2, the associated direct aerosol radiative forcing should also be below -50 W m^{-2} and -15 W m^{-2} for BOA and TOA in absolute values respectively; if AOT (500 nm) values were above 0.3, the direct ARF at BOA and TOA should also be above -50 W m^{-2} and -15 W m^{-2} (absolute values) respectively.

Previous analyses of aerosol optical properties demonstrated significant seasonal and spatial variability of aerosol loads in southern Africa.

Consequently, if aerosol class values are used to infer the direct aerosol radiative forcing in southern Africa, based on available information of aerosol optical properties, the following perspectives should be considered:

General perspective

(i) Overall aerosol optical thicknesses averages were 25% higher at Mongu than at Skukuza;

Seasonal perspectives

Aerosol optical thicknesses in southern Africa were below medium aerosol loading conditions (AOT at 500 nm < 0.2) from December to May, with the special note that aerosol loadings at Skukuza were approximately 20% higher when compared with Mongu for the same period:

(ii) Between June and August (JJA), aerosol optical thicknesses were within medium loading conditions (0.2 < AOT at 500 nm < 0.3), with the special note that AOT at Mongu was approximately 25% higher than at Skukuza;

(iii) For the period of September to November (SON), seasonal AOT peaks for high aerosol loading conditions (0.3 < AOT at 500 nm < 0.5), sub regional differences were quite significant, with Skukuza being well represented by the lower peak and Mongu by the higher peak; during the same period AOT at Mongu was approximately 35% higher than Skukuza.

The above perspectives, combined with the direct aerosol radiative forcing magnitudes (in Table 5.5), may contribute significantly to the future characterisations of direct ARF in southern Africa. Of particular interest is the finding that there was a clear reversal gradient on direct aerosol forcing magnitude between Mongu and Skukuza. More specifically, from

December to May direct aerosol forcing magnitude was higher at Skukuza than at Mongu; vice versa from June to November.

The results also call attention to the need to consider the seasonal and spatial dynamics of aerosols when assessing the direct aerosol radiative forcing in the region. The next section will build on the current study results, together with previous studies, to move forward on defining the integrated regional features of direct aerosol radiative forcing.

5.3 What is the direct aerosol radiative forcing of aerosols over southern Africa?

Previous findings on direct aerosol radiative forcing estimates for southern Africa

Aerosol radiative forcing calculations in southern Africa are few in number (few previous case studies have been conducted) and limited in spatial and temporal coverage. All previous studies (and this current study) coincide quite well on determining the aerosol radiative forcing magnitudes at TOA (Magi B. I., 2006; Abel *et al*., 2005; Keil and Haywood, 2003; Ichoku *et al*., 2003; Bergstrom *et al*., 2003). Estimates for BOA, however, differ from one study to other. There is also a common understanding that, during the high levels of aerosol optical thickness, strong surface and TOA aerosol forcing are created.

Published estimates of direct ARF for southern Africa and a comparison of the results are presented here. Bergstrom *et al*. (2003) computed the radiative effects of aerosols for 24 August 2000. The TOA effects of aerosols were -13 W m^{-2} and -57 W m^{-2} for BOA. This study, for this same day, suggests aerosol radiative forcing classes between -20 and -25 W m^{-2} and -70 to -80 W m^{-2} for TOA and BOA respectively.

Based on Bergstrom calculations, the AOT values have been underestimated; the values on 24 August 2000 were classified as having low AOT conditions; from AERONET measurements in this current analysis, 24 August 2000 has been re-classified differently – i.e. as having high aerosol loading conditions leading to strong forcing.

From a regional perspective, Keil and Haywood (2003) used in situ data, collected in Namibia during SAFARI 2000, and estimated direct aerosol radiative forcing from -12 to -14 W m^{-2} for TOA and -22 to -28 W m^{-2} for BOA. Ichoku *et al*. (2003), using aerosol information from the MODIS, calculated direct aerosol radiative forcing over the southern Africa as -10 W m^{-2} for TOA, and -26 W m^{-2} for BOA. Subsequently, Magi (2006)

reported that Abel *et al*. (2005) had suggested direct aerosol radiative forcing occurred in the ranges -7 to -9 W m^{-2}, and -32 to -35 W m^{-2}, for the TOA and BOA respectively, for southern Africa region.

Current results arising from this study

Moving from case studies, to regional integration of radiative effects of aerosols and estimates of the regional direct aerosol forcing represent the challenges of this research. AERONET has developed a database of comprehensive measurements and estimates of aerosol optical properties at two key sites in southern Africa. These data may help to answer the question: *What is the direct radiative forcing of aerosols for southern Africa?*

Careful analyses of aerosol optical properties and aerosol direct effects have demonstrated that static values in terms of regional and temporal representation are not suitable to describe the aerosol effects in southern Africa. Consequently, a dynamic approach should be used.

This approach should be based on combining: the given aerosol loading classification; the correspondent direct radiative forcing magnitudes; the frequency distribution for all data points and the separation of biomass burning and non-biomass burning seasons for BOA and TOA.

Table 5-6 and Table 5-7 give summaries of the values and attributes of direct aerosol radiative forcing, at BOA and TOA, for different states of the atmosphere and different seasons at Mongu and Skukuza. The obtained results are an intermediate step towards achieving reliable regional figures.

Table 5-6 Summary of values and attributes of direct radiative forcing for BOA at Mongu and Skukuza.

Aerosol loadings classes	Aerosol radiative forcing magnitudes (W m^{-2})	Probability within the range (%)					
		Mongu			Skukuza		
	BOA	All data points	ASO	AMJ	All data points	ASO	AMJ
Very Low	[-20, 0]	28.2	1.6	56.5	40.9	18.6	51.8
Low	[-40, -20]	30.0	14.9	30.6	40.6	39.0	42.1
Medium	[-60, -40]	19.1	27.5	11.2	12.3	24.7	5.9
High	[-80, -60]	14.0	28.5	----	3.8	10.6	0.3
Very High	[-100, -80]	9.6	21.9	----	2.1	6.0	----

Table 5-7 Summary of values and attributes of direct radiative forcing for TOA at Mongu and Skukuza.

Aerosol loadings classes	Aerosol radiative forcing magnitudes (W m^{-2})	Probability within the range (%)					
		Mongu			Skukuza		
	TOA	All data points	ASO	AMJ	All data points	ASO	AMJ
Very Low	[-5, 0]	49.9	17.8	72.5	50.1	29.2	59.4
Low	[-10, -5]	34.7	46.8	26.6	35.4	44.6	32.9
Medium	[-20, -10]	12.5	29.0	----	12.2	22.4	6.6
High	[-25, -20]	2.8	6.4	----	2.00	3.8	1.0
Very High	[-30, -25]	----	----	----	----	----	----

The frequency distribution presented in the above tables, alongside the direct ARF ranges, gives the weight of the particular aerosol loading class to the total forcing in each time line. By using the middle point values of each direct radiative forcing range and the corresponding weight in aerosol loading classes, single values of direct aerosol radiative forcing were computed for each time line, for both the sub regions and the overall region. The results of these estimates are presented in Table 5.8.

Table 5-8 Direct aerosol radiative forcing values computed for each sub region and all regions. The seasonal changes are also expressed.

Time period	Radiative Forcing (W m^{-2})					
	Mongu		Skukuza		All Region	
	BOA	*TOA*	BOA	TOA	BOA	TOA
All year	-40	-6	-27	-6	-33	-6
ASO	-58	-10	-39	-8	-48	-9
AMJ	-20	-4	-21	-5	-20	-4

From the results given in Table 5-8 and aiming regional perspective, the following can be expressed:

(i) Direct aerosol radiative forcing values for all southern Africa have been estimated as -33 W m^{-2} for BOA and -6 W m^{-2} for TOA; these values are consistent with the findings of (Abel *et al*. 2005);

(ii) Biomass burning exerted strong forcing in region, with direct aerosol forcing magnitudes reaching -48 W m^{-2} for BOA and -9 W m^{-2} for TOA, these values are consistent with the findings of (Garcia *et al*. 2011);

(iii) The difference of forcing magnitude between biomass burning and non-biomass burning season was shown to be a factor of two;

(iv) There were significant sub regional differences in direct aerosol forcing magnitudes between Mongu and Skukuza, particularly for BOA;

(v) In general the direct aerosol forcing magnitude for TOA was similar for Mongu and Skukuza; however differences were observed between the biomass burning and non-biomass burning seasons;

(vi) During the non-biomass burning season direct aerosol radiative forcing at Skukuza exceeded the value at Mongu for the same period, thus indicating the reverse gradient on aerosol optical thickness.

5.4 Comparison of direct aerosol radiative forcing magnitudes between southern Africa and Middle East

In Chapter 3 a brief analysis of the aerosol optical properties for Middle East were given and an outline of how aerosol properties of southern Africa differ from the Middle East environment. In general terms aerosol loading levels in Middle East are higher than southern Africa and aerosol size particles in Middle East are dominated by coarse particles (desert dust), whereas fine particles (mainly from biomass burning) dominate in southern Africa.

This short section will present the main results of direct aerosol forcing estimates in Middle East, based on AERONET data and published literature, and compare them with the southern Africa values. Garcia *et al. (*2008) reported annual and regional averages of direct aerosol radiative forcing of -40 W m^{-2} for BOA and -4 W m^{-2} at TOA for Arabian Peninsula and -46 W m^{-2} for BOA and -11 W m^{-2} for TOA in southern Africa region. Satheesh *et al*. (2006), based on AERONET and MODIS data, found that the direct aerosol radiative forcing at BOA over Saudi Arabia varies in the range of -30 to -70 W m^{-2} ; at TOA the forcing is nearly at zero because of the large surface albedo. Dey *at al. (*2004) also reported a strong seasonal direct forcing at BOA over Arabian Sea, which had not been found at the TOA. The following section summarises the direct aerosol forcing magnitudes and their temporal variation over the sites used in this study (based on AERONET estimates).

Table 5.9 shows more detailed results of the monthly and annual direct aerosol radiative forcing magnitudes over four sites, two in southern Africa (Mongu and Skukuza) and two

in the Middle East (Solar Village and Dhadnah). Overall results show that direct aerosol forcing magnitudes at the two Middle East sites are higher than at the southern Africa sites. Bottom of atmosphere annual means of direct aerosol radiative forcing range between -33 W m^{-2} and -42 W m^{-2} at Skukuza and Mongu respectively; these vary between -46 W m^{-2} and -56 W m^{-2} at Solar Village and Dhadhah. Direct aerosol radiative forcing at the top of atmosphere is lower over the inland desert site of Solar Village in Saudi Arabia when compared to Skukuza and Mongu in southern Africa. In contrast, at the coastal site of Dhadnah in the UAE, direct aerosol radiative forcing at TOA is significantly higher. The reasons for these high direct aerosol forcing values at TOA over Dhadnah are not part of this study.

Monthly means of direct aerosol radiative forcing also shows seasonal variation of forcing magnitudes for both bottom and top of atmosphere (see bold and italic values in Table 5.9, to highlight the magnitude differences with other months). The monthly aerosol forcing magnitudes and their variability follow the season changes of the aerosol optical thicknesses in both the Middle East and in southern Africa (detailed analysis on AOT variability is given in Chapter 3 of this study).

Table 5-9 Monthly aerosol radiative forcing magnitudes at selected sites in southern Africa and Middle Least, based on AERONET estimates. The values in last column are the overall annual average and are negative.

Atmos. Level	Site	Monthly means of aerosol radiative forcing												
		J	F	M	A	M	J	J	A	S	O	N	D	Ann
BOA	Mongu	-25.8	-20.5	-16.4	-15.4	-24.1	-36.2	**-50.1**	**-73.4**	**-97.8**	**-75.8**	-43.7	-26.2	**42.1**
	Skukuza	-24.6	-24.7	-23.2	-27.2	-25.4	-26.0	-31.9	**-44.7**	**-60.2**	**-50.5**	-32.3	-27.8	**33.3**
	Solar Village	-28.7	-41.3	**-48.9**	**-55.8**	**-65.4**	**-60.3**	**-52.1**	**-54.3**	**-47.5**	-40.6	-36.2	-28.8	**46.6**
	Dhadnah	-28.3	-44.7	**-58.5**	**56.6**	**-61.6**	**-65.9**	**-83.9**	**-83.0**	**-62.4**	-47.8	-36.5	-44.9	**56.2**
TOA	Mongu	-7.3	-7.8	-6.2	-6.9	-8.0	-8.5	-8.5	**-12.4**	**-20.4**	**-21.7**	**-12.8**	-7.7	**10.7**
	Skukuza	-7.9	-7.2	-9.0	-11.1	-9.2	-8.9	-9.7	**-12.4**	**-16.4**	**-16.5**	-10.4	-8.2	**10.6**
	Solar Village	-3.7	-7.0	**-8.0**	**-10.6**	**-12.1**	**-8.3**	**-7.7**	**-7.3**	-5.3	-3.4	-3.9	-3.3	**6.70**
	Dhadnah	-14.5	-23.1	**-29.2**	**-28.1**	**-27.4**	**-26.1**	**-35.2**	**-35.1**	**-27.3**	-24.8	-20.2	-17.7	**25.7**

The results obtained in this study will contribute to the characterisation of direct aerosol forcing, on a seasonal basis and for each sub region in southern Africa. Improved characterisation will advance the understanding of the impacts of aerosol loadings on the climate of southern Africa. However the limited number of aerosol measurements sites need to be address.

****

The magnitude and temporal variation of direct aerosol forcing estimates at bottom of atmosphere (BOA) and top of atmosphere (TOA) were presented as a first assessment of the changes in radiation fluxes being attributed to variations in aerosol concentration in the atmosphere of southern Africa. Combined analyses, projected from the study of selected cloud free days, the climatology of aerosol optical properties and model estimates of direct aerosol forcing contributed to the final assessment of direct aerosol forcing in southern Africa. The next chapter will summarise and outline the key results of this research.

Chapter 6.

6 Summary and Conclusions

A successful ground based and readily accessible database for long-term monitoring and characterisation of aerosols, combined with good international collaboration from within the scientific community, has been a crucial factor in the study of aerosol climate effects worldwide. The valuable and unique long-term measurements of atmospheric aerosols and their solar effects in southern Africa, plus the intensive field experiments (such as SAFARI 2000) provided key information - contributing towards a better overall understanding of the main characteristics of tropospheric aerosols in this region (and how these aerosols impact the direct aerosol forcing). The main conclusions of this study are summarised below (in response to the research questions posed in Chapter 1, under research aim and objectives):

1. *What are the aerosol optical properties (AOP) over southern Africa?*

Aerosol optical properties in southern Africa display significant day-to-day and interannual variability. Daily averages of AOT (500 nm) range from very low (AOT < 0.1) to very high (AOT > 0.5) conditions, with annual averages between 0.2 and 0.3. Ångström exponent values indicate a wide range of particle sizes (0.5 – 2.0); fine particles are the most predominant in this region (with median Ångström exponent values between 1.4 and 1.7). The proportion of fine particles versus coarse fluctuates around 70 % to 30 % depending on the season. This proportion is well illustrated by typical bimodal size distribution of fine and coarse mode particles, with varying concentrations seen along the timeline of a year. Single Scattering Albedo (SSA) in the visible range (440 and 670 nm) decreases with wavelength - a characteristic of the absorption by small elemental carbon particles. This study suggests that (SSA = 0.85 ± 0.02) is the most representative level for the northern region (the area most affected by biomass burning emissions). However this SSA range is not appropriate south of 20º S; here a different value (showing less absorbing aerosols) would be more realistic, i.e. SSA = 0.90 ± 0.01.

2. *How do these AOPs change within different seasons and are there likely to be long-term trends?*

Aerosol optical properties in southern Africa can be distinguished in three periods:

(i) from December to May with relatively clean atmosphere (with monthly averages AOT values at 500 nm between 0.1 to 0.2) – mainly associated with the aerosols washed out from the atmosphere (wet season) and minimal biomass burning;

(ii) followed by a transition period towards high AOT values from June to August with a moderately turbid atmosphere (0.2 – 0.3);

(iii) from September to November, with high levels of AOT (0.3 – 0.5) - mainly associated with biomass burning.

Within this region a reversal gradient of AOT is observed along the year: the north has higher magnitudes than the south, i.e. a north – south gradient, during the biomass-burning season and the opposite applies in the non-biomass burning season, i.e. a south – north gradient.

A typical bimodal size distribution is always present along the year with the concentrations of fine mode particles rising as AOT values increases. Low aerosol concentrations (less than 0.02 $\mu m^3 \mu m^{-2}$) and a well balanced mixture of both coarse and fine particle size characterises the relatively clean period (December to May). The winter period and the early stage of biomass burning activities (June, July and August) are characterised by the increase in fine particle concentrations; this increase continues and reaches remarkably high values during the peak of the biomass burning season (September and October).

The present aerosol data in southern Africa display significant interannual variability, recording years with relative abundance or paucity of total aerosol amounts. However, no long-term discernible trends in the total aerosol loads are observable in this region. The data strongly suggests large-scale extreme events, e.g. El Niño or La Niña, have impacts on the annual aerosols amounts and these impacts should be further investigated.

Several results of aerosol trends analyses consistently indicate a negative global tropospheric AOT trend in the last decade; the results differ from one region to other. Of particular interest in this study is the southern Africa region, and more specifically the two sites at Mongu and Skukuza. De Meij *et al*. (2010), using MODIS and MISR data, indicated an average negative trend for the African continent, with caution that these negative trends are not statistically robust because of the limited number of ground stations

used for comparison. More recently, Xia (2011), using aerosol data from 79 AERONET stations worldwide, investigated the trends on AOT. For Mongu and Skukuza Xia concluded that AOT had decreased, but the trends were small and were not significant.

3. *What are the main characteristics of AOP in southern Africa that differ from other environments?*

The selected secondary area of study to fulfil this evaluation is the Middle East. The comparison of aerosol optical properties (between Southern Africa and Middle East) indicates clear differences exist:

(i) aerosol loading magnitudes in Middle East are higher than Southern Africa;

(ii) annual averages of AOT (500 nm) vary between 0.3 – 0.4 for Middle East and 0.2 – 0.3 for southern Africa;

(iii) aerosol size particles in Middle East are dominated by coarse particles (desert dust); fine particles (mainly from biomass-burning) dominate in Southern Africa;

(iv) aerosol volume size distribution is clearly bimodal (coarse and fine) in Southern Africa but almost mono modal (coarse) in Middle East;

(v) the single scattering albedo (SSA) in visible range, indicates that aerosol particles in Middle East (mainly desert dust) are less absorbent when compared to southern Africa (with mainly biomass burning particles). Desert dust has higher absorption at wavelengths close to the ultraviolet wavelengths; for biomass burning, by contrast, the absorption increases in the near infrared region. In addition SSA increases with wavelength in Middle East but decreases for Southern Africa;

(vi) long-term data on aerosol optical thickness indicate a trend towards increased aerosols over Middle East (particularly for coarse particles). However, in southern Africa, no discernible trend was identified. The reasons associated with this possible increase of aerosols in Middle East do not form part of this study.

The overall differences outlined above lead to significant difference in the aerosol optical properties and thereby the aerosol radiative effects of these two environments. Furthermore, these differences emphasise the need for obtaining further data for defining the aerosol optical characterisations by regions or sub regions.

4. *What is the direct radiative forcing of aerosols for southern Africa? What are the magnitudes of daily and seasonal direct aerosol radiative forcing (ARF) at bottom of atmosphere (BOA) and top of atmosphere (TOA) in southern Africa?*

Daily estimates of direct aerosol forcing magnitudes cover a wide range of intervals, from -2 to -200 W m^{-2} at BOA, and ~0 to -50 W m^{-2} at TOA, throughout the year. In general, there is a strong north-south gradient of direct ARF at BOA; the overall mean from model estimates provided by AERONET indicates values between -50 W m^{-2} (northern part) to -35 W m^{-2} (southern part). For the TOA, the direct ARF gradient appears to be nearly zero, with a mean value of -11 W m^{-2}.

Direct ARF over southern Africa changes significantly from one season to another because of the strong seasonal cycle of biomass burning activity. The impact of biomass burning on the direct aerosol forcing is not limited to the BOA, but also influences the forcing at TOA. Forcing magnitudes during biomass burning period are almost double those during the non-biomass burning season at both BOA and TOA.

Monthly averages of direct ARF at BOA are frequently less than -30 W m^{-2} from December to May (non-biomass burning period) with a slightly south-north gradient. From July to October, a strong north-south gradient of direct ARF is observed and forcing magnitudes are frequently recorded at -50 W m^{-2} (and, on occasion, well above that level) during September, i.e. at the peak of biomass burning. June and November are regarded as transitional months when levels move towards the higher or and lower values of forcing respectively.

Monthly averages of direct ARF at TOA are frequently less than -9 W m^{-2} from December to May and, during biomass burning, direct ARF values almost double. From the seasonal perspective, it is also possible to depict the reversal gradient behaviour at TOA.

5. *How does the change of aerosol amounts in tropospheric column influence the change of direct ARF at bottom of atmosphere and at top of atmosphere?*

Accurate estimates of direct ARF require solar radiation fluxes data to be recorded in cloud-free conditions. However, solar radiation fluxes are hampered, most of the time, by persistent broken cloud fields, making it difficult to assess the aerosol radiative forcing.

The use of the accurately assessed cloud free days (best case days) from the SAFARI 2000 field campaign, generated by a varied set of instruments, reduced the wide range of variability initially observed in the AERONET model estimates.

For instance: in the previous analyses (based on model estimates), it was found that daily direct ARF values were between -2 and -200 W m^{-2} for BOA and 0 and -50 W m^{-2} for TOA. A multiple combination of data, corresponding to the best cloud free days, showed that daily direct ARF values range between 0 and -100 W m^{-2} for BOA and 0 and -30 W m^{-2} for TOA. The high values from the model estimates may possibly be because of cloud contaminations by high cirrus clouds. The impact of cloud contaminations can be removed by focussing the case study on the cloud free days. Therefore, it appears that the model estimates of direct ARF tend to overestimate the forcing magnitudes for both BOA and TOA, especially in the presence of thin cloud contamination.

The direct ARF magnitudes, corresponding to the different aerosol amounts in the atmosphere on cloud free days, clearly indicate direct ARF magnitudes are proportional to the aerosol loading. Direct aerosol radiative forcing at TOA is less sensitive to the variation of aerosols amounts in the tropospheric column; conversely direct aerosol radiative forcing at BOA is demonstrably more sensitive to this variation.

When the aerosols amounts are insignificant, i.e. a very clean atmosphere, direct aerosol radiative forcing at BOA and TOA is very small and both forcing levels are almost of the same magnitude. Differences between direct ARF magnitudes at BOA and TOA increase with the amounts of aerosols in the tropospheric column.

6. *What is the likely regional magnitude of direct radiative forcing of aerosols for southern Africa?*

Based on the results of this study, the direct aerosol radiative forcing values for all southern Africa are estimated at -33 W m-2 for BOA and -6 W m-2 for TOA. These values are consistent with the findings of Abel *et al*. (2005). However, seasonal values may differ considerably from these numbers.

Direct aerosol radiative forcing magnitudes are estimated at -48 W m^{-2} for BOA and -9 W m^{-2} for TOA during the biomass burning period and -20 W m^{-2} for BOA and -4 W m^{-2} for TOA during the non-biomass burning period. These results corroborate the findings of Garcia *et al*. (2011)

For a more accurate assessment it is important to take into account the sub regional differences of direct aerosol forcing magnitudes (between the south and the north) and the seasonal reversal in behaviour.

The conclusion drawn from this study is: the aerosol optical properties and the direct aerosol radiative forcing both change significantly from one season to another in southern Africa, following the strong seasonal cycle of aerosol optical properties.

Consequently the evaluation of forcing, using static values (throughout the year), is not suitable for describing the aerosol climate effects in this region. Furthermore improving the understanding and knowledge of the aerosol direct radiative effects in this region is a necessary step in order to address the indirect and semi-direct aerosol effects. This process will require improving the quantity and quality of aerosol measurements in southern Africa.

Biomass burning in southern Africa is a significant source of fine mode aerosols; these aerosols interact efficiently with the solar radiation and affect the radiation budget of this region. Assuming that most forest fires are, to some extent, related to human activities, it is believed that positive changes in human behaviour and practices can contribute significantly to the reduction of the amount of tropospheric aerosols in this region and thereby improve the air quality.

6.1 Significance of the study

This study (specifically over southern Africa) was part of a global effort coordinated by NASA Goddard Space Flight Center (GSFC) to better characterise the aerosol radiative effects at regional levels and so improve the understanding of the role of aerosols in the climate system.

The author was actively engaged, as part of the research team, in two major regional field campaigns. The Southern Africa Science Initiative (SAFARI 2000), conducted between 1999 and 2001; the Unified Aerosol Experiment in United Arab Emirates (UAE^2) in 2004. The author also spent time at GSFC with the AERONET and SMART teams (for instrumental training and data analysis).

The data acquired from the ground-based radiometers during the regional experiments have contributed significantly to many aerosol case studies, including the validation of space and airborne instruments, e.g. MODIS, TERRA and AQUA.

Mainly this study contributes to a deeper understanding of the particular features of the aerosol sources, spatial patterns, seasonal variations, trends and atmospheric dynamics and a deeper understanding of direct aerosol radiative forcing over southern Africa (and the spatial and seasonal changes). This research has developed an approach for assessing the average direct ARF, based on given aerosol optical thickness magnitude. In addition the study emphasises the use of a dynamic values approach, rather than using static values (where one number is used throughout the year) as in previous studies. It is hoped that the information collected and the approach used will be able to contribute significantly to the estimates of regional radiation balance and improve local understanding on climate dynamics. One crucial challenge for southern Africa to improve the knowledge of the aerosol radiative effects on climate system is the need for more long-term measurement stations equipped with multiple radiation measurement instruments. Finally, but not least, parts of this study have been published in the Journal of Atmospheric Environment. Moreover, the overall research has contributed significantly to develop capacities of African scientists on the matter of aerosol studies, as result the author contributed as reviewer of the IPCC fourth assessment report under the aerosol chapter.

References

Abel, S. J., Highwood, E. J., Haywood, J. M., Stringer, M. A., 2005: The direct radiative effects of biomass burning aerosols over southern Africa, *Atmospheric Chemistry and Physics*., 5, 1999–2018.

Anderson, T. L., Charlson, R. J., Bellouin, N., Boucher, O., Chin, M., Christopher, S. A., Haywood, J., Kaufman, Y. J., Kinne, S., Ogren, J. A., Remer, L. A., Takemura, T., Tanré, D., Torres, O., Trepte, C. R., Wielicki, B. A., Winker, D. M., Yu, H., 2005: An "A-Train" strategy for quantifying direct aerosol forcing of climate, *Bulletin of American Meteorological Society*, 86 (12), 1795–1809.

Ångström, A., 1930: On the atmospheric transmission of sun radiation. *II. Geografiska Annaler*, 12, 130–159.

Ångström, A., 1929: On the atmospheric transmission of sun radiation and on dust in the air, *Geografiska Annaler*, 11, 156–166.

Annegarn, H. J., Otter, L., Swap, R. J., Scholes, R. J., 2002: Southern Africa's ecosystem in test tube: A perspective on the Southern African Regional Science Initiative (SAFARI 2000), *South African Journal of Science*, 98, 111–113.

Anyamba, A., Justice, C. O., Tucker, C. J. , Mahoney, R., 2003: Seasonal to inter-annual variability of vegetation and fires at SAFARI 2000 sites inferred from advanced very high resolution radiometer time series data, *Journal of Geophysical Research*, 108 (D13), 8507, doi: 10.1029/2002/JD002464.

Barenbrug, M., 2003: The transport of aerosols and their effects on direct solar radiation over Southern Africa, Unpublished MSc Thesis, University of the Witwatersrand, Johannesburg, South Africa.

Bergstrom, R. W., Pilewskie, P., Schmid, B., Russell, P. B., 2003: Estimates of the spectral aerosol single scattering albedo and aerosol radiative effects during SAFARI 2000, *Journal of Geophysical Research*, 108(D13), 8465, doi:10.1029/2002JD002435.

Bergstrom, R. W., Russell, P. B, Hignett, P., 2002: On the Wavelength Dependence of the Absorption of Black Carbon Particles: Predictions and Results from the TARFOX Experiment and Implications for the Aerosol Single Scattering Albedo, *Journal of Atmospheric Science*, 59, 567–577.

Bohren, C. F., Huffman D. R., 1983: *Absorption and Scattering of Light by Small Particles*, Wiley, Canada.

Campbell Scientific, 2001: Application note 2RA-A, http://www.campbellsci.com.

Charlson, R. J., Schwartz, S. E., Hales, R. D., Cess, J. A., Coakley, Jr., Hansen, J. E., Hofman, D. J., 1992: Climate forcing by anthropogenic aerosols, *Science*, 255, 423–430.

Coakley, J. A., Cess, R. D., 1985: Response of the NCAR Community Climate Model to the radiative forcing by the naturally-occurring tropospheric aerosol, *Journal of Atmospheric Science*, 42, 1677–1692.

Coakley, J. A., Cess, R. D., Yurevich, F. B., 1983: The effect of tropospheric aerosols on the Earth's radiation budget: a parameterisation for climate models, *Journal of Atmospheric Science*, 40, 116–138.

Collins, W. D., Rasch, P. J., Eaton, B. E., Khattatov, B., Lamarque, J. F., Zender, C. S., 2001: Simulating aerosols using a chemical transport model with assimilation of satellite aerosol retrievals: Methodology for INDOEX, *Journal of Geophysical Research*, 106, 7313–7336.

Cosijn, C., Tyson, P. D., 1996: Stable discontinuities in the atmosphere over South Africa, *South African Journal of Science*, 92, 381–386.

Crutzen, P. J., Andreae, M. O., 1990: Biomass burning in tropics: impact on atmospheric chemistry and biogeochemical cycles, Science, 250, 1669–1678.

Dey, S., Sarkar, S., Singh, R. P., 2004: Comparison of aerosol radiative forcing over the Arabian Sea and the Bay of Bengal, Advances in Space Research, 33, 1104–1108.

Draxler R., Stunder B., Rolph G., Stein A., Taylor A., 2009: HYSPLIT4 user's guide, Ver. 4.9, http://www.arl.noaa.gov/documents/reports/hysplit user guide.pdf .

Draxler, R. R., Hess, G. D., 1998: Description of the HYSPLIT_4 modelling system, NOAA Technical Memorandum ERL ARL-224, Silver Spring, Maryland, 27 pp.

de Meij, A., Pozzer, A., Lelieveld, J., 2010: Global and regional trends in aerosol optical depth based on remote sensing products and pollutant emission estimates between 2000 and 2009, Atmospheric Chemistry and Physics Discussions, 10, 30731–30776, doi:10.5194/acpd-10-30731.

Diner, D. J., Ackerman, T. P., Anderson, T. L., 2004: Progressive Aerosol Retrieval and Assimilation Global Observing Network (PARAGON): An integrated approach for characterizing aerosol climatic and environmental interactions, *Bulletin of American Meteorological Society*, 85(10), 1491–1501.

Dubovik, O., Sinyuk, A., Lapyonok, T., Holben, B. N., Mishchenko, M., Yang, P., Eck, T. F., Volten, H., Munoz, O., Veihelmann, B., van der Zande, W. J., Leon, J. F., Sorokin, M., Slutsker, I., 2006: Application of light scattering by spheroids for accounting for particle non-sphericity in remote sensing of desert dust, *Journal of Geophysical Research*, 111, D11208, doi:10.1029/2005JD006619.

Dubovik, O., Holben, B. N., Eck, T. F., Smirnov, A., Kaufman, Y. J., King, M. D., Tanré, D., Slutsker, I., 2002: Variability of absorption and optical properties of key aerosol types observed in worldwide locations, *Journal of Atmospheric Science*, 59, 590–608.

Dubovik, O., Smirnov, A., Holben, B. N., King, M. D., Kaufman, Y. J., Slutsker, I., 2000: Accuracy assessments of aerosol optical properties retrieved from AERONET sun and sky radiance measurements, *Journal of Geophysical Research*, 105, 9791–9806.

Dubovik, O., King, M. D., 2000: A flexible inversion algorithm for retrieval of aerosol optical properties from sun and sky radiance measurements, *Journal of Geophysical Research*, 105, 20673–20696.

Dubuisson, P., Dessailly, D., Vesperini, M., Frouin, R., 2004: Water vapor retrieval over ocean using near-infrared imagery, *Journal of Geophysical Research*, 109, D19106, doi:10.1029/2004JD004516.

Eck, T.F., Holben, B. N., Reid, J. S., Sinyuk, A., Dubovik, O., Smirnov, A., Giles, D., O'Neill, N.T., Tsay, S.-C., Ji, Q., Al Mandoos, A., Ramzan Khan, M., Reid, E. A., Schafer J. S., Sorokine, M., Newcomb, M., Slutsker, I., 2008: Spatial and temporal variability of column-

integrated aerosol optical properties in the southern Arabian Gulf and United Arab Emirates in summer, Journal of Geophysical Research, 113, (D01204), doi:10.1029/2007JD008944.

Eck, T. F., Holben, B. N., Dubovik, O., Smirnov, A., Goloub, P., Chen, H. B., Chatenet, B., Gomes, L., Zhang, X. Y., Tsay, S. C., Ji, Q., Giles, D., Slutsker, I., 2005: Columnar aerosol optical properties at AERONET sites in central eastern Asia and aerosol transport to the tropical mid-Pacific, *Journal of Geophysical Research*, 110, (D06202), doi:10.1029/2004JD005274.

Eck, T. F., Holben, B. N., Ward, D. E., Mukelabai, M. M., Dubovik, O., Smirnov, A., Schafer, J. S., Hsu, N. C., Piketh, S. J., Queface, A. J., Le Roux, J., Swap, R. J. and Slutsker, I., 2003: Variability of biomass burning aerosol characteristics in southern Africa during the SAFARI 2000 dry season campaign and a comparison of single scattering albedo estimates from radiometric measurements, *Journal of Geophysical Research*, 108 (D13), 8465, doi: 10.1029/2002JD002321.

Eck, T. F., Holben, B. N., Ward, D. E., Dubovik, O., Reid, J. S., Smirnov, A., Mukelabai, M. M., Hsu, N. C., O'Neill, N. T., Slutsker, I., 2001: Characterization of the optical properties of biomass burning aerosols in Zambia during the 1997 ZIBBEE field campaign, *Journal of Geophysical Research* 106, 3425–3448.

Eck, T. F., Holben, B. N., Reid, J. S., Dubovik, O., Smirnov, A., O'Neill, N. T., Slutsker, I., Kinne, S., 1999: The wavelength dependence of the optical depth of biomass burning, urban and desert dust aerosols, *Journal of Geophysical Research*, 104, 31333–31349.

Freiman, M. T., Piketh, S. J., 2003: Air Transport Into And out of The Industrial Highveld Region of South Africa, *Journal of Applied Meteorology*, 42, 994–1002.

Fu, Q., Liou, K. N., 1993: Parameterization of the radiative properties of cirrus clouds, *Journal of Atmospheric Science*, 50, 2008–2025.

Garcia, O. E., Diaz, J. P., Expósito, F. J., Diaz, A. M., Dubovik, O., Derimian, Y., Dubuisson, P., Roger, J.-C., 2011: Shortwave radiative forcing and efficiency of key aerosol types using AERONET data, *Atmospheric Chemistry and Physics Discussions*, 11, 32647–32684.

Garcia, O. E., Diaz, A. M., Expósito, F. J., Diaz, J. P., Dubovik, O., Dubuisson, P., Roger, J.-C., Eck, T. F., Sinyuk, A., Derimian, Y., Dutton, E. G., Schafer, J. S., Holben, B. N., Garcia, C. A., 2008: Validation of AERONET estimates of atmospheric solar fluxes and aerosol radiative forcing by ground-based broadband measurements, *Journal of Geophysical Research*, 113, doi:10.1029/2008JD010211.

Garstang, M., Tyson, P. D., Swap. R. J., Edwards, M., Kallberg, P., Lindesay, J. A., 1996: Horizontal and vertical transport of air over southern Africa, *Journal of Geophysical Research*, 101, 23721–23736.

Giglio, L., van der Werf, G. R., Randerson, J. T., Collatz, G. J., Kasibhatla, P., 2006: Global estimation of burned area using MODIS active fire observations, *Atmospheric Chemistry and Physics*, 6, 957– 974.

Hansen, J., Travis, L. D., 1974: Light scattering in planetary atmospheres, *Space Science Reviews*, 16, 527–610.

Harrison, R. M., Van Grieken, R. E., 1998: *Atmospheric Particles*, John Wiley, Chichester, UK.

Haywood, J., Frances, P., Dubovik, O., Glew, M., Holben, B., 2003: Comparison of aerosol size distributions, radiative properties, and optical depths determined by aircraft observations and Sun photometers during SAFARI 2000, *Journal of Geophysical Research*, 108 (D13), 8465, doi: 10.1029/2002JD002250.

Haywood, J., Boucher, O., 2000: Estimates of the direct and indirect radiative forcing due to tropospheric aerosols: A review, *Reviews of Geophysics*, 38, 513–543.

Haywood, J. M., Shine, K. P., 1995: The effect of anthropogenic sulfate and soot aerosol on the clear sky planetary radiation budget. *Geophysical Research Letters*, 22, 602–606.

Henyey, L. G., Greenstein, T. L., 1941: Diffuse radiation in the galaxy, *Astrophysics Journal*, 93, 70–83.

Hinds, W. C., 1982: *Aerosol Technology: Properties, Behaviour and Measurements of Airborne Particles*, John Wiley, Toronto.

Hobbs, P. V., 2003: Clean air slots amid dense atmospheric pollution in southern Africa, *Journal of Geophysical Research*, 108 (D13), 8465, doi: 10.1029/2002JD002156.

Holben, B. N., Tanré, D., Smirnov, A., Eck, T. F., Slutsker, I., Abuhassan, N., Newcomb, W. W., Schafer, J. S., Chatenet, B., Lavenu, F., Kaufman, Y. J., Vande Castle, J., Setzer, A., Markham, B., Clark, D., Frouin, R., Halthore, R., Karneli, A., O'Neill, N. T., Pietras, C., Pinker, R. T., Voss, K., Zibordi, G., 2001: An emerging ground-based aerosol climatology: Aerosol optical depth from AERONET, *Journal of Geophysical Research*, 106, 12067–12097.

Holben, B. N., Eck, T. F., Slutsker, I., Tanré, D., Buis, J. P., Setzer, A., Vermote, E., Reagan, J. A., Kaufman, Y. J., Nakajima, T., Lavenu, F., Jankowiak, I., Smirnov, A., 1998: AERONET - A federated instrument network and data archive for aerosol characterization, *Remote Sensing Environment*, 66, 1–16.

Hsu, N. C., Herman, J. R., Weaver, C., 2000: Determination of radiative forcing of Saharan dust using combined TOMS and ERBE data, *Journal of Geophysical Research*, 108 (D16), 20649-20661.

http://www.campbellsci.com, Campbell Scientific Instruments. (Accessed [August, 2011]).

http://www.yesinc.com, Yankee Environmental Systems. (Accessed [September, 2011]).

Ichoku, C., Remer, L. A., Kaufman, Y. J., Levy, R., Chu, D. A., Tanré, D., Holben, B. N., 2003: MODIS observation of aerosol and estimation of aerosol radiative forcing over southern Africa during SAFARI 2000, *Journal of Geophysical Research*, 108 (D13), 8465, doi: 10.1029/2002JD002310.

IPCC, 2007: *Climate Change 2007: The Physical Science Basis*. Contribution of Working Group I to the Fourth Assessment Report of the Intergovernmental Panel on Climate Change. Cambridge, UK; New York, US, Cambridge University Press.

IPCC, 2001: *Climate Change 2001: The Scientific Basis.* Contribution of Working Group I to the Third Assessment Report of the Intergovernmental Panel on Climate Change, Houghton, J. T., Ding, Y., Griggs, D. J., Noguer, M., van der Linden, P. J., Maskell, D. K., Johnson, C. A. (eds), Cambridge University Press, Cambridge, UK; and New York, NY, USA, 881 pp.

IPCC, 1995: *Climate Change 1995: The Science of Climate Change*. Contribution of Working Group I to the Second Assessment Report of the Intergovernmental Panel on Climate Change,

Houghton, J. T., Meira Filho, L. G., Callander, B. A., Kattenberg, A., Maskell, D. K., (eds), Cambridge University Press, Cambridge, UK; and New York, NY, USA, 572 pp.

Iqbal, M., 1983: *An Introduction to Solar Radiation*, Academic Press, Toronto.

Ito, A., Akimoto, H., 2007: Seasonal and interannual variations in CO and BC emissions from open biomass burning in Southern Africa during 1998 to 2005, *Global Biogeochemistry Cycles*, 21, GB2011, doi:10.1029/2006GB002848.

Junge, C. E., 1955: The size distribution and aging of natural aerosols as determined from electrical and optical data on the atmosphere, *Journal of Meteorology*, 12, 13–25.

Kanyanga, J. K., 2008: EL Niño Southern Oscillation (ENSO) and Atmospheric Transport over Southern Africa, Unpublished PhD Thesis, University of Johannesburg, South Africa.

Kaufman, Y. J., Tanre, D., Holben, B. N., Mattoo, S., Remer, L. A., Eck, T. F., Vaughan, J., Chatenet, B., 2002: Aerosol Radiative Impact on Spectral Solar Flux at the Surface, Derived from Principal-Plane Sky Measurements, *Journal of Atmospheric Science*, 59, 635–646.

Kaufman, Y. J., Fraser, R. S., 1997: The effect of smoke particles on clouds and climate forcing, *Science*, 277 (1350), 1636–1639.

Kaufman, Y. J., Tanre, D., Gordon, H. R., Nakajima, T., Lenoble, J., Frouin, R., Grassl, H., Herman, B. M., King, M. D., Teillet, P. M., 1997: Passive remote sensing of tropospheric aerosol and atmospheric correction for the aerosol effect, *Journal of Geophysical Research*, 102, 16815–16830.

Keil, A., Haywood, J. M., 2003: Solar radiative forcing by biomass burning aerosol particles during SAFARI 2000: A case study based on measured aerosol and cloud properties, *Journal of Geophysical Research*, 108 (D13), 8465, doi:10.1029/2002JD002315.

King, M. D., Byrne, D. M., Herman, B. M., Reagan, J. A., 1978: Aerosol size distribution obtained by inversion of spectral optical depth measurements, *Journal of the Atmospheric Sciences*, 21, 2153–2167.

Kirkman, G., Piketh, S. J., Andreae, M. O., Annegarn, H. J., Helas, G., 2000: Distribution of aerosols, ozone and carbon monoxide over southern Africa, South African Journal of Science, 96, 423–431.

Kondratyev, K. Y., 1999: *Climatic Effects of Aerosols and Clouds*. ISBN: 1-85233-110-0, 264 pp.

Koren, I. Y., Kaufman, Y. J., Remer, L. A., Martins, J. V., 2004: Measurement of the effect of Amazon smoke on inhibition of cloud formation, *Science*, 303, 1342–1345.

Lacis, A. A., Mishchenko, M. I., 1994: Climate forcing, climate sensitivity, and climate response radiative modeling perspective on atmospheric aerosols, In: *Aerosol Forcing of Climate*, R. L. Charlson, J. Heintzenberg (eds), John Wiley, p. 12.

Leahy, L. V., Anderson, T. L., Eck, T. F., Bergstrom, R. W., 2007: A synthesis of single scattering albedo of biomass burning aerosol over southern Africa during SAFARI 2000, *Geophysical Research Letters*, 34, L12814, doi:10.1029/2007GL029697.

Lindesay, Y. J., 1988: South African rainfall, the Southern Oscillation and Southern Hemisphere semi-annual cycle, Journal of Climatology, 8 , 17–30.

Maenhaut, W., Schwarz, J., Cafmeyer, J., Annegarn, H. J., 2002: Study of elemental mass size distributions at Skukuza, South Africa, during the SAFARI 2000 dry season campaign, *Nuclear Instruments and Methods in Physics Research B*, 189, 254–258.

Magi, B. I., Ginoux, P., Ming, Y., Ramaswamy, V., 2009: Evaluation of tropical and extratropical Southern Hemisphere African aerosol properties simulated by a climate model, *Journal of Geophysical Research*, 114, D14204, doi:10.1029/2008JD011128.

Magi, B. I., 2006: Optical Properties and Radiative Forcing of Southern African Biomass Burning Aerosol, Unpublished PhD Thesis, University of Washington, USA.

Magi, B. I., Hobbs, P. V., Schmid, B., Redemann, J., 2003: Vertical profiles of light scattering, light absorption and single-scattering albedo during the dry, biomass burning season in southern Africa and comparisons of in-situ and remote sensing measurements of aerosol optical depth, *Journal of Geophysical Research*, 108(D13), doi:10.1029/2002JD002361.

Mishchenko, M. I., Geogdzhayev, I. V., Rossow, W. B., Cairns, B., Carlson, B. E., Lacis, A. A., Liu, L., Travis, L. D., 2007: Long-term satellite record reveals likely recent aerosol trend, *Science*, 315, 1543.

Miron, O., Tyson, P. D., 1984: Wet and dry conditions and pressure anomaly fields over South Africa and the adjacent oceans 1963–1979, *Monthly Weather Review*, 112, 2127–2132.

Nemani, R. R., Keeling, C. D., Hashimoto, H., Jolly, W. M., Piper, S. C., Tucker, C. J., Myneni, R. B., Running, S. W., 2003: Climate – Driven Increases in Global Terrestrial Net Primary Production from 1982 to 1999, *Science*, 300, 1560–1563.

O'Neill, N. T., Eck, T. F., Smirnov, A., Holben, B. N., Thulasiram, S., 2006. Spectral deconvolution algorithm, AERONET Technical Memo, 14 pp.

O'Neill, N. T., Eck, T. F., Smirnov, A., Holben, B. N., Thulasiram, S., 2003. Spectral discrimination of coarse and fine mode optical depth, *Journal of Geophysical Research* 108(D17), 4559, doi: 10.1029/2002JD002975.

O'Neill, N. T., Eck, T. F., Holben, B. N., Smirnov, A., Dubovik, O., Royer, A., 2000a: Uni- and bi-modal size distribution influences on the variation of Ångström derivatives in spectral and optical depth space. *Journal of Geophysical Research* (accepted, in press).

O'Neill, N. T., Ignatov, A., Holben, B. N., Eck, T. F., 2000b: The lognormal distribution as a reference for reporting aerosol optical depth statistics; Empirical tests using multi-year, multi-site AERONET sunphotometer data, *Geophysical Research Letter*, 27(20), 3333–3336.

Penner, J. E., Charlson, R. J., Hales, J. M., 1994: Quantifying and minimizing uncertainty of climate forcing by anthropogenic aerosols, *Bulletin of American Meteorology Society*, 75, 375–400.

Piketh, S. J., Annegarn, H. J., Tyson, P. D., 1999: Lower tropospheric aerosol loadings over South Africa: The relative contribution of aeolian dust, industrial emissions and biomass burning, *Journal of Geophysical Research*, 104, 1597–1607.

Queface, A. J., Piketh, S. J., Eck, T. F., Tsay, S.-C., Mavume, A. F., 2011: Climatology of aerosol optical properties in Southern Africa, *Journal of Atmospheric Environment*, 45, 2910–2921.

Queface, A. J., Piketh, S. J., Annegarn, H. J., Holben, B. N., Uthui, R. J., 2003: Retrieval of aerosol optical thickness and size distribution from CIMEL sun photometer over Inhaca Island, Mozambique, *Journal of Geophysical Research*, 108(D13), 8465, doi: 10.1029/2002JD002374.

Raes, F., Wilson, J., Vandingenen, R., 1995: Aerosols dynamics and its implications for the global aerosol climatology, in *Aerosol Forcing of Climate*, Charlson, R. J., Heintzenberg, J. (eds), John Wiley, New York, NY, Chapter 8.

Ramanathan, V., Crutzen, P. J., Kiehl, J. L., Rosenfeld, D., 2001: Aerosols, climate and the hydrological cycle, *Science*, 294, 2119–2124.

Ramanathan, V., Cess, R. D., Harrison, E. F., Minnis, P., Barkstrom, B. R., Ahmad, E., Hartmann, D., 1989: Cloud radiative forcing and climate: results from the Earth radiation budget experiment, *Science*, 243, 57–63.

Reason, C. J. C., Jagadheesha, D., 2005: A model investigation of recent ENSO impacts over southern Africa, *Journal of Meteorology and Atmospheric Physics*, 89, 181–205.

Reason, C. J. C., Allan, R. J., Lindesay, J. A., Ansell, T. J., 2000: ENSO and climatic signals across the Indian Ocean Basin in the global context: Part I, interannual composite patterns, *International Journal of Climate*, 20 (11), 1285–1327.

Reid, J. S., Gatebe, Holben, B. N., King, M., Piketh, S., Westphal, D. L., 2004: Science Plan - United Arab Emirates Unified Aerosol Experiment (UAE2), Prepared for DWRS, NASA, NRL, and ONR.

Reist, P. C., 1993: *Aerosol Science and Technology*, McGraw-Hill, New York, NY.

Richard, Y., Trzaska, S., Roucou, P., Rouault, M., 2000: Modification of the southern African rainfall variability/ENSO relationship since the late 1960s, *Journal of Climate Dynamics*, 16, 883–895.

Rocha, A., Simmonds, I., 1997: Interannual variability of south-eastern African summer rainfall. Part 1: Relationship with air-sea interaction process, *International Journal of Climatology*, 17, 235–265.

Rosenfeld, D., Lensky, I. M., 1998: Satellite-based insights into precipitation formation processes in continental and maritime convective clouds, *Bulletin of American Meteorology Society*, 79, 2457–2476.

Ross, K. E., Piketh, S. J., Bruintjes, R. T., Burger, R. P., Swap, R. J., Annegarn, H. J., 2003: Spatial and seasonal variations in CCN distribution and the aerosol-CCN relationship over southern Africa, *Journal of Geophysical Research*, 108(D13), 8465, doi:10.1029/2002JD002384.

Sabbah, I., Hasan, F. M., 2008: Remote sensing of aerosols over the Solar Village, Saudi Arabia, *Journal of Atmospheric Research*, 90, 170–179.

Satheesh S., Deepshikha, K. S., Srinivasan, J., 2006: Impact of dust aerosols on Earth-atmosphere clear-sky albedo and its short wave radiative forcing over African and Arabian regions, *International Journal of Remote Sensing*, 27, 1691–1706.

Schmid, B., Ferrare, R., Flynn, C., Elleman, R., Covert, D., Strawa, A., Welton, E., Turner, D., Jonsson, H., Redemann, J., Eilers, J., Ricci, K., Hallar, A. G., Clayton, M., Michalsky, J., Smirnov, A., Holben, B., Barnard, J., 2006: How well do state-of-the-art techniques measuring the vertical profile of tropospheric aerosol extinction compare?, *Journal of Geophysical Research*, 111, D05S07, doi:10.1029/2005JD005837.

Schmid, B., Redemann, J., Russell, P. B., Hobbs, P. V., Hlavka, D. L., McGill, M. J., Holben, B. N., Welton, E. J., Campbell, J. R., Torres, O., Kahn, R. A., Diner, D. J., Helmlinger, M. C., Chu, D. A., Robles-Gonzalez, C., De Leeuw, G., 2003: Coordinated airborne, spaceborne, and ground-based measurements of massive thick aerosol layers during the dry season in southern Africa, *Journal of Geophysical Research*, 108(D13), 8465, doi:10.1029/2002JD002297.

Schmid, B., Michaslky, J. J., Slater, D. W., Barnard, J. C., Halthore, R. N., Liljegren, J. C., Holben, B. N., Eck, T. F., Livingston, J. M., Russell, P. B., Ingold, T., Slutsker, I., 2001: Comparison of columnar water vapor measurements during the fall 1997 ARM Intensive Observation Period: solar transmittance methods, *Applied Optics*, 40 (12), 1886–1896.

Schmid, B., Michalsky, J., Halthore, R., Beauharnois, M., Harrison, L., Livingston, J., Russell, P., Holben, B., Eck, T., Smirnov, A., 1999: Comparison of Aerosol Optical Depth from Four Solar Radiometers during the Fall 1997 ARM Intensive Observation Period, *Geophysical Research Letter*, 26, 2725–2728.

Seinfeld, J. H., Kahn, R. A., Anderson, T. L., Charlson, R. J., Davies, R., Diner, D. J., Schwartz, S. E., Wielicki, B., 2004: Scientific objectives, measurement needs & challenges motivating the PARAGON aerosol initiative, *Bulletin of American Meteorology Society*, 85(10), 1503–1509.

Shugart, H. H., Macko, S. A., Lesolle, P., Szuba, T. A., Mukelebai, M. M., Dowty, P., Swap, R., 2004: The SAFARI 2000 – Kalahari transect wet season campaign of year 2000, *Global Change Biology*, 10, 273–280.

SMART-Surface Sensing Measurements for Atmospheric Radiative Transfer, http://smartlabs.gsfc.nasa.gov.

Smirnov, A., Holben, B. N., Eck, T. F., Dubovik, O., Slutsker, I., 2000: Cloud screening and quality control algorithms for the AERONET database, *Remote Sensing Environment* 73, 337–349.

Stamnes, K., Tsay, S.-C., Wiscombe, W., Jayaweera, K., 1988: Numerically stable algorithm for discrete-ordinate-method radiative transfer in multiple scattering and emitting layered media, *Applied Optics*, 27: 2,502–2,509.

Stein, D. C., Swap, R. J., Greco, S., Piketh, S. J., Macko, S. A., Doddridge, B. G., Elias, T., Bruintjes, R. T., 2003: Haze layer characterization and associated meteorological controls along the eastern coastal region of southern Africa, *Journal of Geophysical Research*, 108 (D13), 8465, doi: 10.1029/2002JD003237.

Stohl, A., 1998: Computation, accuracy and applications of trajectories a review and bibliography, *Journal of Atmospheric Environment*, 32, (6), 947–966.

Swap, R. J., Annegarn, H. J., Suttles, J. T., King, M. D., Platnick, S., Privette, J. L., Scholes, R. J., 2003: Africa burning: A thematic analysis of the Southern African Regional Science Initiative (SAFARI 2000), *Journal of Geophysical Research*, 108(D13), 8465, doi: 10.1029/2003JD003747.

Twomey, S., 1977: *Atmospheric Aerosols*, Elsevier Scientific, Amsterdam.

Tyson, P. D., Garstang, M., Swap, R. J., Kållberg, P., Edwards, M., 1996: An air transport climatology for subtropical southern Africa, *International Journal of Climatology*, 16, 265–291.

Yoon, J., von Hoyningen-Huene, W., Vountas, M., Burrows, J. P., 2011: Analysis of linear long-term trend of aerosol optical thickness derived from SeaWiFS using BAER over Europe and South China, *Journal Atmospheric Chemistry and Physics*, 11, 12149–12167.

Yu, H., Kaufman, Y. J., Chin, M., Feingold, G., Remer, L. A., Anderson, T. L., Balkanski, Y., Bellouin, N., Boucher, O., Christopher, S., DeCola, P., Kahn, R., Koch, D., Loeb, N., Reddy, M. S., Schulz, M., Takemura, T., Zhou, M., 2006: A review of measurement-based assessments of the aerosol direct radiative effect and forcing, *Journal of Atmospheric Chemistry and Physics*., 6, 613– 666.

Yu, H., Dickinson, R. E., Chin, M., Kaufman, Y. J., Zhou, M., Zhou, L., Tian, Y., Dubovik, O., Holben, B. N., 2004: The direct radiative effect of aerosols as determined from a combination of MODIS retrievals and GOCART simulations, *Journal of Geophysical Research.*, 109, D03206, doi:10.1029/2003JD003914.

Yu, H., Liu, S. C., Dickinson, R. E., 2002: Radiative effects of aerosols on the evolution of the atmospheric boundary layer, *Journal of Geophysical Research*., 107(D12), 4142, doi:10.1029/2001JD000754.

van de Hulst, H. C., 1981: *Light Scattering by Small Particles*, Dover Publications, New York, NY.

Vignola, F., Lin, F., 2010: Evaluating calibrations of normal incident pyrheliometers, *Proceedings of SPIE*, Volume 7773.

Vogelmann, A. M., Flatau, P. J., Szczodrak, M., Markowicz, K. M., Minnett, P. J., 2003: Observations of large aerosol infrared forcing at the surface, *Geophysical Research Letters*, 30(12), 1655, doi:10.1029/2002GL016829.

Ward, D. E., Hao, W. M., Susott, R. A., Babbitt, R. E., Shea, R. W., Kaufman, J. B., Justice, C. O., 1996: Effect of fuel composition on combustion efficiency and emission factors for African savanna ecosystems, *Journal of Geophysical Research*, 101, 23,569–23,576.

Welton, E. J., Campbell, J. R., 2002: Micropulse lidar signals - Uncertainty analysis, *Journal of Atmospheric and Ocean Technology*, 19, 2089–2094.

Xia, X., 2011: Variability of aerosol optical depth and Angstrom wavelength exponent derived from AERONET observations in recent decades, I, 6, doi:10.1088/1748-9326/6/4/044011.

Zhang, J., Reid, J. S., 2010: A decadal regional and global trend analysis of the aerosol optical depth using a data-assimilation grade over-water MODIS and Level 2 MISR aerosol products, *Journal of Atmospheric Chemistry and Physics*, 10, 10949–10963, doi:10.5194/acp-10-10949-2010.

Zhao, T. X.-P., Laszlo, I., Guo, W., Heidinger, A., Cao, C., Jelenak, A., Tarpley, D., Sullivan, J., 2008: Study of long-term trend in aerosol optical thickness observed from operational AVHRR satellite instrument, *Journal of Geophysical Research*, 113, D07201, doi:10.1029/2007JD009061.